

Technische Universität München  
Physik-Department  
Lehrstuhl für Biophysik E22

**The interaction of conotoxins with voltage gated ion channels:  
influence of membrane potential and ionic milieu on  
the binding of  $\kappa$ -conotoxin PVIIA to *Shaker* K<sup>+</sup>-channels**

Anna Elisabetta Boccaccio

Vollständiger Abdruck der von der Fakultät für Physik  
der Technischen Universität München  
zur Erlangung des akademischen Grades eines

Doktors der Naturwissenschaften  
(Dr.rer.nat.)

genehmigten Dissertation.

Vorsitzender: Univ.-Prof. Dr. M. Kleber  
Prüfer der Dissertation: 1. Univ.-Prof. Dr. E. Sackmann  
2. Hon.-Prof. Dr. W. Stühmer, Universität Göttingen

Die Dissertation wurde am 8.10.2001 bei der Technischen Universität München eingereicht und durch die Fakultät für Physik am 19.11.2001 angenommen.

A mamma e papà

## Summary

Ion channels are integral membrane proteins present in almost all cells and assure selective and high rate transport of ions down the electrochemical gradient. Voltage gated ion channels respond to a depolarization of the membrane potential with a conformational change that opens a permeation pathway for ions. Within this family,  $K^+$  channels, which are selectively permeable to  $K^+$ -ions, are the biggest group and are a requisite for a variety of physiological functions. Due to their functional importance for the electrical excitability of cells, diverse organisms such as scorpions, anemones, snakes and snails have developed highly specific toxins targeting voltage gated  $K^+$  channels of their prey. Some of these toxins have been successfully used as probes for investigating the structure and function of ion channels (for review, Hille 1992).

$\kappa$ -conotoxin PVIIA ( $\kappa$ -PVIIA), isolated from the fish-hunting snail *Conus purpurascens*, blocks *Shaker*  $K^+$  channels (Terlau et al. 1996), by strongly interacting with some amino acid residues that are believed to shape the outer pore (Shon et al. 1998). In this study we investigated the blocking mechanism by  $\kappa$ -PVIIA and the parameters that influence the binding of this peptide to the ion channel protein. Since ion channels are not a rigid structure and they undergo conformational changes during their activity, we investigated the possibility that this might affect, directly or indirectly, i.e. through ion(s) sitting in the pore, the binding of the toxin.

The main results of this study are:

$\kappa$ -PVIIA binds to *Shaker*  $K^+$ -channel with a 1:1 stoichiometry (Garcia et al. 1999, Terlau et al. 1999), but blocks differently the channel in the conductive than in the not conductive state, which can be either the closed or N-type inactivated state (Terlau et al. 1999).

The potency of toxin block of *Shaker* channels in the open conformation decreases with increasing potentials. This feature reflects a destabilization of the toxin due to a  $K^+$  ion bound in the pore: toxin dissociation from the  $K^+$ -occupied channel increases at higher depolarizations and is faster than from channels not occupied by  $K^+$ .

When  $K^+$  is the only permeant cation in solution, the binding properties of  $\kappa$ -PVIIA to open channels are affected only by the composition of the intracellular solution. Accordingly, in the presence of impermeant cations in the intracellular medium, the efficiency of the toxin is increased, due to a lower probability for a  $K^+$  in the pore to efficiently destabilize the toxin. Nevertheless in the presence of bulky non permeant cations, a residual voltage dependence of the toxin block is observed. In addition  $Na^+$  acts like  $K^+$  in destabilizing the bound toxin,

which might indicate that this poorly permeant ion (it is permeable in absence of  $K^+$ ) traverses a substantial length of the pore.

Since  $K^+$ -channels are multi ion pores it is likely that when the toxin is bound, more ions can be present in the pore. Consequently the ion interfering with toxin binding would be the one located at the outer position, in most cases a  $K^+$ , and its destabilizing action would reflect a cooperative movement of all the ions present in the pore. Our results suggest that the movement of the inner ion, maybe within the cavity, accessible to impermeant ions as well, influences the probability of  $K^+$  to be in the outer position, from which it is more effective in repelling the toxin. Alternatively, the toxin could sense a small fraction of the voltage drop across the pore.

In contrast to these findings observed for open channel binding, the properties of the binding of  $\kappa$ -PVIIA to closed channels are exclusively determined by the extracellular solution. This indicates that when the toxin is bound the probability that the channels open is very low. Toxin efficiency decreases at increasing potassium concentrations, suggesting the presence of an external  $K^+$ -selective site near the toxin receptor in the channel vestibule, which interferes with toxin binding.

When the permeant  $Rb^+$  is present in the extracellular and/or intracellular solutions, the toxin block appears to be modified.  $\kappa$ -PVIIA blocks closed channels 2-3 times better when  $Rb^+$  instead of  $K^+$  is trapped by the toxin. For the open channel block, the complicated pattern of toxin efficiencies in all the various solutions used suggests not only that the toxin interacts differently with the two ions, but it is also likely that the occupancy of the pore is different depending on the permeating species. In comparison to the case in which  $K^+$  is the only permeant ion, open channel block is strongly reduced, approximately 7 fold at 0 mV, when  $Rb^+$  is present in the extracellular solution and  $Rb$  ions are flowing, independently on the composition of the intracellular media. This situation corresponds most likely to the presence of two  $Rb$  ions in the pore and seems to be the most destabilizing configuration for the toxin. We conclude that  $\kappa$ -PVIIA can be successfully used as a probe to elucidate the permeation properties of voltage gated  $K^+$  channels and therefore is an useful tool in understanding the pharmacology and physiology of  $K^+$ -channels.

# Contents

<b>1</b>	<b>INTRODUCTION .....</b>	<b>1</b>
1.1	ION CHANNELS: FOCUS ON THE VOLTAGE-GATED <i>SHAKER</i> K <sup>+</sup> CHANNELS.....	1
1.2	CONOTOXINS AND κ-PVIIA, A K <sup>+</sup> CHANNEL BLOCKER .....	5
<b>2</b>	<b>MATERIALS AND METHODS .....</b>	<b>1</b>
2.1	OOCYTES SOLUTIONS .....	9
2.2	PREPARATION OF OOCYTES.....	10
2.3	ELECTROPHYSIOLOGICAL METHODS .....	12
2.3.1	<i>Two-electrode voltage clamp (TEVC)</i> .....	13
2.3.2	<i>Patch clamp</i> .....	14
2.4	INSTRUMENTATION .....	15
2.4.1	<i>Mechanical set-up and electrical recordings</i> .....	15
2.4.2	<i>Micropipettes and electrodes</i> .....	16
2.5	STIMULATION PROTOCOLS AND DATA ANALYSIS.....	17
2.5.1	<i>IV-protocol</i> .....	18
2.5.2	<i>Variable prepulse duration tail protocol</i> .....	19
2.5.3	<i>Double pulse protocol</i> .....	20
2.5.4	<i>Data analysis</i> .....	20
2.5.5	<i>Leakage</i> .....	20
2.6	KINETIC ANALYSIS .....	21
<b>3</b>	<b>RESULTS .....</b>	<b>23</b>
3.1	κ-PVIIA BLOCK IN EXTRACELLULAR NFR.....	23
3.1.1	<i>Shaker-wt</i> .....	23
3.1.2	<i>Shaker-Δ6-46</i> .....	25
3.1.3	<i>Closed-channel block: Shaker-Δ6-46</i> .....	29
3.1.4	<i>Closed-channel block in NFR: Shaker-wt</i> .....	31
3.2	EFFECT OF [K] <sub>o</sub> ON THE BINDING OF κ-PVIIA.....	31
3.2.1	<i>Shaker-wt</i> .....	31
3.2.2	<i>Shaker-Δ6-46: open channel block</i> .....	32
3.2.3	<i>Shaker-Δ6-46: closed channel block</i> .....	34
3.2.4	<i>Closed channel block as a function of [K]<sub>o</sub></i> .....	36
3.3	BINDING OF κ-PVIIA IN ABSENCE OF EXTERNAL K <sup>+</sup> .....	38
3.4	EFFECT OF [Rb] <sub>o</sub> ON THE BINDING OF κ-PVIIA.....	39
3.4.1	<i>115 int KCl, 115 ext RbCl</i> .....	40
3.5	EFFECT OF INTRACELLULAR CATIONS .....	46
3.5.1	<i>Open channel block</i> .....	46
3.5.2	<i>Closed channel block</i> .....	54
3.5.3	<i>Intermediate [K]<sub>i</sub></i> .....	55
3.6	EFFECTS OF TOXIN BINDING ON "TAIL CURRENTS" .....	57
3.7	EFFECT OF SYMMETRICAL [Rb] <sub>o</sub> .....	58
<b>4</b>	<b>DISCUSSION .....</b>	<b>61</b>
4.1	κ-PVIIA IS A PORE BLOCKER.....	61
4.2	κ-PVIIA-BLOCK IS STATE-DEPENDENT .....	61
4.3	κ-PVIIA BLOCK OF OPEN CHANNELS IS VOLTAGE DEPENDENT.....	62
4.4	ANALOGY BETWEEN κ-PVIIA AND CTX .....	63
4.5	A MODEL FOR THE STATE-DEPENDENCY OF κ-PVIIA-BLOCK .....	66
4.5.1	<i>Dependence of the open channel block on the solution composition</i> .....	67
4.5.2	<i>Closed channel block vs [K]<sub>o</sub></i> .....	72
4.5.3	<i>Closed channel block does not depend on the intracellular solution</i> .....	76
4.6	EFFECTS OF TOXIN BINDING ON "TAIL CURRENTS" .....	76
4.7	κ-PVIIA DESTABILIZATION BY Rb <sup>+</sup> .....	78
4.7.1	<i>Closed channel block vs [Rb]<sub>o</sub></i> .....	78

4.7.2 Simulation of closed channel block in [K]O or [Rb]O.....	81
4.7.3 Open channel block vs [Rb]O.....	83
4.8 K <sup>+</sup> CHANNELS HAVE 3 - 4 K <sup>+</sup> -BINDING SITES.....	85
4.9 SUMMARY .....	89
<b>ABBREVIATIONS.....</b>	<b>91</b>
<b>REFERENCES .....</b>	<b>I</b>

# 1 Introduction

## 1.1 Ion channels: focus on the voltage-gated *Shaker* K<sup>+</sup> channels

Many cellular processes rely upon the passive diffusion of ions through biological membranes. Typical cell membranes are constituted by a lipid bilayer that represents an enormous energy barrier to the movement of small ions across it. During evolution a class of proteins known as *ion channels* has evolved in order to facilitate ion movements between the intracellular and extracellular aqueous compartments. These proteins are integrally embedded in the membrane, spanning the lipid bilayer to provide an expeditious and selective pathway for ions to cross down their electrochemical gradient, therefore without direct expenditure of metabolic energy. Despite their high selectivity, ion channels conduct ions at extremely high rates ( $10^6$ - $10^9$  ions transported through a single channel per second). In this sense, ion channels are not merely open holes of different diameter, since channels that allow the passage of a certain ion do not allow the passage of other types larger or even smaller. Accordingly, ion channels can be classified in respect to the main ion they are selective for, for instance Na<sup>+</sup> channels, K<sup>+</sup> channels, etc.

Ion channels are widely distributed throughout the biological world appearing in membranes of excitable and non-excitable animal cells, prokaryotes, protozoa, and plant cells. Although ion channels serve a common function allowing the passage of ions through the plasma membrane, they respond to different stimuli that induce the opening (activation) of the permeation pathway in a process called “gating”. The family of voltage-gated ion channels, for example, is activated by a depolarization of the membrane potential resulting in conformational changes that allow ions to permeate (Hille 1992; Armstrong and Hille 1998).

Voltage-gated ion channels are key molecules for the generation of electrical signals in the cells; for instance, the opening of Na<sup>+</sup> channels induce the rapid increase of the membrane permeability, determining the rising phase of the action potential process; Ca<sup>2+</sup> channels have a major role in muscle contraction and in the activation of responses mediated by Ca<sup>2+</sup> as second messengers; moreover, K<sup>+</sup> channels are required for all electrical activity in the nervous system. They are responsible for maintaining and regulating the resting potential and play a key role in excitability by controlling the repolarization phase of the action potential. Consequently, there has been a big interest in the study of ion channels for many years, but it was only recently that the combination of molecular biology tools and electrophysiological techniques allowed the successful study of the correlation between molecular structure and function of such proteins. In 1984 the first voltage-gated Na<sup>+</sup> channel was cloned from the eel

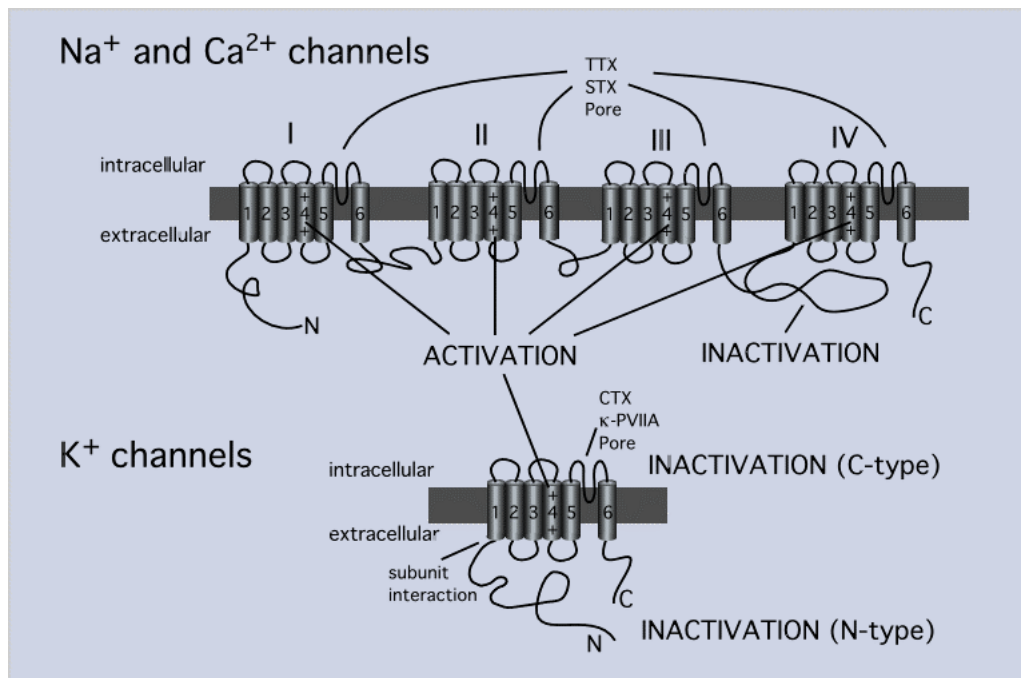


**Figure 1.1 Topology of voltage-gated ion channels** Schematic representation of the proposed transmembrane topology of voltage-gated Na<sup>+</sup>, K<sup>+</sup> and Ca<sup>2+</sup> channels. The regions of the protein whose function has been identified are indicated. (Modified from Terlau and Stühmer 1998).

electroplax (Noda et al. 1984), whereas the *Shaker* K<sup>+</sup> channel from the fruit fly *Drosophila melanogaster* was cloned in 1987 (Tempel et al. 1987).

All voltage-gated ion channels have a similar architecture and functional mechanisms (fig. 1.1; Hille 1992; Armstrong and Hille 1998). The pore forming  $\alpha$ -subunit consists of four repeats of a basic motif composed of six highly hydrophobic transmembrane segments (S1-S6). The S5-S6 segments are connected through the extracellular side of the membrane by a loop that forms the pore, known as the P-region, hence the selectivity filter of the channel. A single  $\alpha$ -subunit of voltage-gated Na<sup>+</sup> or Ca<sup>2+</sup> channels contains four of these repeats. In contrast, K<sup>+</sup> channels are composed of four separate  $\alpha$ -subunits (MacKinnon 1991) each containing one repeat homologous to the repeats of Na<sup>+</sup> and Ca<sup>2+</sup> channels. Accessory subunits have been cloned and proven that they associate to the  $\alpha$ -subunit with modulatory effects (Isom et al. 1992; Rettig et al. 1994).

A common feature of the voltage-gated channels is the presence of a “voltage sensor” that confers part of the sensitivity to the voltage. It has been identified as highly conserved positively charged amino acids in the 4<sup>th</sup> transmembrane segment (S4). The voltage sensor reacts to a change in the membrane potential with a conformational change accompanied by a movement of electrical charges that can be detected as a transient current (gating current). The gating process of the channel protein finally leads to the opening of the pore structure



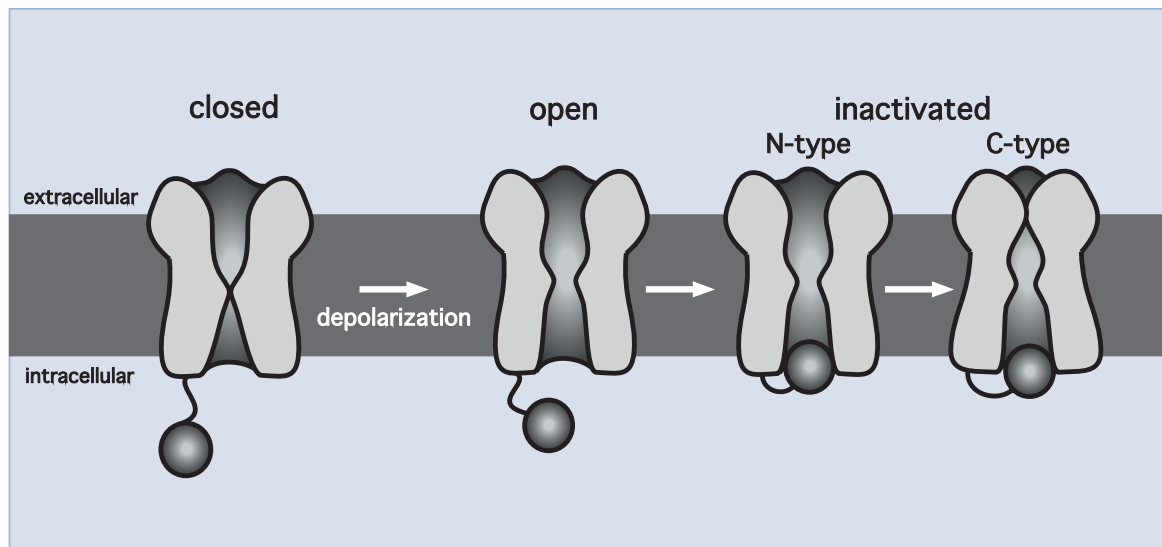


**Figure 1.2 Inactivation mechanisms** According to the “ball and chain” model of inactivation, ion channels contain a domain (“ball”) tethered to the cytoplasmic side of the protein. Following a conformational change the inactivation ball is free to bind to its receptor, occluding the ion conducting pore. This fast inactivation process (N-type inactivation) can be distinguished for  $K^+$  channels from a second inactivation process (C-type inactivation) that involves a conformational change in the extracellular part of the protein. (Modified from Terlau and Stühmer 1998).

resulting in an ionic current (for  $Na^+$  channels Stühmer et al. 1989, for *Shaker*  $K^+$  channels Papazian et al. 1991, for review Yellen 1998).

The ion flux through the permeation pathway can be interrupted by diverse mechanisms that involve different conformational changes in the protein. The voltage-gated ion channels can be either inactivated from the open state by an additional conformational change, which leads to a non conducting state of the channel, or they might be deactivated through repolarization of the membrane potential. For  $K^+$  channels two mechanisms of inactivation have been identified and named “N-type” and “C-type” (fig. 1.2). The N-type -or fast inactivation- occurs through a “ball and chain” mechanism previously proposed for the inactivation of  $Na^+$  channels (Armstrong and Bezanilla 1977) in which a cytoplasmic domain of the protein blocks the pore of the channel once it has opened (Hoshi et al. 1990; Zagotta et al. 1990). In the *Shaker*  $K^+$  channel the inactivation process normally occurs in tens of milliseconds following activation and involves the N-terminal region of the protein. It has been shown that deletion of the so-called ball-peptide disrupts the inactivation process (Hoshi et al. 1990). Furthermore, fast inactivation can be conferred by association with  $\beta$ -subunits (Rettig et al. 1994; Morales et al. 1995). C-type - or slow inactivation - is usually slower than N-type inactivation and involves conformational changes in the extracellular mouth of the channel (Hoshi et al. 1991). External permeant ions and tetraethylammonium (TEA) antagonize the C-type inactivation process by preventing the channel from entering the inactivated state (Choi et al. 1991; López-Barneo et al. 1993), as a result there is a slowing of the inactivation

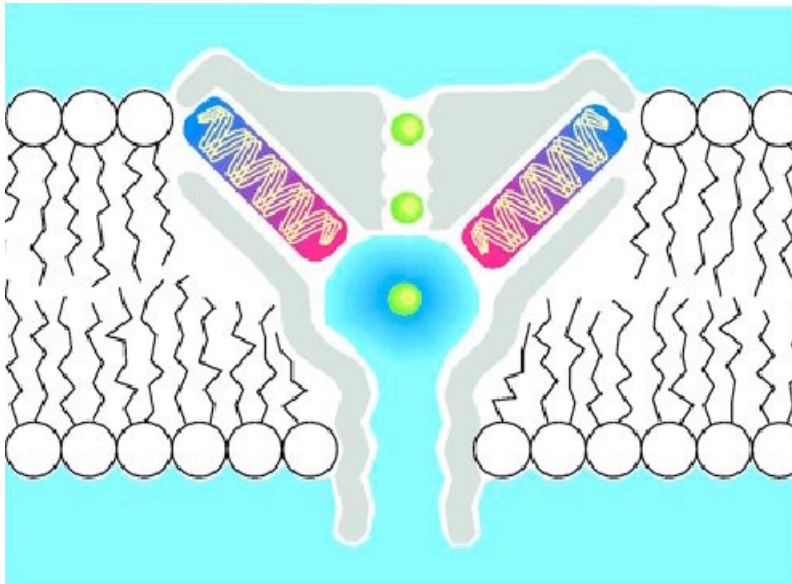


**Figure 1.3. Picture of the KcsA K<sup>+</sup> channel based on the X-ray crystallographic structure.**

Two K<sup>+</sup> ions are located at the opposite ends of the selectivity filter separated by 8 Å. A third ion, presumably surrounded by water molecules, is in a large water filled cavity (roughly 10 Å in diameter) at the center of the pore near to the cytoplasmic end of the selectivity filter (from Doyle et al. 1998).

kinetics. This suggested that the conformational change for C-type inactivation strongly depends on the occupancy of a K<sup>+</sup> binding site at the outer mouth of the channel pore (for review Yellen 1998).

Due to the amphiphilic character and the large size of ion channels, it is relatively difficult to solve their three-dimensional structure by X-ray crystallography or nuclear magnetic resonance (NMR) techniques. Recent structural data of the pore region of a K<sup>+</sup> channel from *Streptomyces lividans* have been obtained by X-ray crystallography (Doyle et al. 1998).

Although this K<sup>+</sup> channel contains only two transmembrane segments, the amino acid sequence is very close to the one of K<sup>+</sup> channels with six transmembrane segments particularly in the pore region. The crystal structure revealed that the bacterial K<sup>+</sup> channel could contain three ions in its conduction pathway (fig. 1.3). One K<sup>+</sup> ion, presumably surrounded by water molecules, was detected in a large water filled cavity (roughly 10 Å in diameter) at the center of the pore near to the cytoplasmic end of the selectivity filter. The other two K<sup>+</sup> ions were located at opposite ends of the selectivity filter separated by 8 Å, almost completely dehydrated and presumably coordinated by the carbonyl groups backbone. This structural data are consistent with earlier reports where three sites for K<sup>+</sup> in the pore region of K<sup>+</sup> channels have been hypothesized (Hodgkin and Keynes 1955; Armstrong 1971; Hille et al. 1999).

The three-dimensional crystal structures of two voltage-gated channels were recently elucidated using electron microscopy. Both structures, the Na<sup>+</sup> channel from the eel *Electrophorus electricus* (Sato et al. 2001) and the *Shaker* K<sup>+</sup> channel (Sokolova et al. 2001) from *Drosophila melanogaster*, were determined with a resolution of 19 and 25 Å respectively. *Shaker* K<sup>+</sup> channels showed fourfold symmetric structure with a large domain embedded in the membrane linked by thin connectors to a smaller cytoplasmatic domain. The

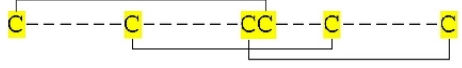
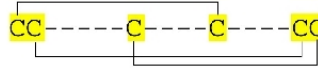
structure of the smaller bacterial channel KcsA overlaps the membrane domain. The cytoplasmic part is composed by the so called T1 domains which are highly conserved portions of the N-terminus of the protein, responsible for driving and regulating the tetramerization of the  $\alpha$ -subunits (Kreusch et al. 1998; Cushman et al. 2000).

Voltage-gated ion-channels have a fundamental role in the electrical excitability of cells, thus diverse organisms such as scorpions, anemones or snakes have developed highly specific toxins targeting ion channel proteins of their prey (Adams and Olivera 1994). Depending on the binding site, different toxins produce an occlusion of the permeation pathway or a change in the activation or inactivation kinetics of the channel. Toxins affecting voltage-gated ion channels have been indispensable for investigating the localization of the ion channel pore-structure either in  $\text{Na}^+$  (Terlau et al. 1991) and  $\text{K}^+$  channels. A peptide called Charybdotoxin ( $\alpha$ -KTx or CTX), found in the venom of the scorpion *Leiurus quinquestriatus*, targets a specific receptor site within the ion permeation pathway blocking  $\text{K}^+$  channels by a plugging mechanism (Miller 1995). Using site-directed mutagenesis, the negatively charged amino acids of the *Shaker*  $\text{K}^+$  channel protein that influence the binding affinity of the CTX molecule were identified, indicating the localization of the pore region (P-region) of  $\text{K}^+$  channels in the S5-S6 linker (MacKinnon and Miller 1989). Because ion conduction is similar in all  $\text{K}^+$  channels regardless of the gating mechanism, the pore region is a remarkably conserved structure (present in at least 50 cloned  $\text{K}^+$  selective channels) and it is comprised of a stretch of 8 amino acids, recognized as the signature sequence. This stretch in the *Shaker* channel corresponds to the sequence TMTTVGYG.

## 1.2 Conotoxins and $\kappa$ -PVIIA, a $\text{K}^+$ channel blocker

Several toxins affecting voltage-gated ion-channels have been identified from marine cone snails (Adams and Olivera 1994; Olivera and Cruz 2001). These snails predate by injecting highly effective venom into their victims, which are worms, snails, or fish. The venom of the cone snail species consists of a cocktail of up to 200 different peptides, usually small, typically 10-30 amino acids, if compared with most polypeptide toxins from other venomous animals such as scorpions, anemones, and snakes. Conotoxins are usually highly crosslinked by disulfide bonds forming a limited number of typical backbones: toxins with the same cystein arrangement can have different targets. Therefore, they have been grouped into several families according to their pharmacological action (fig. 1.4). Most of the peptides identified so far exhibit very high specificity with regard to the target molecule and are capable to differentiate between different subtypes of channels.

$\kappa$ -conotoxin PVIIA ( $\kappa$ -PVIIA), isolated from the fish-hunting snail *Conus purpurascens*, was

Toxin	Sequence	Species
<b>δ - Conotoxins</b>		
TXVIA	W <b>C</b> KQSGEM <b>C</b> NLLDQ <b>NCC</b> DGY- <b>C</b> IVLV <b>C</b> T	<i>C. textile</i>
PVIA	E <b>A</b> CW <b>A</b> PGT <b>F</b> C <b>G</b> IK <b>P</b> GL <b>CC</b> SE <b>F</b> - <b>C</b> LP <b>G</b> V <b>C</b> FG*	<i>C. purpurascens</i>
<b>ω - Conotoxins</b>		
GVIA	<b>C</b> K <b>S</b> O <b>G</b> S <b>S</b> <b>C</b> S <b>O</b> T <b>S</b> Y <b>N</b> <b>CC</b> R- <b>S</b> C <b>N</b> O <b>Y</b> T <b>K</b> R <b>C</b> Y*	<i>C. geographus</i>
MVIA	<b>C</b> K <b>G</b> K <b>G</b> A <b>K</b> <b>C</b> S <b>R</b> L <b>M</b> Y <b>D</b> <b>CC</b> T <b>G</b> S <b>C</b> R <b>S</b> -- <b>G</b> K <b>C</b> *	<i>C. magus</i>
<b>κ - Conotoxins</b>		
PVIA	<b>C</b> R <b>I</b> O <b>N</b> <b>Q</b> <b>K</b> <b>C</b> <b>F</b> <b>Q</b> H <b>L</b> D <b>D</b> <b>CC</b> S <b>R</b> K <b>C</b> N <b>R</b> F- <b>N</b> K <b>C</b> V	<i>C. purpurascens</i>
Disulfide Bridges		
<b>μ - Conotoxins</b>		
GIIA	R <b>D</b> <b>CC</b> T <b>O</b> O <b>K</b> K <b>C</b> K <b>D</b> R <b>Q</b> <b>C</b> K <b>O</b> <b>Q</b> R <b>CC</b> A*	<i>C. geographus</i>
PIIA	Z <b>R</b> L <b>CC</b> G <b>F</b> O <b>K</b> S <b>C</b> R <b>S</b> R <b>Q</b> <b>C</b> K <b>O</b> H <b>R</b> <b>CC</b> *	<i>C. purpurascens</i>
Disulfide Bridges		

**Figure 1.4 Primary structure of conotoxins binding to voltage-gated ion channels.**  $\mu$ - and  $\delta$ -conotoxins interact with  $\text{Na}^+$  channels,  $\omega$ - with  $\text{Ca}^{2+}$  channels and  $\kappa$ - with  $\text{K}^+$  channels. Other identified conotoxins families interact with acetylcholine receptor, NMDA subtype of glutamate receptor or 5HT<sub>3</sub> receptors.  $\text{K}^+$  channels peptide blockers seem to possess a common functionally important dyad consisting of a hydrophobic residue and key lysine protruding from a relatively flat surface (Ménez 1998). These residues are highlighted in bold in the  $\kappa$ -PVIA primary sequence. (Modified from Adams and Olivera 1994).

the first conopeptide detected which blocks  $\text{K}^+$  channels (Terlau et al. 1996). It was shown that  $\kappa$ -PVIA blocks the *Drosophila Shaker*  $\text{K}^+$  channel but not the rat homologues of the Kv1 family. The peptide contains 27 amino acids and three disulfide-bonds.  $\kappa$ -PVIA is a key molecule for the rapid effects of the snail venom since it acts synergistically with a  $\delta$ -conotoxin, that slows sodium channels inactivation in order to produce a massive hyperexcitation of the victim which results in almost instant tetanic paralysis of the prey. Like scorpion toxins of the CTX family,  $\kappa$ -PVIA appears to bind to the extracellular mouth of the ion pore (Shon et al. 1998). Indeed, interactions with the channel protein are strongly modified by mutations of some of the amino acid residues that are believed to shape the outer pore vestibule. Nevertheless the binding of  $\kappa$ -PVIA to the channel is mediated through a different set of interactions than those observed with scorpion toxins (Terlau et al. 1996; Shon et al. 1998; Jacobsen et al. 2000).  $\kappa$ -PVIA interacts also with the external TEA binding site competing with this toxin for blocking the channel. All these features make  $\kappa$ -PVIA an interesting tool for obtaining additional information on the molecular structure of potassium channels.

With the aid of functional assays and alanine substitutions in the amino acid sequence of the toxin peptide, Jacobsen et al. (2000) identified the binding surface of  $\kappa$ -PVIIA that is crucial for the high affinity block of K<sup>+</sup> channel. Furthermore, by combining pairs of mutations in the toxin and in the channel (mutant cycle analysis), they found that Lysine in position 7 and an aromatic residue, a Phenylalanine in position 9, share key roles for the channel-toxin interaction as it was hypothesized by Savarin and coworkers (1998) from the NMR structure of  $\kappa$ -PVIIA (Scanlon et al. 1997; Savarin et al. 1998). The fold adopted by  $\kappa$ -PVIIA is unrelated to any of the three other folds of toxins from scorpions (Bontems et al. 1991), sea anemones (Dauplais et al. 1997) and snakes (Skarzinsky 1992; Imredy and MacKinnon 2000) that block Kv1 potassium channels (Ménez 1998). However, all these seem to possess a common functionally important dyad consisting of a hydrophobic residue and key lysine protruding from a relatively flat surface formed by the residues that surround its side chain (Ménez 1998).

Since ion channels undergo conformational changes during their activity, it is possible that this might affect the “binding pocket” for the toxin.

Thus, in this study we addressed the following questions:

- Is the interaction of the toxin with the channel protein identical for the different conformational states of the channel?
- Does the ion permeation play a role in the interaction of the toxin with the channel?
- In how far is the binding of  $\kappa$ -PVIIA to the channel protein influenced by the ionic composition of the extra- or intracellular milieu and by the membrane voltage?

Furthermore, is it possible to correlate mechanisms that influence the interaction of the toxin with the channel with important functional features of the pharmacology and physiology of voltage gated K<sup>+</sup>-channels?

$\kappa$ -PVIIA could be an useful tool in investigating the intimate properties of the permeation process and help answer these questions.



## 2 Materials and methods

### 2.1 Oocytes solutions

#### Oocytes Solutions

<b>Barth</b>  pH 7.4	84 mM	NaCl
	10 mM	KCl
	2.5 mM	NaHCO <sub>3</sub>
	6.5 mM	Ca(NO <sub>3</sub> )
	0.6 mM	CaCl <sub>2</sub>
	7.5 mM	Tris-HCl
<b>Ca<sup>2+</sup>-free Barth</b>  pH 7.4	84 mM	NaCl
	10 mM	KCl
	2.5 mM	NaHCO <sub>3</sub>
	7.5 mM	Tris-HCl
<b>Skinning solution</b>  pH 7.4	200mM	K-aspartate
	20 mM	KCl
	1 mM	MgCl <sub>2</sub>
	10 mM	EGTA
	10 mM	Hepes
<b>Collagenase solution</b>	1 mg/ml	collagenase Type2 Ca <sup>2+</sup> -free Barth
<b>Antibiotics</b>	4 mg/l	Cefuxorixim / Zinacef750
	100U/ml	Penicillin / streptomycin

#### Extracellular recording solutions

<b>NFR</b>  pH 7.3	112.5 mM	NaCl
	2.5 mM	KCl
	1.8 mM	CaCl <sub>2</sub>
	10 mM	Hepes
<b>X-Ringer</b> pH 7.3 (XOH)	115 mM	XCl
	1.8 mM	CaCl <sub>2</sub>
	10 mM	Hepes
X= K, Rb, Na, Tris		

### **Intracellular recording solutions**

<b>X-intra</b>  pH 7.3 (XOH)	115 mM	XCl
	1.8 mM	CaCl <sub>2</sub>
	10 mM	Hepes
	10 mM	EGTA
	X= K, Rb, Na, Li, NMDG, Tris	

Intermediate solutions were made by mixing different ratios of the X-Ringer solutions.

Collagenase Type 2 was purchased from Worthington Biochemical Corporation, (Lakewood, NJ), Cefuxorixim/Zinacef750 by Hoechst (now Aventis, Strasbourg, France), Penicillin / streptomycin by Gibco. All other chemicals were purchased from Sigma (S. Louis, MO, USA) or Merck (Darmstadt, Germany).

$\kappa$ -PVIIA was synthesized at the peptide synthesis facility of the University of Utah. The folding and testing for biological activity of the synthetic peptide was performed at the Department of Biology, University of Utah, Salt Lake City (Shon et al. 1998).

$\kappa$ -PVIIA stock solutions (10 or 50  $\mu$ M in X-Ringer) were prepared from lyophilized material and stored at 4 °C.

## **2.2 Preparation of oocytes**

The *Xenopus* oocyte expression system was used to study the interaction of  $\kappa$ -PVIIA with *Shaker* K<sup>+</sup> channel from the fruit fly *Drosophila melanogaster* (Tempel et al. 1987). *Xenopus* oocytes contain only very few endogenous voltage activated channels and are relatively large (about 1 mm diameter) which make them a very useful system to study heterologously expressed ion channels (Methfessel et al. 1986; Goldin 1992; Stühmer and Parekh 1995).

Oocytes were surgically extracted from the frog *Xenopus laevis* under anesthesia (20-30 min in a Tricaine solution, 2.5 g/l) and the follicular cell layer was removed by 2-3 hours incubation under shaking in the collagenase solution (fig 2.1). To stop the enzymatic reaction, oocytes were extensively washed in Barth medium and selected with fine forceps (No. 5 Dumont and Fils, Montignez, Switzerland).

Oocytes between stage IV and VI were micro-injected with ~ 50 nl of solution containing 0.25  $\mu$ g/ $\mu$ l of cRNA coding for *Shaker-wt* (Tempel et al. 1987) and *Shaker  $\Delta$ 6-46* (Hoshi et al. 1994) channels. The cRNAs were kindly provided by Dr. Martin Stocker.

The injection pipettes were pulled using a standard pipette puller. The tips of the pipettes were broken under a microscope until they had an opening diameter of about 10  $\mu$ m. To avoid that the rough rim damages the oocyte, the tip was fire polished and a sharp tip pulled, by



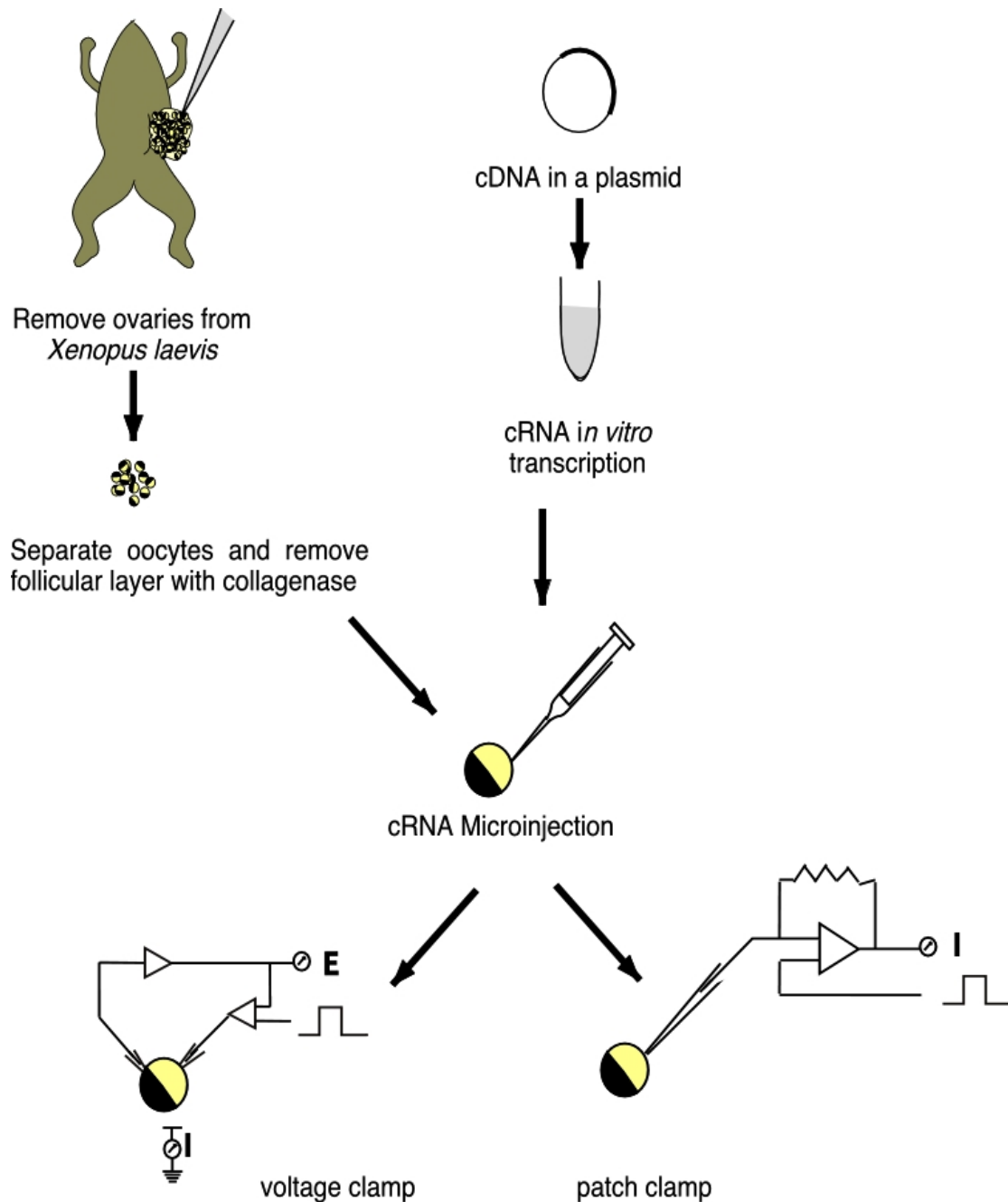


**Figure 2.1 The *Xenopus laevis* oocytes expression system.** Steps involved in the preparation of oocytes for electrophysiological recordings with either the two-electrode voltage clamp or the patch clamp technique.

approaching the injection pipette with a heated microfilament that had a small drop of melted glass on the tip. A sharp, needlelike protrusion could be obtained by rapidly removing the glass-covered filament after touching the injection pipette. Injected oocytes were then incubated at 18°C in Barth solution containing penicillin-streptomycin and cefuroxime for 1-2 days prior to electrophysiological analysis to allow expression of the protein.

The vitelline membrane surrounding the cytoplasmic membrane of the oocytes was mechanically removed during an incubation in a hypertonic skinning solution that favors the

detachment between the vitelline and the plasma membrane. The removal of the vitelline membrane is usually not necessary for voltage clamp experiments, but was performed in order to have optimal access and wash-out of solutions. Control experiments had shown that the  $IC_{50}$  of  $\kappa$ -PVIIA in the presence of the vitelline envelope was about 4 times higher compared to experiments where this membrane had been removed. Finally the oocyte was placed in the measuring chamber containing the appropriate medium for the electrophysiological experiment (section 2.1). Our experiments were performed at room temperature 20-22 °C.

### 2.3 Electrophysiological methods

Voltage clamp recordings are heavily used to investigate the properties of heterologous expressed voltage activated ion channels (Methfessel et al. 1986; Goldin 1992; Stühmer et al. 1992) and allow the measurement of electric currents due to the ion flow across a cell membrane. This is achieved by clamping the membrane potential at the desired value through a feedback amplifier.

Following a stepwise change in membrane potential a transient capacitive current flows, charging the membrane capacitance  $C$  ( $I_C$ ) to the desired value with an exponential time course with  $\tau = RC$  with  $R$  = membrane resistance. The total current flowing is the sum of the capacitive current ( $I_C$ ), a passive so called leakage current ( $I_L$ ), and the current associated to the voltage gated ion channels. For ion channels, the current reflects both the gating (due to molecular rearrangements in the new electric field;  $I_G$ ) and the ionic components (from ion permeation across the channel pore;  $I_{ION}$ )

$$I = I_G + I_{ION} + I_C + I_L = I_G + I_{ION} + C(dV/dt) + I_L$$

$I_G$  flows only transiently and is usually very small compared to  $I_{ION}$  and therefore can be neglected. However, the contribution of the transient capacitive current  $I_C$  as well as  $I_L$  must be subtracted in order to estimate the ionic current. For this purpose a P/n pulse protocol it is commonly used. It is based on the assumption that these terms depend linearly on the applied potential, as described in Heinemann (1995; see below, section 2.5.5 ).

Different electrophysiological techniques can be used according to the requirements of the experiments. We used the two-electrode voltage clamp technique when very stable conditions during long experiments were needed and the control the intracellular solution composition was not required. Alternatively we used the *outside-out* configuration of the patch clamp technique when the control of the intracellular solution and a better clamp for the inward currents was required, especially in the region of negative slope.

### 2.3.1 Two-electrode voltage clamp (TEVC)

Macroscopic currents generated by ion channels expressed in oocytes can be investigated by the two-electrode voltage clamp technique (TEVC). During TEVC experiments one intracellular electrode measures the membrane potential (the voltage electrode), and the second (current electrode) injects sufficient current to maintain the desired voltage clamp using a feedback circuit (fig. 2.2). The amount of current that passes through the current electrode is the measured parameter and is determined by the discrepancy between the membrane potential and the command potential. To limit possible voltage clamp artifacts the electrodes should be close as possible to the center of the oocyte (without damaging the cell): at small penetration depth the injected current close to the membrane would charge faster this part of the cell respect to the other side and the voltage controlled by the clamp would be not homogeneous and quite different form the command potential. In any case the oocyte membrane cannot be considered isopotential on time scales of  $300 \mu\text{s}$  or less, or when the total current is larger than  $\sim 20 \mu\text{A}$  (Baumgartner et al. 1999).

In addition there is a resistance in series with the membrane (series resistance) that is due to

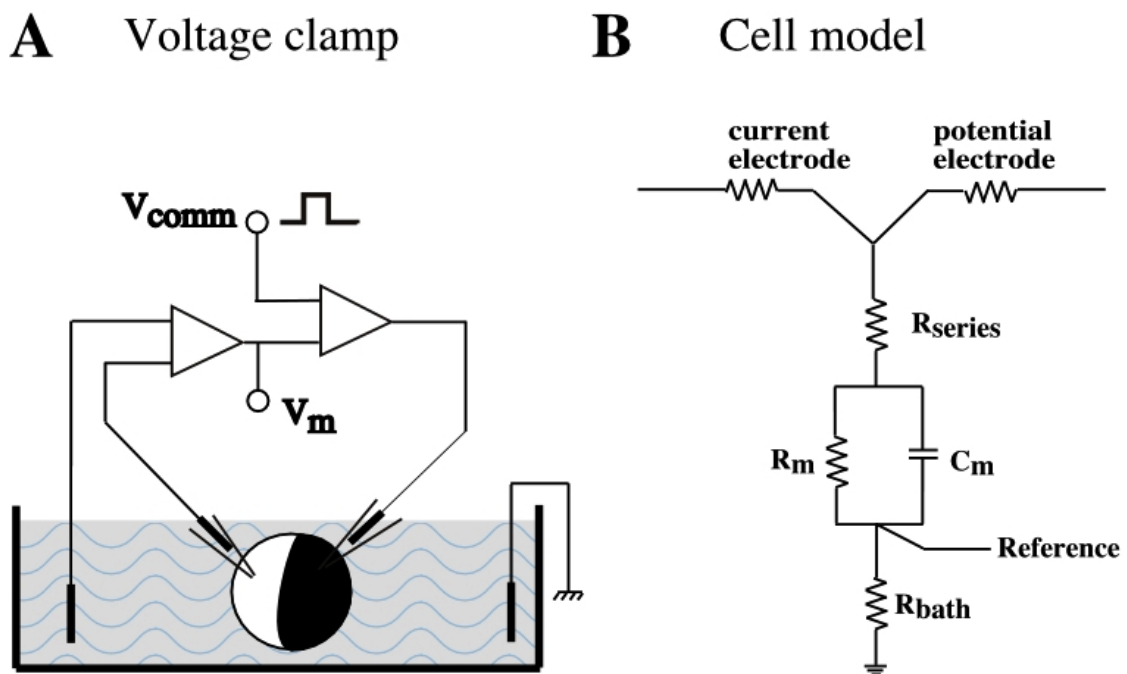


**Figure 2.2 Two-electrode voltage clamp and electrical equivalent circuit.** A) Schematic diagram of the main components of a two-electrode voltage clamp: the difference in potential between the bath and the potential electrode (left),  $V_m$ , is compared to the command potential,  $V_{\text{comm}}$  and determines the amount of current injected into the oocyte through the current electrode (right). B) Electrical circuit representing a model cell. Typical values for the electrodes' resistance is  $0.5 - 1 \text{ M}\Omega$ , for the membrane resistance  $R_m$  and capacitance  $C_m$  respectively  $100 \text{ K}\Omega$  and  $200 \text{ nF}$ , for the  $R_{\text{bath}}$  and  $R_{\text{series}}$   $1 \text{ K}\Omega$ . The error induced by the series resistance is  $I \cdot R_{\text{series}} = 1 \text{ mV} / \mu\text{A}$  if  $R_{\text{series}}$  is  $1 \text{ K}\Omega$ .

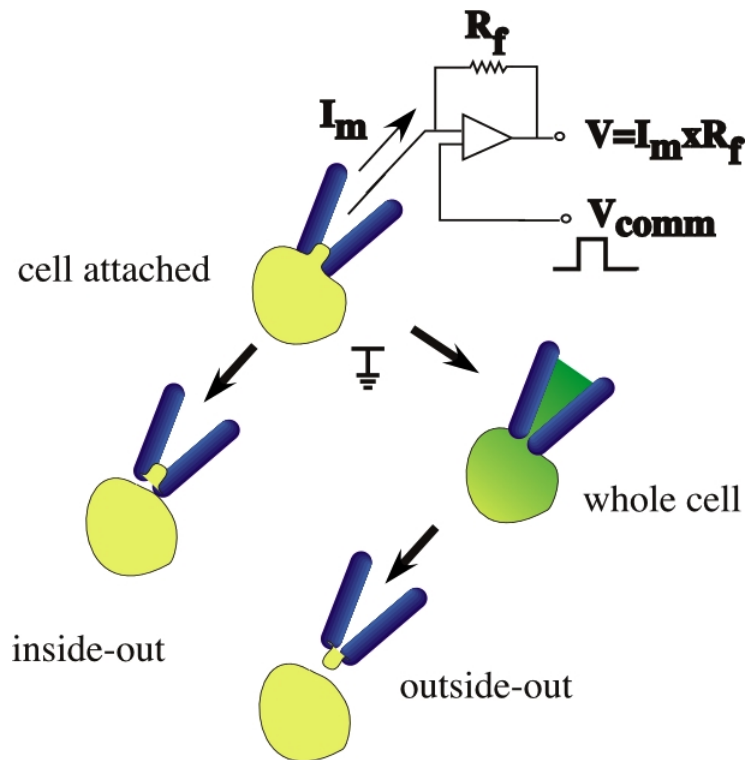


**Figure 2.3 Simplified schematic patch clamp configuration.**

The *cell-attached* configuration is obtained when the tip of a glass pipette makes a very tight seal on the cell membrane. Pulling-up a patch of membrane from the cell, leads to the *inside-out* configuration. Alternatively breaking the membrane by suction the *whole cell* configuration is obtained. By withdrawing slowly the pipette a small membrane vesicle can be formed on the tip of the pipette resulting in the *outside-out* configuration.

the elements that the injected current has to traverse: the bath, mainly the cytoplasm and the electrodes. When a current flows across the membrane, this resistance leads to a discrepancy between the measured membrane potential (controlled by the amplifier) and the true potential difference across the membrane (fig. 2.2B).

### 2.3.2 Patch clamp

The patch clamp technique is based on the control of the membrane potential across a small area of membrane by measuring the current necessary to maintain the membrane potential equal to that of the command circuit. The main part of the patch clamp amplifier is constituted by a current-voltage converter (fig. 2.3) that makes the membrane potential rapidly follow the variations of the command potential. The injected current is proportional to the potential drop at the edges of the feedback resistance  $R_f$ .

The patch of membrane is isolated by attaching the clean and smooth tip of a glass pipette on the surface of the cell membrane and obtaining a very tight seal between the pipette and the membrane (the adhesion can be so good to reach a shunt resistance bigger than 10 G $\Omega$ ; fig. 2.3). Under these conditions (*cell attached configuration*) the currents flowing through the ion channels enclosed by the pipette tip are measured by the patch-clamp amplifier. The tightness of the gigaseal prevents leak currents flowing between the pipette and the reference electrode.

When the *cell-attached* configuration is obtained, the pipette can be pulled-away and a patch of membrane can be excised from the cell, forming the *inside-out* patch-clamp configuration. In this configuration the internal membrane surface is exposed to the bath solution.

Another possibility after the *cell-attached* patch is obtained, is to perforate the membrane through the application of negative pressure (*whole cell configuration*). As the direct communication is established between the pipette and the intracellular compartment, the intracellular solution is rapidly dialyzed by the pipette solution, giving a control of the internal composition of the cell. From the whole-cell configuration it is possible to achieve a new excised patch configuration named *outside-out*. By slowly withdrawing the pipette from the cell the patch of membrane at the tip reseals with the outer surface exposed to the bath solution, and the internal surface to the pipette solution. In this configuration the pipette potential is equal to that of the membrane and negative currents are interpreted as cationic currents flowing into the cell, while positive currents represent outward cationic currents (Neher et al. 1978; Hamill et al. 1981; Moran 1996).

We used the *outside-out* configuration because in this configuration it is possible to apply different substances to the external surface of the membrane by adding them to the bath solution. In this configuration the composition of the intracellular solution is determined by the pipette solution. In order to obtain high current density measurements we performed macro patches from large portions of oocytes membrane, using pipettes with a resistance between 0.7 and 1.5 M $\Omega$ , corresponding to a diameter tip of about 3-1.5  $\mu\text{m}$ .

## 2.4 Instrumentation

### 2.4.1 Mechanical set-up and electrical recordings

The patch clamp set-up requires mechanical stability and electrical shielding.

The support system of the cell, the micromanipulators and the microscope (inverted microscope Zeiss Axiovert 100, magnification objectives 5X and 10X ) were located on an antivibration table, mechanically separated by a second table and from the Faraday cage. An optimal shielding was obtained by connecting the individual pieces to a single ground, avoiding current ("ground") loops between the instruments.

Hydraulic micromanipulators (Narishige, Tokio, Japan) were used to control the movement of the current and potential electrodes in the two-electrode voltage clamp technique, while a stepper motor driven manipulator (Luigs and Neumann, Ratingen, Germany) was used for the movement of the patch clamp pipette.

The amplifier used for the voltage clamp recordings was a Turbo TEC 10CD (Turbo Tec, npi electronics, Tamm, Germany) with an electronic built-in  $R_{\text{series}}$ -compensation and for patch

<b>Table 2.1</b>		<b>glass</b>	<b>Øi</b>	<b>Øo</b>	<b>resistance</b>	<b>company</b>
			mm	mm	MΩ	
Injection glass	Borosilicate		1.6	2		Hilgenberg
TEVC	Borosilicate filament glass		1.16	2	0.6 - 1	Hilgenberg
Patch <i>out-out</i>	Aluminum		1.22	1.6	0.8 - 1.4	Hilgenberg
	Kimax (hard borosilicate)		1.5	1.8	0.8 - 1.4	Kible products

**Table 2.1 Types of glass used**

clamp experiments an EPC9 amplifier (HEKA Elektronik, Lambrecht, Germany). In both techniques the electrical stimulation and registration of the current was performed through the EPC9 built-in ITC-16 AD/DA converter, controlled by a Macintosh, Quadra700, microcomputer (Apple computer, Cupertino, Ca, USA).

Extracellular solutions were exchanged through a gravity perfusion system by using a mechanical valve (Hamilton Deutschland, Darmstadt, Germany) which allows the change of up to 6 different solutions. The solution level of the recording chamber was maintained constant through a pressure driven level sensor system (Lorenz, Lindau, Germany).

#### 2.4.2 Micropipettes and electrodes

For the different recording conditions several types of glass capillaries were used (table 2.1). According to the melting temperatures the capillaries' glass can be classified as soft (as soda glass), hard (as borosilicate glass), and extra hard (as aluminum glass; Sakmann and Neher 1995). Selection of the glass is made optimizing the requirements of low noise-recording characteristics (hard glass has higher resistivity and lower dielectric constant) and the facility to work with each type of glass (with soft glass it is easier to get very steep tips).

After having been cut to the appropriate length the edges of the glass capillary were rounded using a Bunsen flame. This improves the junction between the pipette and the holder and also protects the Ag/Ag|Cl electrode in the holder against scraping with the glass. Pipettes were pulled in a two steps vertical puller (List Medical Electronic, Darmstadt, Germany). To improve noise characteristics and to reduce the tip capacity, pipettes were coated with RTV (GE Silicone), a low dielectric and highly hydrophobic polymer. Silicone rubber was applied as near as possible to the tip for patch electrodes (about 5 to 20  $\mu\text{m}$ ), further away for voltage clamp electrodes (about 1 mm) to avoid contact with the oocyte. A hot air stream induced the polymerization of the rubber.

The two-electrode voltage clamp pipettes were made from capillary glass containing a thin filament, which ensures that the electrode filling solution reaches the tip. To avoid creeping of the pipette filling solution to the back end of the electrode a small amount of wax was applied

to the end after moderate heating in a small flame. Pipettes were filled with 3M KCl and could be stored for several days in a closed container under moist environment. Before use the tip was broken to decrease the resistance into the range of 500 k $\Omega$  to 1 M $\Omega$  which corresponded to a tip diameter 2-10  $\mu$ m. As long as the electrodes maintain their low resistance they can be reused for several oocytes.

To smooth the surface tip, clean it and improve the patch formation, the patch pipettes were fire-polished just before use. Polishing was achieved by bringing the pipette tip close to a hot platinum wire. The patch pipettes were fabricated the day of the experiment and stored in a closed container. The electrical contact between the pipette solution and the amplifier is achieved through a silver wire covered with silver chloride. The wire converts the ionic current in electronic current in the metal, according to the  $\text{Cl} + \text{Ag} \leftrightarrow \text{AgCl} + e^-$  reaction which occurs at the liquid/metal interface. When two electrodes are immersed in the same solution there is no potential difference between them. When one electrode (the ground electrode) is immersed in the bath solution and the second one in the pipette solution, a difference of potential between the two electrodes can arise due to the different mobility of the ions in the two solutions (liquid junction potential; Barry and Lynch 1991; Neher 1995). This offset can be compensated before starting the measurements. Solution exchange can introduce an uncompensated offset that can be subtracted offline. In some experiments we replaced  $\text{K}^+$  with  $\text{Na}^+$ , that has a lower mobility ( $u_{\text{Na}}/u_{\text{K}}=0.682$ , Barry and Lynch 1991), in the concentration range of 115 mM to 2.5 mM. Because the differences were always smaller than 4.5 mV (Barry and Lynch 1991), we decided not to compensate for them.

## 2.5 Stimulation protocols and data analysis

The membrane was kept at a holding potential between  $-100$  and  $-80$  mV, where the probability of the ion channels under investigation to be closed was almost 1. The pulse interval between two stimulations was always kept long enough to ensure reequilibration of the channel states and toxin binding. Current signals were sampled at 250-100  $\mu$ s (sampling rate: 4 – 10 kHz) for voltage clamp experiments and at 50  $\mu$ s (sampling rate: 20 kHz) for *outside-out* patches. The signals were low pass filtered with a Bessel filter at a frequency 4 times lower than the inverse of the sampling time, 1-2.5 kHz for voltage clamp recordings and 5 kHz for patch clamp recordings.

To obtain the different parameters for the characterization of the channel protein and the toxin binding several stimulation protocols were generated.

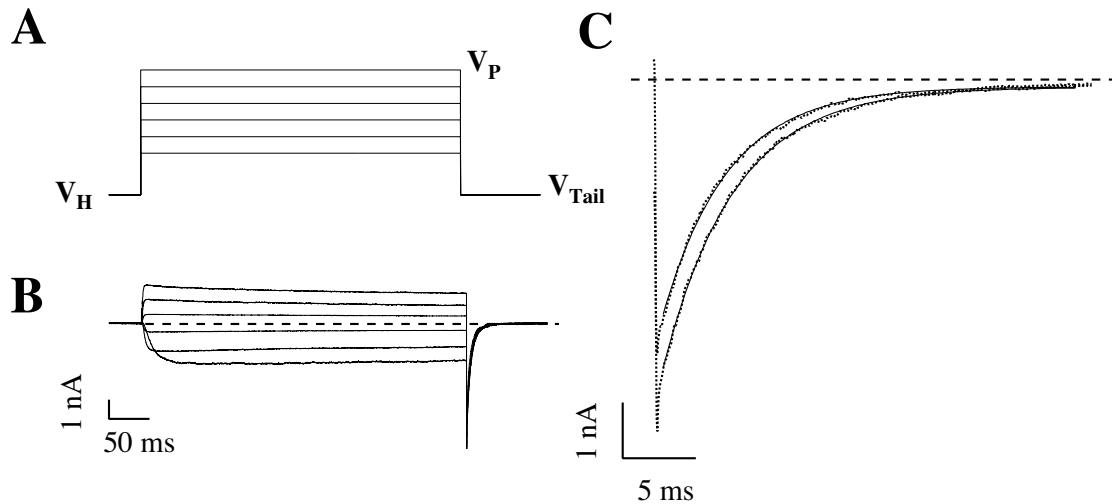


**Figure 2.4 IV protocol** **A)** Starting from the holding potential depolarizing pulses with a duration of 400 ms are applied.  $V_H$ ,  $V_P$  and  $V_{Tail}$  indicate respectively the holding, the test and the tail potentials. **B)** Current responses to the protocol of panel A (with  $V_H = V_{Tail} = -100$  mV,  $V_P$  from  $-50$  mV, every 20 mV) recorded in an *outside-out* patch experiment in symmetrical 115 mM KCl ( $V_{Rev} = 0$  mV). **C)** The deactivation during the step repolarization at  $V_{Tail} = -100$  mV can be fitted by a single exponential.

### 2.5.1 IV-protocol

The IV protocol can be used to evaluate the activation curve of the ion channels under investigation. This protocol was used to study the voltage dependence of the toxin binding. Starting from the holding potential we applied depolarizing pulses from a potential between  $-80$  and  $-60$  mV and up to  $+60$  or  $+80$  mV (fig 2.4). The duration of these pulses was between 40 and 500 ms, depending on the time necessary for the reequilibration of the toxin binding to open channels. This process was faster at high depolarizing potentials and depends also on the composition of the solutions.

The current amplitude elicited by the voltage pulse depends on the number of channels, the open probability of the channels and on the driving force of the permeating ion. When the driving force was small it was not possible to compare the control and the toxin traces. Therefore we evaluated the current at potentials where the driving force was big enough to result in currents amplitudes which could be analyzed (fig 2.4). The currents elicited by the tail potential,  $V_{Tail}$ , were proportional to the steady state current, elicited by  $V_P$ , through the factor  $C = (V_{Tail} - V_{Rev}) / (V_P - V_{Rev})$ . The factor  $C$  depended on the applied potential, but was the same in control and with toxin, therefore this scaling factor was cancelled in the evaluation of the dissociation constant,  $K_D$ , or the unblock probability. In addition the instantaneous tail current was proportional to the open probability at all potentials and therefore could be used to evaluate the activation curve. The activation could be characterized by a Boltzmann fit with the two parameters  $V_{1/2}$ , the potential at which half of the channels



were open, and the e-fold slope  $s$ , that gave an estimate of the steepness of the dependence of the open probability on the voltage:

$$I_{\text{Tail}} \propto \frac{1}{1 + e^{\left(-\frac{V - V_{1/2}}{s}\right)}} \quad \text{eq. 2.1}$$

To evaluate the instantaneous tail current, the deactivating current was fitted with a single exponential and extrapolated to the time of the beginning of the pulse plus the delay due to the filter (200  $\mu\text{s}$ ). The first 5 – 15 points were skipped from the fit to avoid errors from capacitive compensation artifacts.

In some experiments the analysis of the tail currents was not possible because they were contaminated by chloride currents endogenously present in oocytes (Takahashi et al. 1987).

### 2.5.2 Variable prepulse duration tail protocol

For small steady state currents it was not possible to obtain the kinetics of the toxin binding relaxation process from the IV protocol. Alternatively, we applied a pulse of variable duration, between 5 and 200 ms, at the potential at which we wanted to measure the relaxation process and we estimated the current, measuring it at a potential (typically  $-100$ ,  $-70$  mV) where the driving force was considerably larger (fig 2.5).

This evaluation was not so precise as performing a calculation of current ratio in the absence and presence of the toxin, because much less points were available. For control measurements we tested some potentials at which the ratios were also available and the results were in good agreement. To evaluate the instantaneous tail current we used the same procedure explained in the previous paragraph.

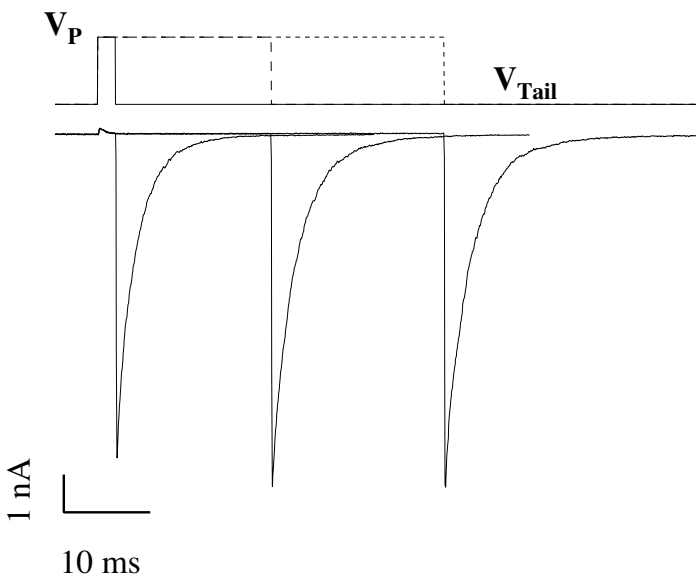


**Figure 2.5 Tail protocol with variable prepulse duration** Pulse of variable duration,  $T_P$ , between 2 and 200 ms (shown 2, 20 and 40 ms), at  $V_P$  (+ 60 mV) is followed by a repolarization at  $V_{\text{Tail}}$  ( $-100$  mV, typically between  $-100$  and  $-70$  mV). The deactivation during the repolarization (bottom) can be fitted by a single exponential and the instantaneous tail current is evaluated by extrapolating the fit at the time of the repolarization plus the delay due to the filter (200  $\mu\text{s}$ ).

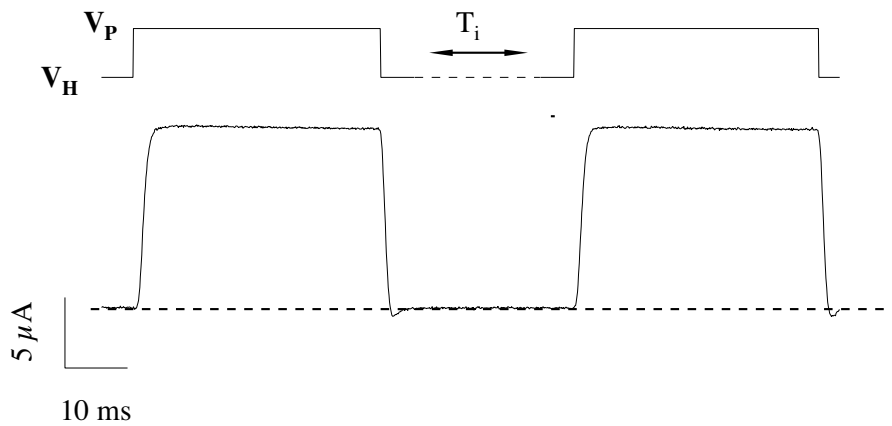


**Figure 2.6 Double pulse protocol** Two identical voltage steps are separated by a variable interpulse at  $V_H$  (top). The bottom panel shows the current responses elicited by the double pulse protocol for  $V_P = +40$  mV and  $T_i = 30$  ms.

### 2.5.3 Double pulse protocol

To measure the kinetics of  $\kappa$ -PVIIA-binding to closed channels we used a double pulse protocol. Two identical voltage steps ( $V_P$  typically  $+40$  mV or  $-30$  mV), separated by an increase time interval (between 5 ms and 6 s) at holding potential were used to test at different times the after-pulse re-equilibration of  $\kappa$ -PVIIA-binding to closed channels (fig 2.6).

### 2.5.4 Data analysis

Off-line analysis was performed with a Macintosh G3 microcomputer (Apple, Cupertino, CA, U.S.A.) with self-written programs in the Igor (Wavemetrics, Lake Oswego, OR) environment.

### 2.5.5 Leakage

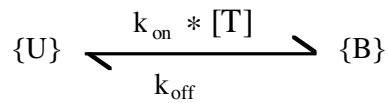
We subtracted the contribution of passive currents with a standard P/n protocol (Heinemann 1995): in a voltage range where voltage dependent channels are not active a scaled down version of the pulse protocol is applied  $n$  times and the resulting current is averaged, scaled and subtracted from that elicited by the main test pulse. We used a scaling factor of 0.25 and we averaged four or eight leak responses to decrease the noise. In patch experiments sometimes the activity of stretch-activated channels which are present in oocyte membranes produced high noise in the leakage traces, due to the high conductance of these endogenous channels (about 40 pS; Taglietti and Toselli 1988; Yang and Sachs 1989; 1990). In these experiments we subtracted the leakage off-line, using a weighted average of the recorded leak traces. The weight of each trace  $I_i^j$  was proportional to the square of the stimulation potential  $\Delta V_p^i$ :

$$\frac{\partial I_1(t)}{\partial V} = \frac{\sum (\Delta V_P^i)^2 (I_1^i(t) / \Delta V_P^i)}{\sum (\Delta V_P^i)^2} = \frac{\sum \Delta V_P^i \cdot I_1^i(t)}{\sum (\Delta V_P^i)^2} \quad \text{eq. 2.2}$$

Therefore the correction to a stimulus of amplitude  $\Delta V_P$  was made by subtracting the new leakage as  $(\partial I_1(t) / \partial V) \cdot \Delta V_P$ .

## 2.6 Kinetic analysis

To interpret the experimental data we used a simple bimolecular reaction scheme to describe the interaction between the toxin and the channel, schematized by



**Scheme 2.1**

where  $\{U\}$  represents the toxin-free channels and  $\{B\}$  the channels bound to a toxin molecule. The transition rates are the product of the second order dissociation constant and the toxin concentration,  $k_{\text{on}} [T]$ , and the dissociation constant,  $k_{\text{off}}$ .

Since we could demonstrate that the toxin binding to the channel molecule is a bimolecular reaction (see results) we could make some predictions about the binding process:

1) Following a step-like perturbation,  $U(t)$  should follow a single-exponential relaxation from the resting value ( $U_0$ ) towards the equilibrium value set by the new binding conditions ( $U_\infty$ ):

$$U(t) = (U_0 - U_\infty) \cdot e^{-t/\tau} + U_\infty \quad \text{eq. 2.3}$$

The parameters  $\tau$  and  $U_\infty$ , experimentally measurable, are related to the kinetic parameters in scheme1 and to the toxin concentration.

2) Both for open and closed channels the resting unblock probabilities,  $U^O$  and  $U^C$ , depend on the toxin concentration,  $[T]$ , following a simple Langmuir isotherm, where  $K_D$  is the equilibrium dissociation constant ( $K^O$  for open and  $K^C$  for closed channels)

$$U_\infty = \frac{k_{\text{off}}}{k_{\text{off}} + k_{\text{on}} \cdot [T]} = \frac{1}{1 + [T]/K_D} \quad \text{eq. 2.4}$$

$$\text{with } K_D = k_{\text{off}} / k_{\text{on}} \quad \text{eq. 2.5}$$

3) A third expectation is that the time constant of the relaxation  $\tau$  should depend on  $[T]$  according to

$$\tau = \frac{1}{k_{\text{off}} + k_{\text{on}} \cdot [T]} \quad \text{eq. 2.6}$$

Therefore at any given toxin concentration it is possible to evaluate  $K_D$ ,  $k_{\text{off}}$  and  $k_{\text{on}}$  from  $U$  and  $\tau$  according to the inverse relationships:

$$K_D = \frac{[T] \cdot U}{1 - U}; \quad k_{\text{off}} = \frac{U}{\tau}; \quad k_{\text{on}} = \frac{1 - U}{[T] \cdot \tau} \quad \text{eq. 2.7}$$

We used a step-like voltage perturbation and a double pulse protocol to evaluate open-channel and closed-channel kinetic parameters, respectively  $K^O$ ,  $k_{\text{off}}^O$ ,  $k_{\text{on}}^O$  and  $K^C$ ,  $k_{\text{off}}^C$ ,  $k_{\text{on}}^C$ .

## 3 Results

$\kappa$ -conotoxin PVIIA blocks *Shaker* mediated potassium currents. We studied the mechanism of inhibition for the *Shaker* wild type (*Shaker-wt*) channel (Tempel et al. 1987) and for the deletion mutant *Shaker-Δ6-46* (*Shaker-Δ*) that lacks fast N-type inactivation (Hoshi et al. 1990). For the *Shaker-Δ6-46* channel the dependence on the ionic composition of the extra- and intracellular solutions was investigated.

### 3.1 $\kappa$ -PVIIA block in extracellular NFR

#### 3.1.1 *Shaker-wt*

Fig. 3.1A shows superimposed current responses to three different step depolarizations, recorded with the two electrode voltage clamp technique (TEVC) from an oocyte expressing *Shaker-wt* potassium channels before and after the addition to the bath of 500 nM- $\kappa$ -PVIIA. Each stimulation consisted of a test pulse  $V_p$ , equal to -10, +10 and +30 mV, starting from an holding potential  $V_H = -100$  mV.

All the peak amplitudes are reduced about ten-fold under toxin, corresponding to a dissociation constant of  $\kappa$ -PVIIA-block of about 50 nM. Additionally a closer inspection of the curves reveals that the time course of the current is sensibly modified. When the toxin trace is scaled to control at the peak (fig. 3.1C), the steady state current is clearly less blocked than the current at the peak. The ratio,  $I_{Tx}/I_{Ct}$  of toxin to control responses increases after the time to peak, approaching a late steady-state value that is about 3 times larger at  $V_p = +30$  mV (fig. 3.1B). Although this effect develops during the onset of inactivation, it cannot be attributed to an unblock of inactivated channels because it increases strongly with  $V_p$  in a range where the steady-state probability and the time constant of inactivation are fairly constant, respectively  $\sim 0.9$  and  $\sim 3.5$  ms. The solid lines in fig. 3.1B are single-exponential fits of  $U(t) = I_{Tx} / I_{Ct}$  yielding asymptotic values that increase from 0.19 at  $V_p = -10$  mV to 0.30 at  $V_p = +30$  mV, while the time constants decrease from 70 ms to 8 ms. The fitted asymptotic values of  $U(t)$  can be used to estimate an apparent dissociation constant,  $K_{app}^O$ , of  $\kappa$ -PVIIA-binding to open (non-inactivated) channels.  $K_{app}^O$  estimates in the voltage range of -20 to +60 mV were fairly well fitted by a single exponential,  $K_{app}^O(V) = K_{app}^O(0) \cdot \exp(V/v_S)$ , with  $K_{app}^O(0) = 115$  nM and  $v_S = 45$  mV (squares in fig. 3.1F). We performed the same experiments with the patch clamp technique in the *outside-out* configuration and no significant difference was observed.

Mean values of  $K_{app}^O(0)$  and  $v_S$  from several experiments in different oocytes tested with the TEVC or patch clamp technique are reported in table 3.1. Due to inactivation the amount of

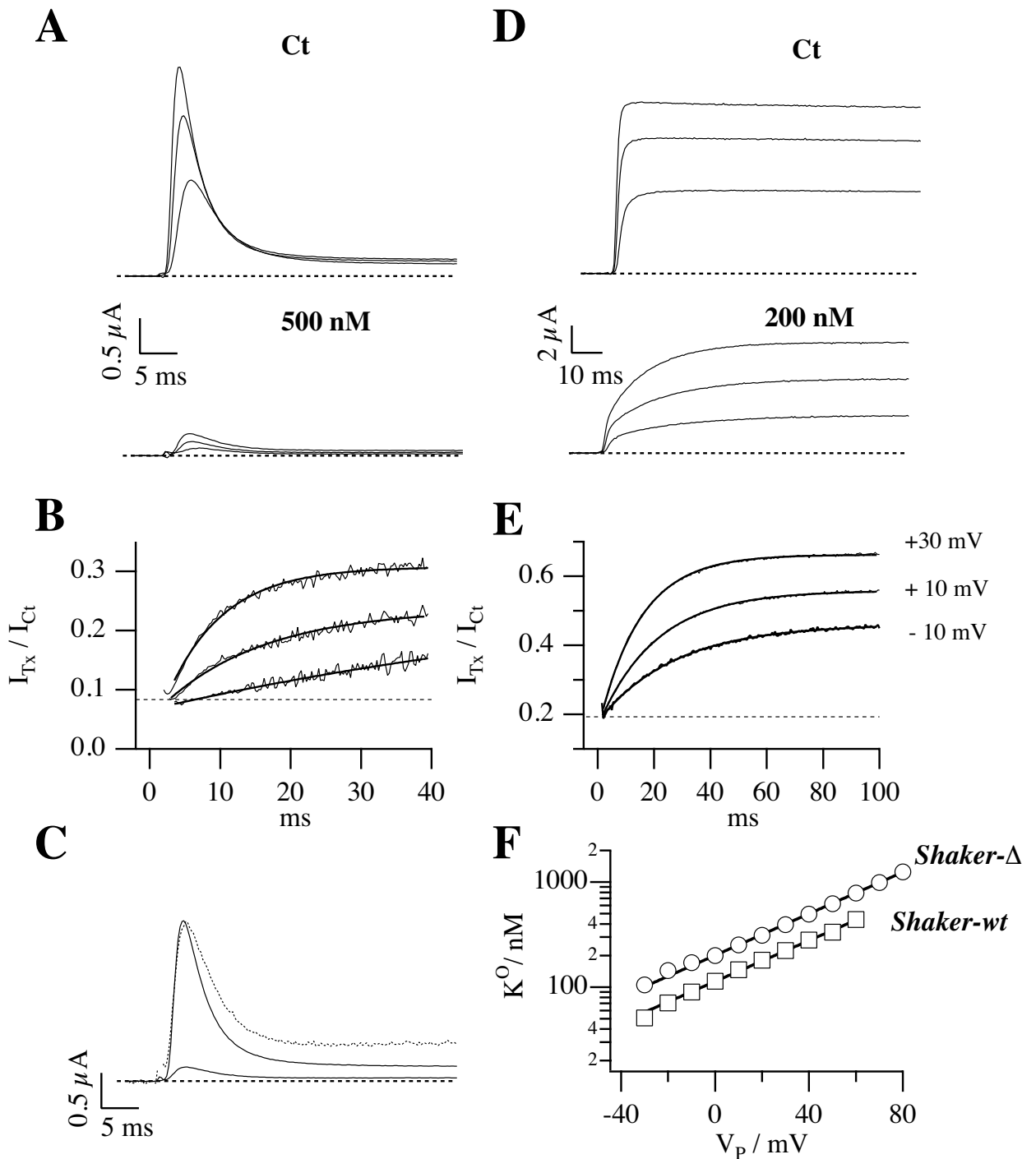


**Figure 3.1 Effect of  $\kappa$ -PVIIA on *Shaker-wt* and *Shaker- $\Delta$*  currents in NFR. **A and D**) Superimposed records of voltage-clamp currents mediated by the *Shaker-wt* (**A**) and *Shaker- $\Delta$*  (**D**) channels before (top) and after (bottom) the addition to the bath of 500 nM and 200 nM  $\kappa$ -PVIIA respectively ( $V_H = -100$  mV;  $V_P = -10, +10, +30$  mV). **B and E**) Toxin to control current ratios for the same voltage steps as in panels A and D. The increase in the fraction of unblocked channels is well fitted by a single exponential (smooth lines) with a plateau level increasing with the test voltage. The dotted line indicates the unblock probability at  $V_H$ , yielding to a dissociation constant of the toxin for the closed channels,  $K^C$ , of 43 nM for *Shaker-wt* (**B**) and of 47 nM for *Shaker- $\Delta$*  (**D**). **C**) Currents mediated by the *Shaker-wt*  $K^+$ -channel at  $V_P = +10$  mV as in panel A. The dotted line represents the toxin peak current scaled to the control by a factor of 11. The steady state current is much less blocked. **F**) Semi-logarithmic plot of the dissociation constants estimated from the experiments of panels A (squares) and D (circles). The straight lines are best fits with the equations  $K^O_{app}/\text{nM} = 115 \cdot \exp(V/45 \text{ mV})$  for *Shaker-wt*, and  $K^O/\text{nM} = 201 \cdot \exp(V/44 \text{ mV})$  for *Shaker- $\Delta$* . (Modified from Terlau et al. 1999).**

steady state current is only about 10% of the peak current value. In patch clamp experiments such a low amplitude does not allow to evaluate easily the steady state block or to perform a kinetic analysis.

### 3.1.2 *Shaker-Δ6-46*

The study of the deletion mutant *Shaker-Δ6-46* shows how the inactivation process masked the toxin effect in *Shaker-wt* channels. The currents mediated by *Shaker-Δ6-46* channels appear strongly modified in the shape by the presence of partially blocking concentrations of extracellular  $\kappa$ -PVIIA. Fig. 3.1D shows currents obtained from TEVC recordings, for step depolarizations to -10, +10 and +30 mV recorded from an oocyte expressing *Shaker-Δ6-46* channels before and after addition of 200 nM- $\kappa$ -PVIIA to the bath. The toxin strongly reduces the current in the early phase, but has much less effect on the steady state. The currents measured in presence of toxin at the half-activation time of the control responses are reduced five times at all voltages. This indicates a  $\kappa$ -PVIIA dissociation constant for the closed channel of ~50 nM for the voltage clamp experiment in fig. 3.1D. These values are close to the estimates obtained previously from the reduction of peak currents in *Shaker-wt* channels. However, this early reduction diminishes during the pulse, and the currents approach asymptotic values that are progressively closer to the toxin-free levels at increasing depolarizations.

These effects can be explained by assuming that  $\kappa$ -PVIIA-binding blocks pore conduction without modifying substantially channel gating and that the channel opening reduces the toxin-binding affinity triggering a re-equilibration towards a lower block probability. This interpretation can be tested by looking if the predictions of a simple second-order reaction for channel-toxin association are fulfilled (see section 2.6).

Fig. 3.2 illustrates a voltage clamp experiment in which the toxin concentration, [T], was changed progressively from 0 to 10, 20, 50, 100, 200, 500 nM, 1  $\mu$ M, and back to 0. At each [T] a standard series of IV responses to various pulse potentials,  $V_p$ , was recorded with 5 s intervals. Fig. 3.2A shows the [T]-dependence of the responses to  $V_p = +20$  mV. Note that the current trace obtained after washing-out the solution containing 1  $\mu$ M  $\kappa$ -PVIIA shows a small "run-up" of the currents and a very small residual unblock that we attribute to the remaining presence of few nM  $\kappa$ -PVIIA around the oocyte. A simple bimolecular interaction would imply a single-exponential relaxation from the resting value towards the equilibrium values for  $U(t)$ , given by the ratio point by point of the toxin trace with the control. Fig. 3.1E shows this property for sample voltage steps to -10, +10, and +30 mV. The smooth lines represent single exponential fits of  $U(t) = I_{Tx}/I_{Ct}$  for the given test potentials which rise from the same

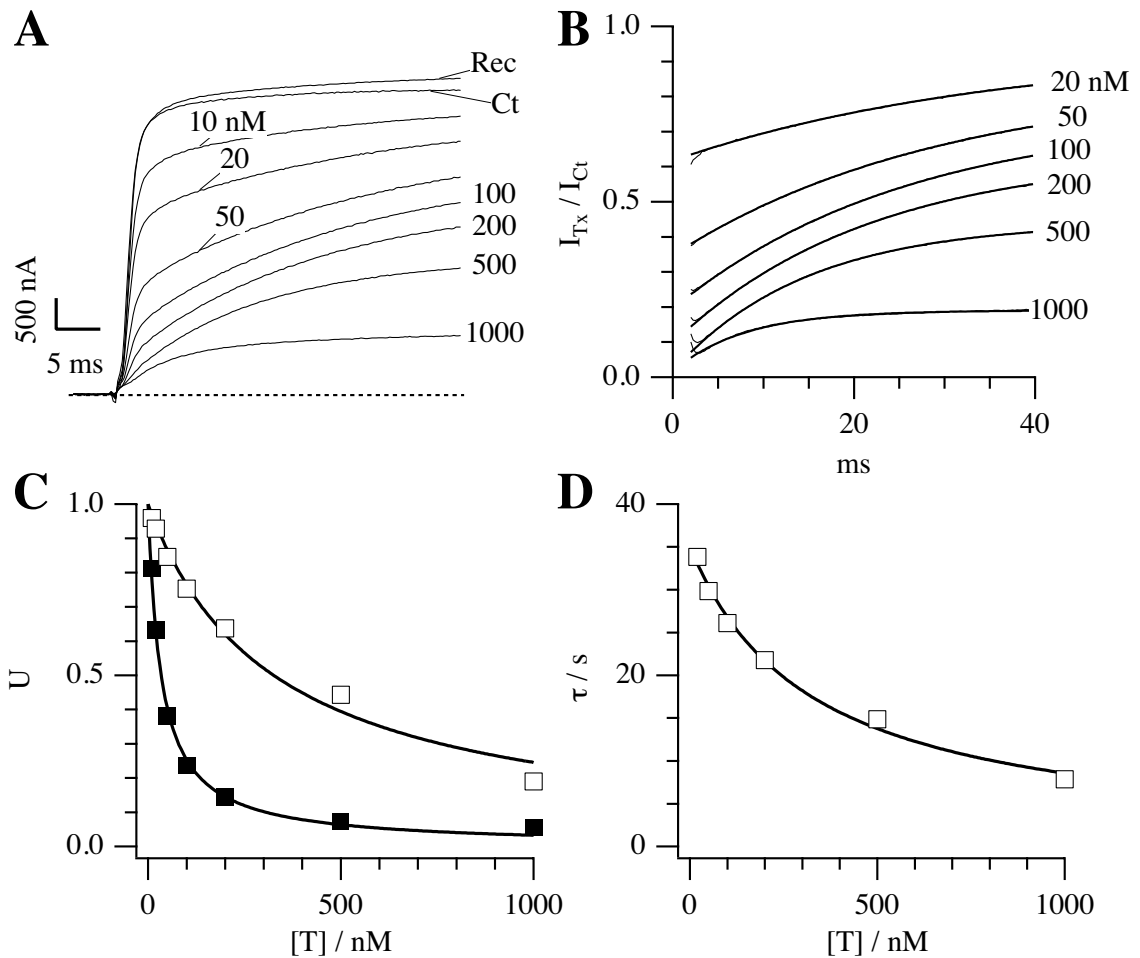


**Figure 3.2 Dose-response of  $\kappa$ -PVIIA effects on *Shaker- $\Delta$*  channels.** **A)** Voltage-clamp currents mediated by the *Shaker- $\Delta$*   $K^+$  channel for  $V_p=+20$  mV from  $V_H= -100$  mV recorded from the same oocyte exposed to increasing values of  $[T]$ . The trace marked "Rec" was recorded after washing-out the  $1 \mu\text{M}$ -PVIIA solution; notice a small "run-up" and a residual slow unblock indicating that few nM- $\kappa$ -PVIIA are still present around the oocyte. **B)** Ratios of the toxin to control currents in panel A; single-exponential fits (smooth lines) are indistinguishable from the data for times bigger than 1 ms; departures at earlier times are likely due to inadequate voltage-step control. **C)**  $[T]$ -dependence of the extrapolated values of the  $U(t)= I_{Tx} / I_{Ct}$  data in panel B at time 0 plus filter delay ( $U^C$ , black squares) and for  $t \rightarrow \infty$  ( $U^O$ , white squares); the solid lines are best fits with eq. 2.4, with respectively  $K^C = 36$  nM and  $K^O = 330$  nM. **D)**  $[T]$ -dependence of the time constant  $\tau$  of the exponential fits in panel B; the solid line is the best fit with eq. 2.6; the fitted parameters are  $k_{off}^O = 29 \text{ s}^{-1}$  and  $k_{on}^O = 88 \mu\text{M}^{-1}\text{s}^{-1}$ ; the ratio  $k_{off}^O / k_{on}^O$  coincides with  $K^O= 330$  nM from the fit of  $U^C$  data in panel C. (Modified from Terlau et al. 1999).

initial value,  $U^C \sim 0.19$  towards asymptotic values  $U^O$  with time constants,  $\tau$ , that depend on the test potential. For  $V_p \geq -20$  mV the open-channel probability is close to its maximum and  $\tau$  is always much larger than the half-activation time of normal currents. Therefore, these relaxations develop almost exclusively while the channels are fully activated and open (indicated by the use of the superscript O for the parameters that characterize them; the superscript C refers to the close channels). We expect that the equilibration process accelerates for increasing toxin concentrations according to the eq. 2.6 that allows an evaluation of  $k_{off}^O$  and  $k_{on}^O$ . Estimates of  $\tau$  from the single exponential fits of fig. 3.2B are plotted as a function of  $[T]$  in fig. 3.2D. The solid line is the least-squares fit of the data



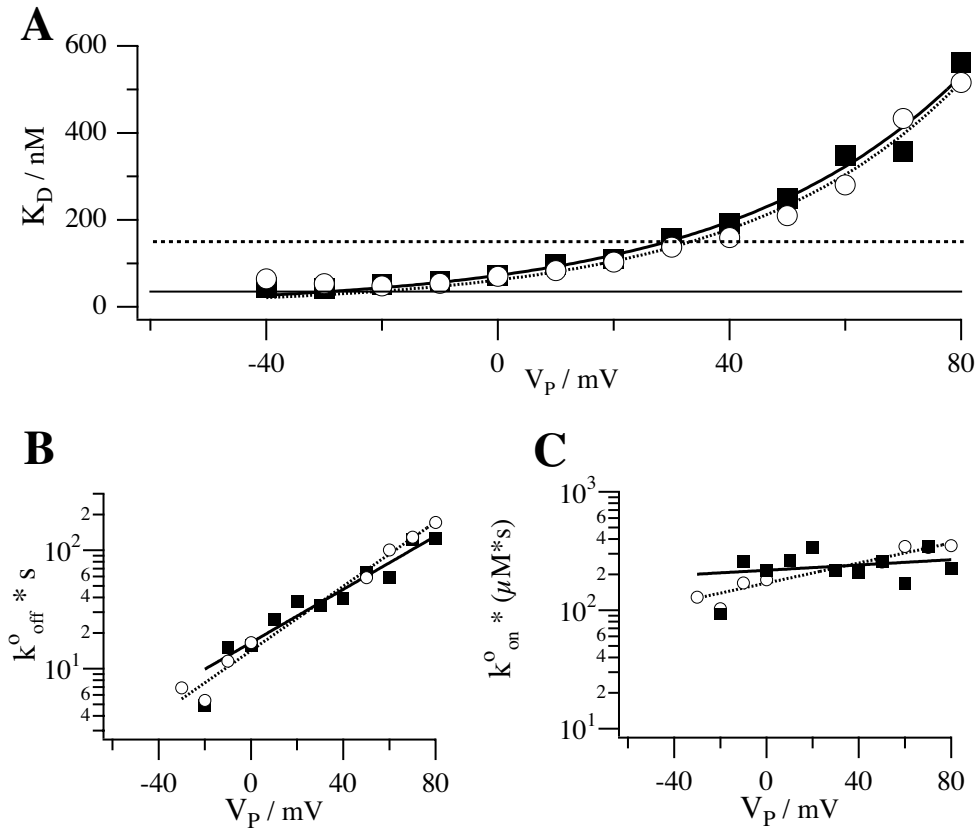


**Figure 3.3 Voltage dependence of  $\kappa$ -PVIIA-binding to open *Shaker-Δ*channels.** **A)** Plot of the dissociation constant vs the applied potential for a patch experiment performed in external NFR (■) and a similar experiment in high  $[K]_O$  (○), with  $[K]_I = 115$  mM, shown in fig. 3.7. The best exponential fits correspond to  $K^O$  /nM =  $72 \cdot \exp(V/40\text{mV})$  in NFR (continuous line) and  $K^O$ /nM =  $62 \cdot \exp(V/38\text{mV})$  in high  $[K]_O$  (dotted line). The horizontal lines correspond to the closed state dissociation constant,  $K^C$ , 35 nM in NFR (continuous line) and 150 nM (dotted line) in high  $[K]_O$ . **B and C)** Semi-logarithmic plot of the estimates of the first-order dissociation rate constant (**B**) and of the second-order association rate constant (**C**) for the same patch experiment shown in panel A. The straight lines are best fits in panel B with the equations  $k_{off}^O \cdot s = 17 \cdot \exp(V/39 \text{ mV})$  in NFR (continuous line) and  $k_{off}^O \cdot s = 14 \cdot \exp(V/32 \text{ mV})$  in high  $[K]_O$  (dotted line) and in panel C with  $k_{on}^O \cdot s = 217 \cdot \exp(V/391 \text{ mV})$  in NFR (continuous line) and  $k_{on}^O \cdot s = 169 \cdot \exp(V/102 \text{ mV})$  in high  $[K]_O$  (dotted line). Because of the shallower voltage dependence of the second-order association rate constant, the experimental data can be described by the mean values  $k_{on}^O \cdot (\mu M \cdot s) = 232$  in NFR and 234 in high  $[K]_O$ .

according to the expression 2.6. Furthermore for a bimolecular reaction we expect that the closed and open state equilibrium unblock probability, respectively  $U^C$  and  $U^O$ , depend on the toxin concentration,  $[T]$ , following simple Langmuir isotherms (eq. 2.4). In fig 3.2C we plotted  $U$  vs  $[T]$  both for closed and open channels and we could evaluate the dissociation constants characterizing the equilibrium binding of  $\kappa$ -PVIIA to resting (closed) or to activated (open) channels,  $K^C$  and  $K^O$  respectively. The solid lines show that the data are indeed well fitted by Langmuir isotherms, yielding in this case  $K^C = 36$  nM and  $K^O = 330$  nM (at  $V_P = +20$  mV).

Finally we expect a simple relationship between the estimates of  $k_{off}^O$  and  $k_{on}^O$  from the above fit of the  $[T]$ -dependence of  $\tau$  and the equilibrium dissociation constant  $K^O$  estimated from the fit of  $U^O$  data, according to the expression 2.5. The values of  $k_{off}^O$  and  $k_{on}^O$  fitting the  $\tau$  data of

fig. 3.2D, respectively  $29 \text{ s}^{-1}$  and  $88 \mu\text{M}^{-1} \text{ s}^{-1}$ , yield the same estimate of  $K^O \sim 330 \text{ nM}$  as the fit of the  $U^O$  data of fig. 3.2C. This analysis shows that the interaction of  $\kappa$ -PVIIA with the pore region of the *Shaker*  $K^+$  channel is indeed a bimolecular reaction.

In most experiments only two toxin concentrations were tested on the same oocyte or experiments were done for a single  $[T]$  value in the range of 100 to 800 nM. The consistency of the results of these experiments with the bimolecular character of the toxin-block reaction was shown indirectly by the agreement of the estimates of  $K^O$ ,  $k_{\text{off}}^O$  and  $k_{\text{on}}^O$  obtained from single measurements of  $U^O$  and  $\tau^O$  at any given condition according to the inverse relationships given in eq. 2.7.

The most interesting feature of  $\kappa$ -PVIIA block relaxations is their strong voltage dependence. Fig 3.3 shows, for a patch experiment performed with 115 mM KCl in the pipette and NFR in the bath (white circles), the dependence on  $V_P$  of  $K^O$ ,  $k_{\text{off}}^O$  and  $k_{\text{on}}^O$ , evaluated from  $U^O$  and  $\tau^O$  according to eq. 2.4 and 2.6. Both  $k_{\text{off}}^O$  and  $K^O$  increase with voltage according to a simple exponential law (see panel A and B). The continuous lines fitting the plots of  $K^O$  and  $k_{\text{off}}^O$  were drawn according to the expressions:  $K^O(V)=K^O(0)\cdot\exp(V/v_S)$ , ( $K^O(0)=72\text{nM}$ ;  $v_S=40\text{mV}$ ) and  $k_{\text{off}}^O(V)=k_{\text{off}}^O(0)\cdot\exp(V/v_S)$ , ( $k_{\text{off}}^O(0)=16.6 \text{ s}^{-1}$ ;  $v_S= 32 \text{ mV}$ ).

Consistently  $k_{\text{on}}^O$  has no systematic trend for different test potentials with a mean value of  $232 \text{ s}^{-1}\mu\text{M}^{-1}$  as illustrated in fig.3.3C. Mean values of  $k_{\text{on}}^O$ ,  $k_{\text{off}}^O(0)$ ,  $K^O(0)$ , and  $v_S$  for experiments performed with either TEVC or patch clamp technique are given in table 3.1.

Fig. 3.1F shows a plot of  $K^O$  for the experiment in fig3.1D compared to the apparent dissociation constant,  $K_{\text{app}}^O$ , estimated for the *Shaker-wt* channels in fig 3.1A.  $K_{\text{app}}^O$  is systematically lower than  $K^O$ , indicating that the reduction of toxin-block occurs in the open state. Thus the effect is strongly reduced if the channels visit frequently and for relatively long periods the inactivated (closed) state.

Type	open channel block					closed channel block		
	$[K]_o$ mM	$K^O(0)$ nM	$v_s$ mV	$k_{\text{on}}^O$ $\mu\text{M}^{-1} \text{ s}^{-1}$	$k_{\text{off}}^O(0)$ $\text{s}^{-1}$	$K^C$ nM	$k_{\text{on}}^C$ $\mu\text{M}^{-1} \text{ s}^{-1}$	$k_{\text{off}}^C$ $\text{s}^{-1}$
<i>Sh-wt</i>	2.5	$125 \pm 30$	$46 \pm 10$	-	-	$49 \pm 23$	$22 \pm 5$	$1.3 \pm 0.4$
<i>Sh-wt</i>	115 #	-	-	-	-	$177 \pm 52$	-	-
<i>Sh-Δ</i>	2.5	$137 \pm 64$	$37 \pm 6$	$176 \pm 82$	$22 \pm 9$	$37 \pm 16$	$23 \pm 7$	$1.0 \pm 0.3$
<i>Sh-Δ</i>	115	$181 \pm 125$	$39 \pm 5$	$130 \pm 69$	$22 \pm 9$	$265 \pm 106$	$2.6 \pm 0.9$	$0.6 \pm 0.2$

**Table 3.1 Parameters of  $\kappa$ -PVIIA-binding to open and closed states of *Shaker* channels.**

Mean values ( $\pm$  SD) over a set of experiment performed either with voltage or patch clamp technique, number of experiments  $\geq 4$  for *Shaker-wt* and 12 for *Shaker-Δ*.

# experiments performed with  $20 \leq [K]_i \leq 115 \text{ mM}$ , resulting in the same  $K^C$  (section 3.5.2).

### 3.1.3 Closed-channel block: *Shaker-Δ6-46*

For voltage activated  $K^+$  channels it has been demonstrated that the conformational change that closes the channel does not involve the extracellular mouth of the pore (Perozo et al. 1999). Our measurements indicate that  $\kappa$ -PVIIA as a pore blocker has free access to the site of block also when the channels are closed during resting hyperpolarizations. The dissociation constant of  $\kappa$ -PVIIA binding to closed channels,  $K^C$ , can be measured by the reduction of the early responses to pulse stimulations under resting conditions with [T]. Our estimates of  $K^C$  in NFR were not significantly different for *Shaker-wt* or *Shaker-Δ* channels (table 3.1). The kinetics of  $\kappa$ -PVIIA binding to closed channels can be measured with a double pulse protocol, shown in fig. 2.6. With such a protocol we test the re-equilibration of the binding to closed channels at different times after the first pulse: the second response in toxin reveals a long memory of the effects induced by the first pulse as shown by the different activation speed, while in control the responses are virtually identical.

Typically a double pulse experiment consisted of two successive pulses of 40 ms to +40 mV separated by a resting period,  $T_i$ , at  $-100$  mV of variable duration (pulse protocol fig. 2.6; *outside-out* patch experiment fig. 3.4). Panel A shows the responses for  $T_i = 8, 128$  and 1024

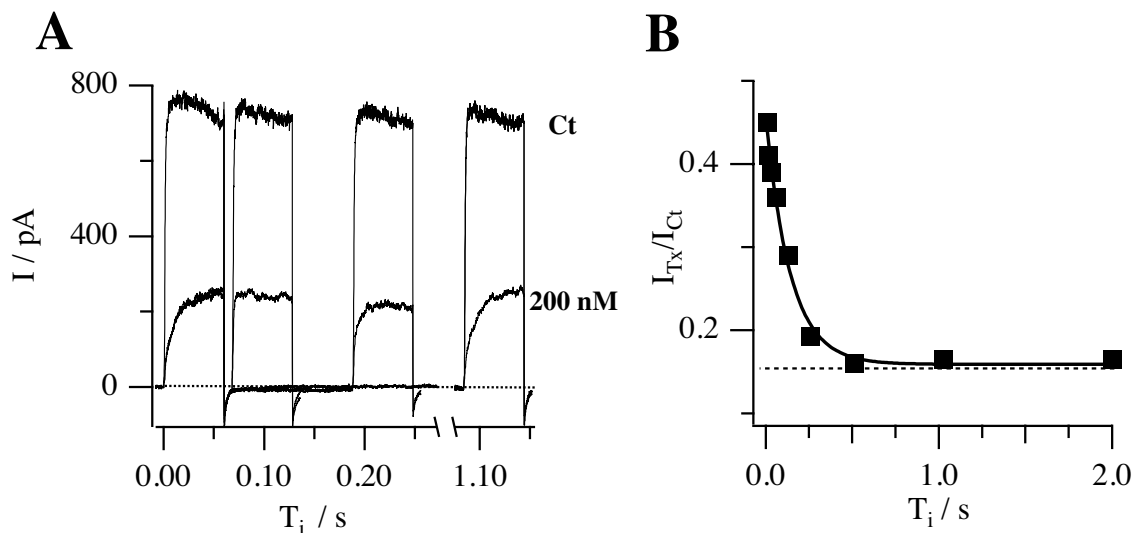


**Figure 3.4 Relaxation of  $\kappa$ -PVIIA-binding to closed *Shaker-Δ* channels after a depolarizing pulse. A)** Superimposed records of responses to double pulse stimulation before and after the addition of 200 nM  $\kappa$ -PVIIA to the NFR-bath. Each stimulation consisted of a conditioning 60-ms pulse to +40 mV, followed by an identical test pulse with a variable pulse interval,  $T_i$  (shown 8, 128 and 1024 ms) at  $V_H = -100$  mV. **B)** Amplitude of the second response at the half activation time of control normalized to the control response and plotted as a function of  $T_i$ . The continuous line is the best exponential fit with  $\tau = 143$  ms and the dotted horizontal line corresponds to the asymptotic value of  $I_{Tx}/I_{Ct}$ ,  $U^C = 0.16$ , giving  $K^C = 38$  nM. From  $\tau$  and  $U$  from eq. 2.6 we estimate  $k_{off}^C = 1.1$  and  $k_{on}^C (\mu M \cdot s) = 39$ .

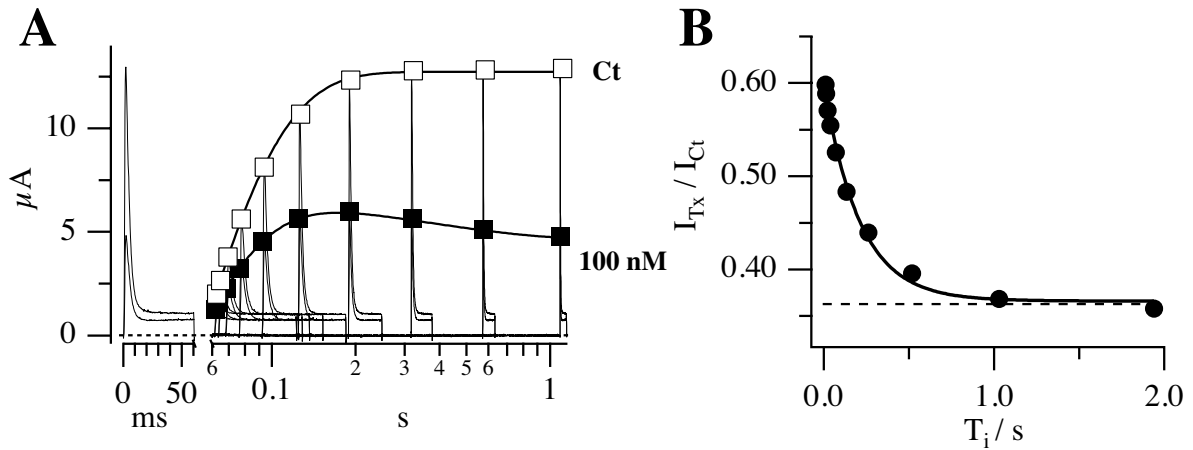


**Figure 3.5 Relaxation of  $\kappa$ -PVIIA-binding to closed Shaker-wt channels after a depolarizing pulse.** **A)** Superimposed records of responses to double pulse stimulation before and after the addition of 100 nM  $\kappa$ -PVIIA to the NFR-bath. Each stimulation consisted of a conditioning 60-ms pulse to 40 mV, followed by an identical test pulse with a variable pulse interval,  $T_i$  (shown between 6 ms and 1 s). The amplitude of the peak current in control ( $\square$ ) and in toxin ( $\blacksquare$ ) is superimposed to the current records. The continuous lines represent in control the single and in toxin the double exponential fit with time constants 36 ms and 29, 360 ms respectively. **B)** Amplitude of the second response at the peak in toxin normalized to the control response and plotted as a function of  $T_i$ . The continuous line is the best exponential fit with  $\tau = 211$  ms and the dotted horizontal line corresponds to the asymptotic value of  $I_{Tx}/I_{Ct}$ ,  $U^C = 0.37$ , giving  $K^C = 59$  nM. From  $\tau$  and  $U$  from eq. 2.6 we estimate  $k_{off}^C \cdot s = 1.7$  and  $k_{on}^C \cdot (\mu M \cdot s) = 30$ .

ms, recorded before and after the addition of 200 nM  $\kappa$ -PVIIA to the extracellular NFR solution. For short interpulses the second response is dominated by a fast rising phase as in the toxin-free response, and its "tonic" characteristics are not fully recovered even after 100 ms. In panel B of fig. 3.4, the ratio of the early currents elicited by the second pulse in toxin and in control, i.e. the fraction of toxin-free channels at the time of onset of the second pulse is plotted as a function of  $T_i$ . This ratio decays with  $T_i$  as a single exponential,  $\tau = 143$  ms, from a starting value of 0.45, close to the toxin-free probability of open channels at the end of the conditioning pulse, up to the steady state value corresponding to the block of closed channels ( $U^C = 0.16 \rightarrow K^C = 38$  nM). We interpret this phenomenon by a relatively slow re-equilibration of  $\kappa$ -PVIIA binding to closed channels. According to eq. 2.7 the association and dissociation rate constants of  $\kappa$ -PVIIA binding to closed channels,  $k_{on}^C$  and  $k_{off}^C$ , can be estimated. From the experiment of fig. 3.4 we obtain:  $k_{on}^C = 39 \mu M^{-1} s^{-1}$ ,  $k_{off}^C = 1.1 s^{-1}$ ,  $K^C = 38$  nM. Mean estimates are given in table 3.1.

In two voltage clamp and one patch experiments the above double-pulse protocol was applied using variable holding potentials between -60 and -120 mV and we observed no significant change in the estimates of the binding parameters (data not shown). Thus, unlike the interaction of  $\kappa$ -PVIIA with open channels, the interaction with closed channels appears to be voltage insensitive.

### 3.1.4 Closed-channel block in NFR: *Shaker-wt*

Due to inactivation, the recovery of the tonic binding of  $\kappa$ -PVIIA to *Shaker-wt* channels after a conditioning stimulus has a biphasic behavior, as shown in fig. 3.5. The control recordings from a double-pulse protocol (fig. 2.6) follow a classical pattern showing that the second response increases with  $T_i$  as more channels recover from the inactivation produced by the conditioning pulse (white squares). The recordings with 100 nM  $\kappa$ -PVIIA added to the bath show instead an overshoot of the second response that subsides very slowly (black squares). This effect has a simple explanation if we assume that the recovery from the unblock induced by the conditioning pulse is much slower than recovery from inactivation. Consistently, as shown in panel B, the fraction of toxin-free channels, estimated from the toxin to control ratio of the second peak response, decreases monotonically with  $T_i$ . Fitting this decay towards the steady-state ratio of the first peak responses with a single exponential yields  $\tau^C = 211$  ms. Combining this estimate with that of the asymptotic toxin-free probability,  $U^C = 0.36$ , we estimate in this experiment:  $k_{\text{off}}^C = 1.6 \text{ s}^{-1}$ ,  $k_{\text{on}}^C = 21 \mu\text{M}^{-1}\text{s}^{-1}$ ,  $K^C = 78$  nM. Mean estimates of the parameters of  $\kappa$ -PVIIA binding to closed *Shaker-wt* channels are given in table 3.1. One can see that they are not significantly different from those of *Shaker-Δ6-46* channels, supporting the idea that  $\kappa$ -PVIIA does not distinguish the resting state of the two phenotypes.

## 3.2 Effect of $[K]_o$ on the binding of $\kappa$ -PVIIA

The voltage-dependence of  $\kappa$ -PVIIA dissociation from open channels is strongly reminiscent of the properties of  $\alpha$ -KTx-block of  $\text{Ca}^{2+}$ -activated potassium channels (McKinnon and Miller, 1988) or *Shaker* channels (Goldstein and Miller, 1993), which arise from the interaction of  $\alpha$ -KTx with potassium ions occupying an outer site in the channel pore. This lead us to investigate the interaction of  $\kappa$ -PVIIA with potassium ions. Thus, we studied the effect of  $\kappa$ -PVIIA on *Shaker-wt* and *Shaker-Δ6-46* channels using high extracellular concentrations of potassium ions,  $[K]_o = 115$  mM. For more reliable measurements in the voltage range of negative-resistance, characteristic of this preparation, most of the experiments were performed with excised *outside-out* patches.

### 3.2.1 *Shaker-wt*

Fig. 3.6A illustrates superimposed current records from standard IV stimulation protocols ( $V_H = -100$  mV,  $V_P$  from  $-40$  mV, every 20 mV) applied to an *outside-out* patch exposed to symmetric 115 mM- $\text{K}^+$  solutions before and after the addition to the external bath of 300 nM  $\kappa$ -PVIIA.  $\kappa$ -PVIIA blocks similarly peak inward currents and outward currents, giving an

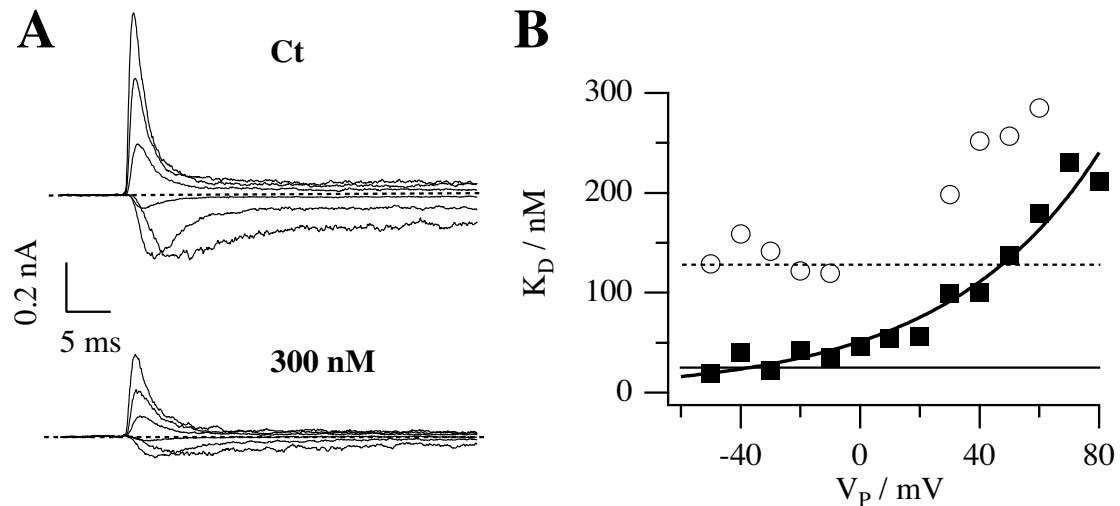


**Figure 3.6 Effect of  $\kappa$ -PVIIA on *Shaker-wt* currents in high  $[K]_O$ .** **A)** Superimposed records of currents from an *outside-out* patch clamp experiment before (top) and after (bottom) the addition to the bath of 300 nM  $\kappa$ -PVIIA ( $V_H = -100$  mV;  $V_P$  from  $-40$  to  $60$  mV in steps of  $20$  mV). The experiment was performed in symmetrical  $115$  mM KCl. **B)** Plot of the dissociation constants estimated from the experiments of panels A (○) and from a similar experiment performed with NFR in the bath (■). The continuous line corresponds to the exponential fit in NFR:  $K_{app}^O/nM = 51 \cdot \exp(V/52 \text{ mV})$ . The horizontal lines correspond to the closed state dissociation constant,  $K^C$ ,  $25$  nM in NFR and  $128$  nM in high  $K^+$ .

estimate of the closed channel dissociation constant of  $185$  nM which is about 4 times higher than the one observed with  $2.5$  mM extracellular  $K^+$  (NFR). Compared to the data recorded in external low  $[K]_O$ , the inward currents at later time points are only two times more blocked than outward currents at large depolarizations. In fig 3.6B the  $K_{app}^O$  (white circles) values for the experiment in panel A are superimposed to the  $K_{app}^O$  (black squares) values for a patch experiment recorded in NFR with toxin from the same batch to minimize errors due to the toxin preparation variations. We evaluated the  $K_{app}^O$  from the mean current between  $20$  and  $25$  ms from the application of the voltage step. At this time the equilibration to the open channels should be complete. The horizontal lines correspond to the closed channel block, evaluated at the half-activation time. We took the half activation time current instead of the peak to minimize the error introduced by the fast unblock of the toxin at depolarizing potential that introduces an apparent voltage dependence of the closed state block. The continuous horizontal line corresponds to the value  $25$  nM, obtained with  $2.5$  mM  $K^+$ , while the broken one corresponds to  $128$  nM, calculated for  $115$  mM  $K^+$ . The toxin block of the steady state currents is much more efficient in high external  $K^+$ .

### 3.2.2 *Shaker-Δ6-46*: open channel block

Fig. 3.7 illustrates a representative experiment on an *outside-out* patch exposed to symmetric  $115$  mM- $K^+$  solutions. Responses to an IV protocol ( $V_H = -100$  mV,  $V_P$  from  $-50$  mV, every  $20$  mV) before and after the addition to the external bath of  $400$  nM- $\kappa$ -PVIIA are shown. At

this concentration  $\kappa$ -PVIIA blocks most of the inward currents but has a much smaller effect on the outward currents at large depolarizations, (panel C), and by the plot of the steady state currents against the applied potential. This is consistent with the results obtained with NFR ( $[K^+]_O=2.5$  mM) in the external bath. Panel D shows a plot of the instantaneous tail current against the applied potential. In control the maximal activation is reached at  $-10$  mV and the current can be fitted with a Boltzmann curve (eq 2.1) with  $V_{1/2} = -37$  mV and  $s = 8$  mV (smooth line).

In presence of the toxin the currents increase almost linearly with the test potential, due to a bigger unblock at higher depolarizations. By interpreting as toxin-free probabilities the ratios of toxin to control for steady state currents and instantaneous tail currents, we obtain for the open-channel dissociation constant,  $K^O$ , similar estimates and the same voltage-dependence as in NFR (fig. 3.7; comparison with NFR in fig. 3.3A; mean values in table 3.1).

The comparison of the whole time course of toxin and control responses reveals that toxin-block relaxations in high  $[K]_O$  exhibit properties similar to those observed in low  $K^+$  solutions, although starting from a different resting-block equilibrium. In fact we estimate a tonic block of 27% in 400nM  $\kappa$ -PVIIA that corresponds to a  $\kappa$ -PVIIA dissociation constant of 150 nM. This value is about 4 times higher than in NFR. Fig. 3.7B shows the ratios for 4 potentials (for  $V_p = -20, +30, +60$  and  $+80$  mV). Depolarizations below  $+30$  mV produce an increased block, while above lead to unblock, as observed for all test voltages in the presence of 2.5 mM extracellular  $K^+$ . At  $+30$  mV the closed channel block is equal to the open channel block and the ratio is well fitted by a straight line. We define this potential as “inversion“ potential,  $V_{Inv}$ : it will be useful below for the comparison of the properties of toxin block at the different experimental conditions tested. The ratios are well fitted by a single exponential for an experiment performed in NFR (white circles). The dissociation rate increases exponentially with the potential with a slope of 34 mV and a value at 0 mV of  $17$  s $^{-1}$ . In this experiment the association rate shows a shallow voltage dependence: in 100 mV the association rate doubles, while the dissociation rate increases of about two orders of magnitude.

A slight voltage dependence of the association rate was observed only in some experiments and because it is much smaller than the one observed for the dissociation rate we neglected it and we considered only the mean values.

In fig. 3.3 the comparison of the data obtained in high  $K^+$  (open circles) with the experiment in NFR (filled squares) shows that both the association and dissociation rate constants of  $\kappa$ -PVIIA-binding to open channels are insensitive to changes of  $[K^+]_O$ . Mean estimates of  $k_{on}^O$ ,  $k_{off}^O(0)$ ,  $K^O(0)$ , and  $v_S$  are given in table 3.1.

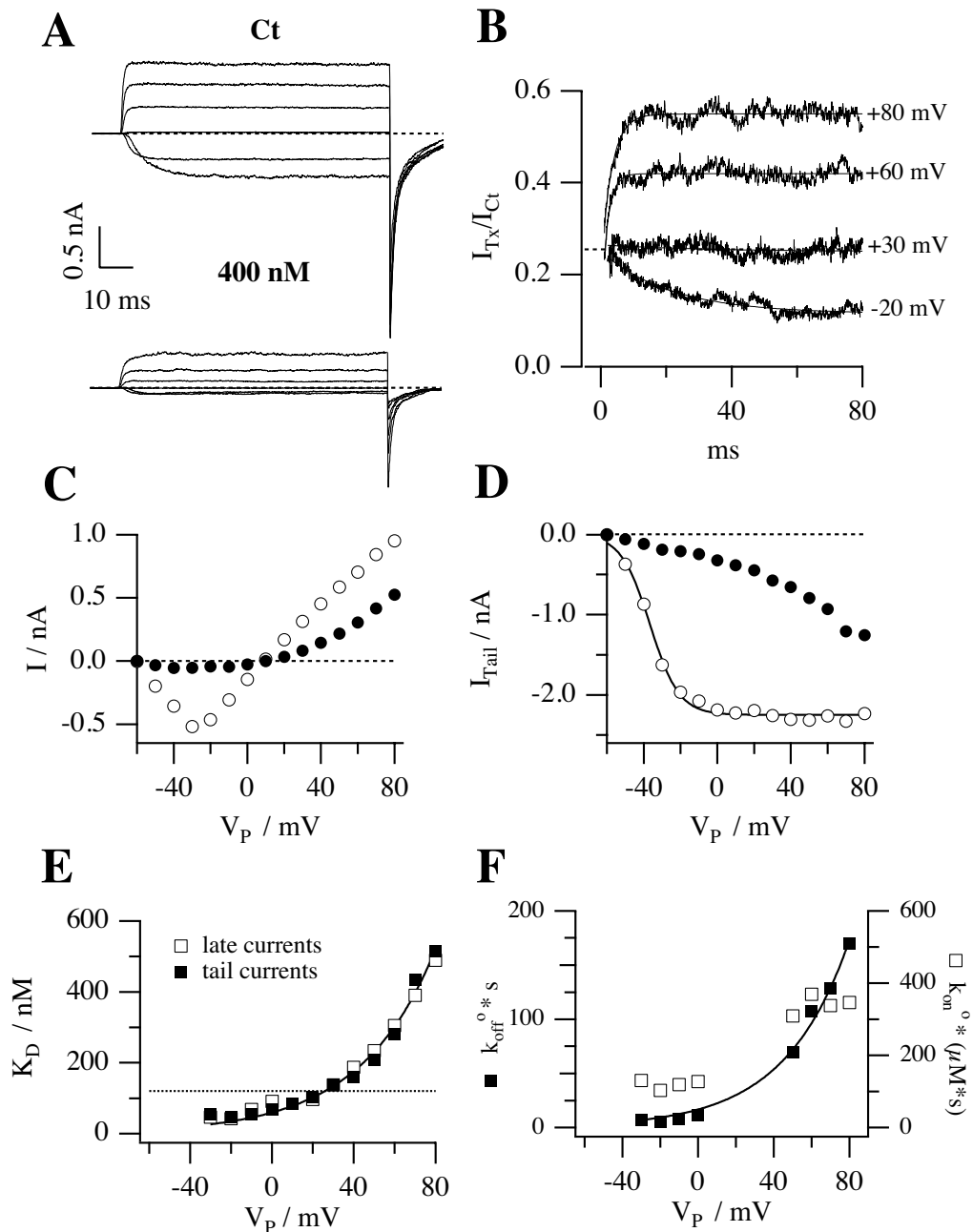


**Figure 3.7 Effect of  $\kappa$ -PVIIA on *Shaker- $\Delta$*  currents in high  $[K]_O$ .** **A)** *Outside-out* patch clamp experiment performed in symmetrical 115 mM KCl. Currents records in response to an IV-protocol, before (top) and after (bottom) the addition to the bath of 400 nM  $\kappa$ -PVIIA ( $V_H = -100$  mV;  $V_P$  from  $-30$  to  $+70$  mV in steps of 20 mV). **B)** Ratios between toxin and control currents for different voltage steps show a block increase (at  $-20$  mV) or decrease (at  $+60$  and  $+80$  mV) that is well fitted by a single exponential (smooth lines). At  $+30$  mV neither unblock nor reblock is observed and the open channel block is equal to the closed channel block (horizontal dotted line), corresponding to  $K^C = 150$  nM. **C)** Plot of the late currents (O control, ● 400 nM  $\kappa$ -PVIIA) show that most of the inward currents, but not so much of the outward currents at large depolarizations, are suppressed by 400 nM  $\kappa$ -PVIIA. **D)** Plot of the instantaneous tail currents (symbols as in panel C) vs the applied potential. The smooth line corresponds to a Boltzmann fit ( $I_{Tail} \propto (1 + \exp(-(V + V_{1/2})/s))^{-1}$ , where  $V_{1/2}$  is the half activation potential and  $s$  is the e-fold slope) with  $V_{1/2} = -37$  mV and  $s = 8$  mV. In presence of the toxin the instantaneous tail current increases continuously due to a bigger unblock at higher depolarizations. **E)** Plot of the dissociation constant calculated from the late currents (panel C, □) or from the instantaneous tail currents (panel D, ■). The continuous line correspond to the exponential fit of the data at positive potentials,  $K^O / \text{nM} = 60 \cdot \exp(V / 37 \text{ mV})$ . The horizontal dotted line corresponds to the closed state dissociation constant, equal to 110 nM. **F)** Plot of the estimates of the  $k_{off}^0$  and  $k_{on}^0$ , calculated from the exponential fit of the ratios between toxin and control currents. The dotted line is the exponential fit of the  $k_{off}^0$  ( $k_{off}^0 \cdot s = 17 \cdot \exp(V / 34 \text{ mV})$ ). In this experiment the  $k_{on}^0$  shows a small voltage dependence with an increase of a factor of 2 in the whole voltage range tested and with an average value of  $230 \mu\text{M}^{-1} \cdot \text{s}^{-1}$ .



### 3.2.3 *Shaker-Δ6-46*: closed channel block

We can ask whether the lower affinity of  $\kappa$ -PVIIA at  $[K]_O = 115$  mM is due to a smaller rate of association or to a larger rate of dissociation by analyzing a double-pulse experiment (fig. 3.8). The *outside-out* patch experiment was performed with 200 nM  $\kappa$ -PVIIA in the bath and the protocol consisted of several double stimulations, with pulses to  $-20$  mV separate by a variable interpulse interval ( $T_i$ ) at  $V_H = -100$  mV, with resting periods of at least 5 s between successive stimulations. Fig. 3.8A shows a sample of responses obtained for the  $T_i$  indicated in the figure. In agreement with the results described above, we observe that the conditioning pulse induces an increase of toxin block that appears as a reproducible hump in the first response of each successive double stimulation. This is due to the fact that at this test potential the open channels are more blocked than the channels that are closed. However, for small  $T_i$  values the second response has a shape similar to control conditions in that no peak is observed. This indicates that the fraction of blocked channels is near the equilibrium for open-channel block at  $-20$  mV that was achieved by the end of the conditioning pulse and corresponded to  $U^O = 0.23$ . Actually after  $T_i = 80$  ms the unblock probability,  $U = 0.19$ , is slightly smaller than the value obtained at the end of the pulse at  $-20$  mV. This observation will be discussed in the section 4.7.2. We can judge qualitatively the slow recovery of the lower equilibrium probability of  $\kappa$ -PVIIA binding to closed channels by the reappearance of a peak in the second response, which is clearly seen in the record with  $T_i = 680$  ms. A

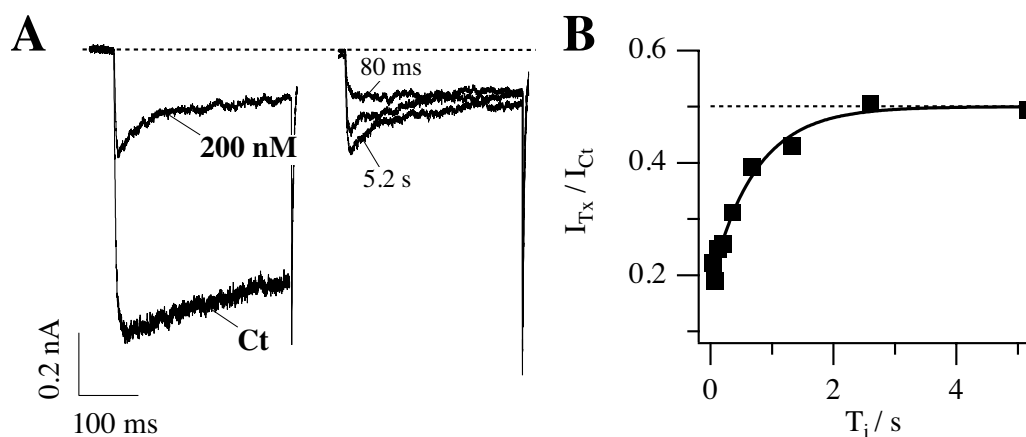


**Figure 3.8 Relaxation in high  $[K]_O$  of  $\kappa$ -PVIIA-binding to closed *Shaker-Δ* channels after a depolarizing pulse.** **A)** *Outside-out* patch clamp experiment performed in symmetrical 115 mM KCl. Superimposed records of responses to double pulse stimulation before and after the addition of 200 nM  $\kappa$ -PVIIA to the bath. Each stimulation consisted of a conditioning 300-ms pulse to  $-20$  mV, followed by an identical test pulse with a variable pulse interval,  $T_i$  (in toxin shown 80, 680 ms and 5.2 s). The holding potential was  $-100$  mV. **B)** Amplitude of the second response at early time normalized to the control response and plotted as a function of  $T_i$ . The continuous line is the best exponential fit with  $\tau = 720$  ms and the dotted horizontal line corresponds to the asymptotic value of  $U = I_{Tx} / I_{Ct} = 0.50$ , giving  $K^C = 200$  nM. From  $U$  and  $\tau$  from eq. 2.7 we estimate  $k_{off}^C = 0.69$  and  $k_{on}^C (\mu M \cdot s) = 3.5$ .

quantitative analysis is shown in fig. 3.8B by plotting, as a function of  $T_i$ , early amplitudes of conditioning responses in toxin normalized to the control value. These data are well fitted by a single exponential increase with  $T_i$  with a time constant of 0.72 s. Assuming this value as an estimate of  $\tau^C$  and using the value of  $U^C = 0.5$  measured from the early fraction of unblocked currents (data not shown), we estimate in this experiment:  $K^C = 200$  nM,  $k_{\text{off}}^C = 0.69$  s $^{-1}$ ,  $k_{\text{on}}^C = 3.5$   $\mu\text{M}^{-1}\text{s}^{-1}$ . Mean estimates are reported in table 3.1. The  $k_{\text{off}}^C$  value at  $[\text{K}]_O = 115$  mM appears equal to that in  $[\text{K}]_O = 2.5$  mM within the experimental error. On the contrary, increasing  $[\text{K}]_O$  from 2.5 to 115 mM decreases the apparent value of  $k_{\text{on}}^C$  by more than one order of magnitude, which seems to be the only kinetic parameter of  $\kappa$ -PVIIA binding to *Shaker* channels that is very sensitive to  $[\text{K}]_O$ .

### 3.2.4 Closed channel block as a function of $[\text{K}]_O$ .

Since increasing the  $[\text{K}]_O$  from 2.5 to 115 mM resulted in a reduction of about 5-7 times of the steady state affinity of the toxin to the closed channel, while the open channel block remains unmodified, we decided to investigate the dependence of the toxin interaction with the closed channel properties on the  $[\text{K}]_O$  in more detail. Intermediate  $\text{K}^+$  concentrations were applied and the kinetic of the unblock / reblock analyzed. For this purpose we used mainly the voltage clamp technique. For increasing  $[\text{K}]_O$  we observed a gradual increase in the  $K^C$  values and a slowing of the kinetics. Current responses to a +40 mV pulse were recorded in a TEVC experiment with 15 mM extracellular KCl in a  $\text{Na}^+$ -based solution (fig 3.9A). Three

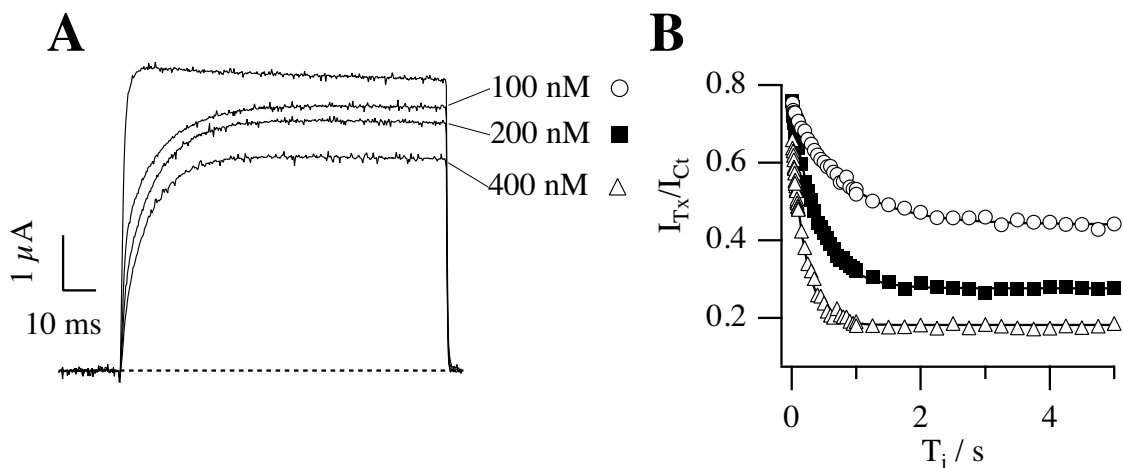


**Figure. 3.9 Relaxation of  $\kappa$ -PVIIA-binding to closed *Shaker*- $\Delta$ channels after a depolarizing pulse in  $[\text{K}]_O=15$  mM. A)** Voltage clamp experiment performed with  $[\text{K}]_O=15$  mM. Superimposed responses to a voltage step to +40 mV from a  $V_H$  of -80 mV in control and with 100, 200 and 400 nM  $\kappa$ -PVIIA added to the bath. **B)** The early currents ( $\circ$  100 nM,  $\blacksquare$  200 nM and  $\Delta$  400 nM  $\kappa$ -PVIIA) elicited by a second pulse and normalized to the control current are plotted vs the interpulse interval  $T_i$ . The continuous lines correspond to a single exponential fit with the following values for  $U$  and  $\tau \cdot \text{s}^{-1}$ : 0.44 and 1.2 in 100 nM, 0.28 and 2.4 in 200 nM and 0.18 and 4.6 in 400 nM  $\kappa$ -PVIIA. From the estimates of  $K^C$ ,  $k_{\text{off}}^C$  and  $k_{\text{on}}^C$  obtained from  $\tau$  and  $U$  through eq. 2.7, the mean values  $K^C / \text{nM} = 81$ ,  $k_{\text{off}}^C \text{ s} = 0.68$  and  $k_{\text{on}}^C \cdot (\mu\text{M} \cdot \text{s}) = 8.4$  are calculated.

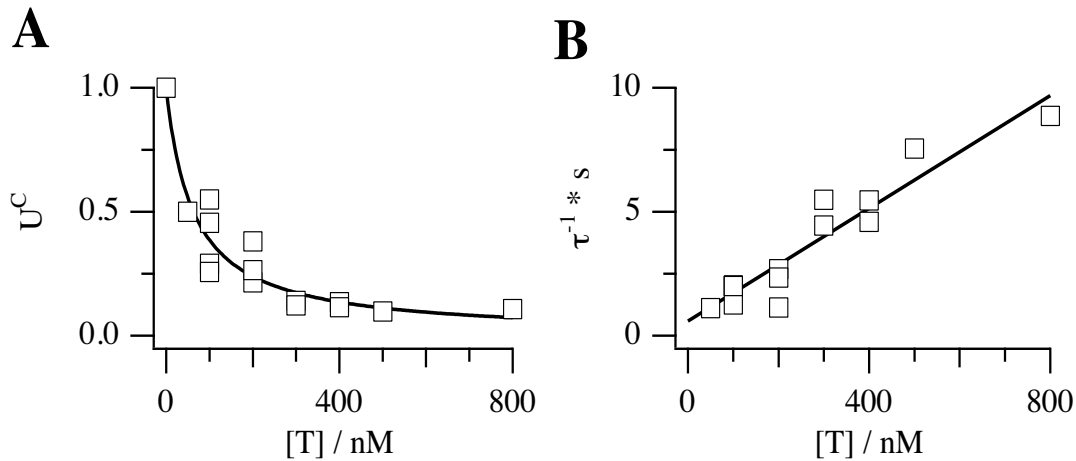


**Fig. 3.10 Dose-response of  $\kappa$ -PVIIA effects on *Shaker*- $\Delta$  channels in  $[K]_0 = 5$  mM.** A)  $[T]$ -dependence of  $U^C$  evaluated from different experiments in  $[K]_0 = 5$  mM. The solid line is the best fit with eq. 2.4, giving  $K^C = 63 \pm 7$  nM. B)  $[T]$ -dependence of the reciprocal of time constant  $\tau$  estimated by fitting with a single exponential the relaxation of the toxin block to closed channels. The solid line is the best fit with a line (reciprocal of the expression 2.6), giving  $k_{off}^C = 0.6 \pm 0.4$  s $^{-1}$  and  $k_{on}^C = 11 \pm 1$   $\mu$ M $^{-1}$ s $^{-1}$ ; the ratio  $k_{off}^C / k_{on}^C$  gives  $K^C = 55$  nM in good agreement with the estimate obtained from the fit of  $U^C$  data in panel A.

increasing toxin concentrations (100, 200 and 400 nM  $\kappa$ -PVIIA) were applied to the bath. The plot of the ratio between the early toxin and control currents toward the interpulse time shows a single exponential relaxation at all  $[T]$  (panel B), with time constants of 0.8, 0.40 and 0.22 s and a tonic  $U^C$  of 0.44, 0.28 and 0.18, respectively. The mean estimate for  $K^C$  is  $81 \pm 6$  nM, for  $k_{off}^C$   $0.7 \pm 0.1$  s $^{-1}$  and  $k_{on}^C = 8.4 \pm 1.3$   $\mu$ M $^{-1}$ s $^{-1}$ . This shows that the kinetics of reblock in these conditions are faster than the one observed in high  $[K]_0$  (fig. 3.8) and slower respect to the NFR experiments (fig. 3.4).

At all  $K^+$ -concentration tested, 2.5, 5, 15, 57.5, 115 mM, in  $Na^+$  based solution, the relaxation was well fitted by a single exponential and slowed for increasing  $[K]_0$ . The case of  $[K]_0 = 0$  will be discussed in a separate section (3.3). A plot of the closed state unblock probability and the reciprocal of the time constant vs the toxin concentration of the values evaluated from different experiments were fitted respectively with eq 2.4 and with a line,  $k_{off} + k_{on} \cdot [T]$ . Fig 3.10 plots in panel A the unblock probability, and in panel B the reciprocal of the time constants vs  $[T]$  for external 5 mM KCl. The best values for  $K^C$ ,  $k_{off}^C$ ,  $k_{on}^C$  obtained by this analysis are given in table 3.2 together with the mean estimate. The values obtained for  $K^C$ ,  $k_{off}^C$  and  $k_{on}^C$  with the two different analysis methods are in excellent agreement, supporting the bimolecular reaction hypothesis. In all conditions tested we did not observe a significant change in the dissociation rate. Thus the reduced affinities in the presence of increased potassium concentrations are due to a change in the association rate, suggesting a competition effect between potassium ions and the toxin in the outer vestibule of the ion channel pore.

<b>Table 3.2</b>		<b>Mean values</b>			<b>Fit with dose response</b>		
$[K]_o$ mM	$[Na]_o$ mM	$K^C$ nM	$k_{off}^C$ $s^{-1}$	$k_{on}^C$ $\mu M^{-1} s^{-1}$	$K^C$ nM	$k_{off}^C$ $s^{-1}$	$k_{on}^C$ $\mu M^{-1} s^{-1}$
0	115	40 ± 14	0.75 ± 0.22	17 ± 7	38 ± 4	0.57 ± 0.35	16.6 ± 1.3
2.5	112.5	37 ± 16	0.96 ± 0.31	23 ± 7	36 ± 3	0.37 ± 0.90	24.0 ± 2.5
5	110	67 ± 29	0.66 ± 0.18	11 ± 3	63 ± 7	0.59 ± 0.39	11.4 ± 1.2
15	100	97 ± 34	0.64 ± 0.15	7 ± 2	93 ± 7	0.58 ± 0.21	7.5 ± 0.9
30	85	125 ± 41	0.88 ± 0.23	7 ± 2	120 ± 14	1.33 ± 0.22	4.9 ± 0.8
57.5	57.5	208 ± 96	0.77 ± 0.21	4.4 ± 1.8	188 ± 18	0.83 ± 0.11	3.9 ± 0.4
115	0	265 ± 106	0.62 ± 0.18	2.6 ± 0.9	249 ± 17	1.05 ± 0.14	0.67 ± 0.46

**Table 3.2 Parameters of  $\kappa$ -PVIIA-binding to closed channels in function of  $[K]_o$**

Mean values (central columns): mean values ± SD from experiments performed either with the TEVC or patch clamp technique, for each concentration number of experiments ≥ 5, with 1-4 toxin application during one experiment.

Fit with dose response (right columns): values (± SD) obtained by fitting for the same set of data  $U^C$  and  $\tau$  with eq. 2.4 and 2.6 respectively.

### 3.3 Binding of $\kappa$ -PVIIA in absence of external $K^+$

We studied the block of  $\kappa$ -PVIIA in complete absence of external potassium where  $K^+$  was exchanged with either external  $Na^+$  or  $Tris^+$ . In both cases properties of the binding to the open channel were not modified. In external NaCl the closed channel block was identical to the one observed with NFR. The mean values of  $K^C$ ,  $k_{off}^C$  and  $k_{on}^C$  under those conditions are shown in table 3.2. Double pulse experiments revealed that the reequilibration kinetics in the presence of 115 mM  $Na^+$  are identical to the kinetics observed in NFR. In external  $Tris^+$  the affinity of the toxin to the closed channels is slightly higher, corresponding to a  $K^C$  of about 20 nM (mean value ± SD:  $K^C$  of 23 ± 10 nM, with 20 experiments and 1 to 3 toxin applications for each experiment; from the fits with the dose response equation, 2.4,  $K^C = 20 \pm 1$  nM).

In the absence of external  $K^+$ , C-type inactivation is much faster than with high  $[K]_o$  and even NFR (López-Barneo et al. 1993). We took advantage of this to measure the block of  $\kappa$ -PVIIA for very long pulses. Fig 3.11 shows current traces from a patch experiment performed with internal 115 mM KCl and external 115 mM NaCl. We applied a 15 s voltage step to +40 mV from a holding potential of -100 mV and recorded the current response in control conditions

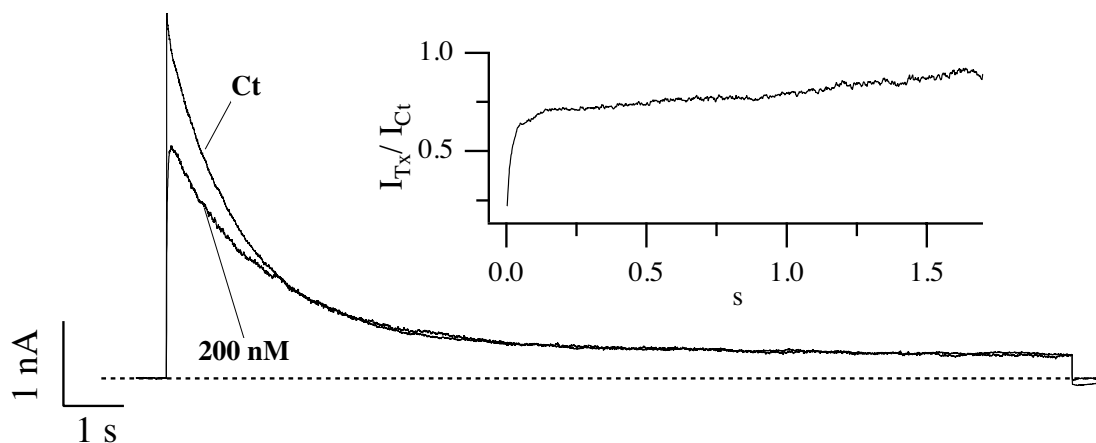


**Figure 3.11 Long pulse in extracellular NaCl.** *Outside-out* patch clamp experiment performed in extracellular 115 mM NaCl and with 115 mM KCl in the pipette solution. Currents in response to a 15 s stimulation at  $V_P = +40$  mV, from  $V_H = -100$  mV in control and in 200 nM  $\kappa$ -PVIIA. The decrease of the current in control is due to the occurrence of the C-type inactivation. After approximately 1.5 s the current recorded in presence of toxin is equal to the control current. **Inset:** Ratio between the toxin and control currents: the early exponential phase is followed by a much slower process. The initial unblock probability, 0.2, corresponds to  $K^C = 50$  nM.

and in presence of 200 nM  $\kappa$ -PVIIA in the bath. The ratio between the toxin and the control, (fig.3.11 inset), starts from a value of 0.2, corresponding to a closed channel block of 50 nM, and reaches a plateau ( $U=0.72$ ,  $K^O(+40\text{mV})=541$  nM) after 100 ms, corresponding to the reached equilibrium of the toxin with the open channel. At about 300 ms after the beginning of the pulse the ratio starts to increase up to a value of one: after about 2 sec the two currents traces overlap and no block is observed. This experiment was repeated with extracellular  $\text{Tris}^+$  and gave the same result, suggesting that there might be incompatibility between toxin binding and C-type inactivated states. In most of the experiments a 15 seconds pulse was not enough to completely abolish the current. The comparison of the toxin with control trace is sometimes difficult because the kinetic of inactivation might change during the time of the experiment (Chen et al. 2000). The interaction of  $\kappa$ -PVIIA with the C-type inactivated state was not investigated further.

### 3.4 Effect of $[\text{Rb}]_o$ on the binding of $\kappa$ -PVIIA

To elucidate the influence of external cations on toxin binding, the next step was to use a permeable cation, such as  $\text{Rb}^+$ . The permeability of  $\text{Rb}^+$  is only slightly smaller than  $\text{K}^+$ : in patch clamp experiments with 115 mM internal  $\text{K}^+$  and equimolar external  $\text{Rb}^+$  the reversal potential is between  $-10$  and  $-5$  mV (see fig. 3.12, Hille 1973).

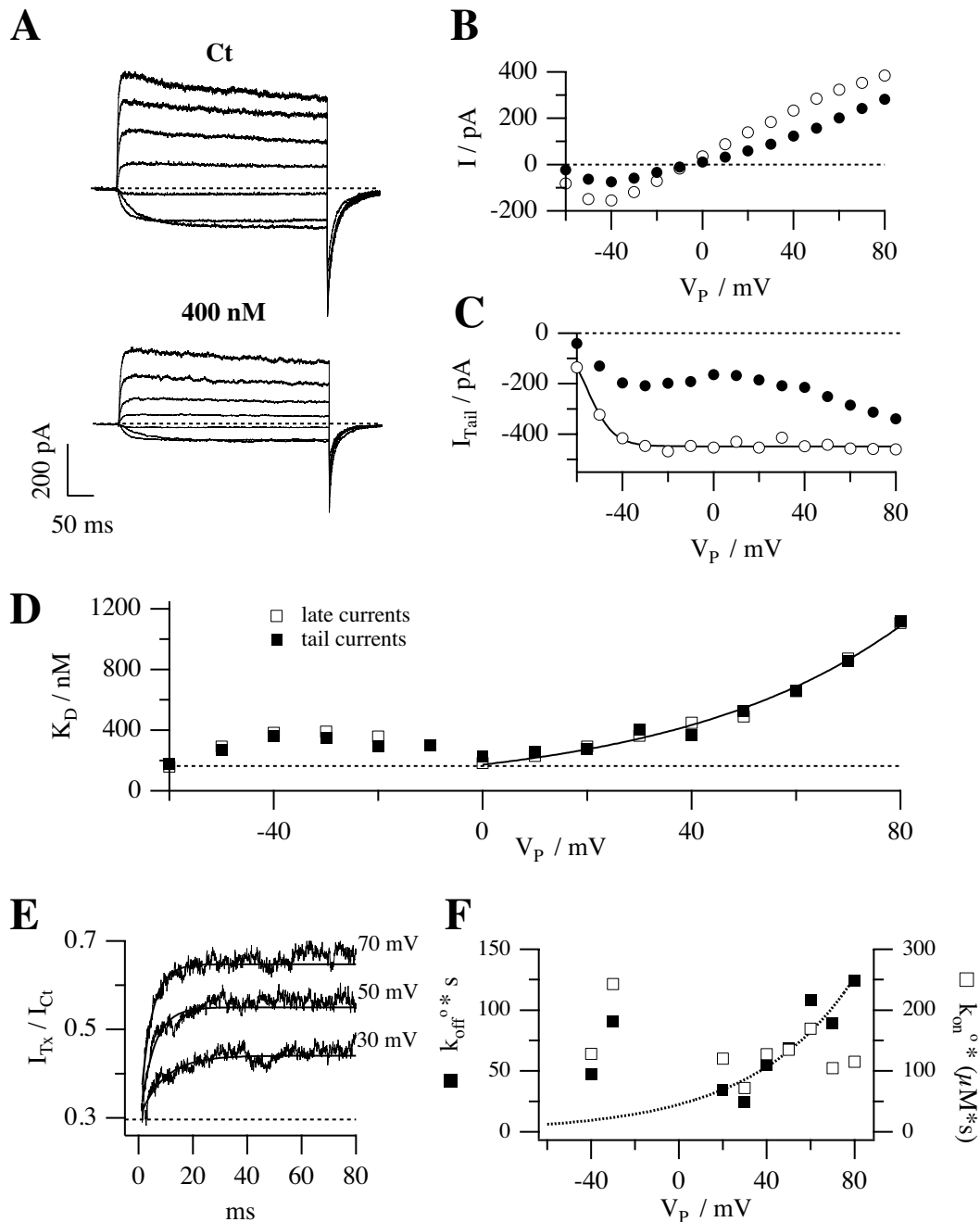


**Figure 3.12 Effect of  $\kappa$ -PVIIA on *Shaker- $\Delta$*  currents in high  $[Rb]_O$**  **A)** *Outside-out* patch clamp experiment performed in  $[K]_I = 115$  mM and  $[Rb]_O = 115$  mM. Current records in response to an IV-protocol, before (top) and after (bottom) the addition to the bath of 400 nM  $\kappa$ -PVIIA ( $V_H = -100$  mV;  $V_P$  from  $-50$  mV, every 20 mV). **B)** The plot of the late currents ( $\circ$  control,  $\bullet$  400 nM  $\kappa$ -PVIIA) shows that inward currents are only partially blocked by 400 nM  $\kappa$ -PVIIA, a concentration that in presence of extracellular 115 mM  $K^+$  almost completely suppressed the currents as shown in fig 3.7. **C)** Plot of the instantaneous tail currents (symbols as in panel B) against the applied potential. The smooth line corresponds to the Boltzman fit eq.2.1, with  $V_{1/2} = -55$  mV and  $s = 6$  mV. In presence of the toxin the instantaneous tail current shows a plateau at negative potentials, while it increases continuously at positive potentials due to the voltage dependence of the toxin block. **D)** Plot of the dissociation constant calculated from the late currents (panel B,  $\square$ ) or from the instantaneous tail currents (panel C,  $\blacksquare$ ) as described in par. 2.5.1. The continuous line correspond to the exponential fit of the data at positive potentials,  $K_D^O / \text{nM} = 173 \cdot \exp(V/44 \text{ mV})$ . The horizontal dotted line corresponds to the closed state dissociation constant, equal to 160 nM. **E)** Ratios between toxin and control currents (shown for voltage steps of 30, 50 and 70 mV) show always a decrease in the block that is well fitted by a single exponential (smooth lines). **F)** Plot of the estimates of the  $k_{off}^O$  and  $k_{on}^O$ , calculated from the exponential fit of the ratios between toxin and control currents. The dotted line is the exponential fit of the  $k_{off}^O$  for positive potentials ( $k_{off}^O \text{ s} = 22 \cdot \exp(V/46 \text{ mV})$ ) extrapolated in the whole potential range studied. The values of  $k_{off}^O$  obtained at negative potentials are much higher than the fit previsions. The  $k_{on}^O$  doesn't show a clear voltage dependence and has a mean value of  $121 \mu\text{M}^{-1} \cdot \text{s}^{-1}$ .

### 3.4.1 115 int KCl, 115 ext RbCl

Fig 3.12 shows the responses to an IV protocol ( $V_H = -100$  mV,  $V_P$  from  $-50$  mV, in steps of 20 mV) for a patch experiment performed with 115 mM intracellular KCl and 115 mM RbCl in the bath, before and after the addition of 400 nM  $\kappa$ -PVIIA to the external bath. Panel B shows the plot of the steady state current vs the applied potential: the reversal potential is  $-7$  mV, indicating a slightly higher permeability of  $K^+$  with respect to  $Rb^+$ . The block of evoked currents decreases with higher applied potentials. Comparing these current traces with the patch experiment of fig. 3.7, performed in symmetrical  $K^+$ , we observe that in presence of extracellular  $Rb^+$  the block of the inward current by  $\kappa$ -PVIIA is similar to the block of the outward currents. This is not the case for symmetrical  $K^+$ . With extracellular  $Rb^+$  the traces with inward currents do not present the typical hump in presence of the toxin as observed with symmetrical  $K^+$ . Panel C shows the plot of the instantaneous tail current as a function of the applied potential: the current exhibits a plateau between  $-40$  and  $0$  mV, indicating that in this range the toxin block is not strongly voltage dependent. The control currents were fitted with a Boltzmann function with  $V_{1/2} = -55$  mV and  $s = 6$  mV. Panel D shows the equilibrium dissociation constants calculated from the steady state current and the instantaneous tail currents: the  $K^O$  is not monotonic and for all test potentials it is bigger than  $K^C$ , indicated by the dashed line and calculated from the initial block shown by the ratios (panel E). The concave region of the  $K^O$  curve corresponds to inward  $Rb^+$  carried currents, while the block of the outward  $K^+$ -currents is identical to the one observed with symmetrical high  $K^+$ . The data

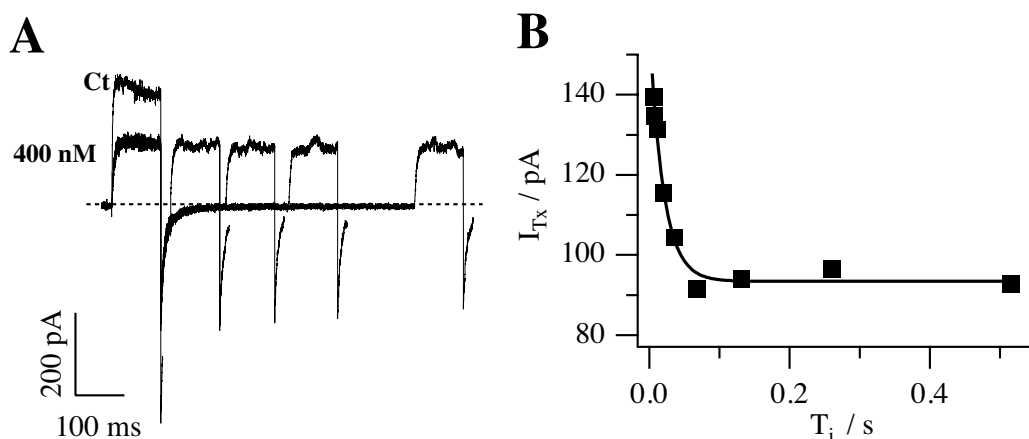


**Figure 3.13 Relaxation of  $\kappa$ -PVIIA-binding to closed *Shaker- $\Delta$* channels after a depolarizing pulse in high  $[Rb]_O$  and high  $[K]_I$**  **A)** Superimposed records of responses to double pulse stimulation before and after the addition of 400 nM  $\kappa$ -PVIIA to the  $Rb^+$ -bath for the same experiment shown in fig 3.12. Each stimulation consisted of a conditioning 100-ms pulse to 40 mV, followed by an identical test pulse with a variable pulse interval,  $T_i$  (in toxin shown 20, 132, 260 and 516 ms). **B)** Amplitude of the second response at the half activation time of control plotted as a function of  $T_i$ . The relaxation is extremely fast and the time constant of the exponential fit is 20 ms (continuous line).

**Table 3.3**

Extracellular		115 RbCl	115 RbCl
Intracellular		115 KCl	115 RbCl
$K^C$	nM	$146 \pm 28$	$259 \pm 21$
$K^O(0)$	nM	$250 \pm 20^*$	$1020 \pm 60^*$
slope	mV	$47 \pm 2^*$	$64 \pm 7^*$
% linear slope	$mV^{-1}$	-	$2.1 \pm 0.4\%^*$
$k_{off}^O(0)$	$s^{-1}$	$29 \pm 10$	$118 \pm 19$
$k_{on}^O$	$\mu M^{-1} s^{-1}$	$113 \pm 40$	$100 \pm 45$

**Table 3.3**  $\kappa$ -PVIIA-binding to *Shaker*- $\Delta$  channels in high extracellular RbCl.

Mean  $\pm$  SD, number of experiments  $\geq 5$ , each with 1-3 toxin applications.

\* from fit of the mean values with a single exponential

of the outward currents are well fitted by a single exponential ( $K^O(V) / nM = 173 \cdot \exp(V/43.5)$ ). The best estimates for  $K^O(0)$  and  $v_s$ , obtained by fitting the mean values of  $K^O$  for  $0 mV \leq V_p \leq 80 mV$  (10 experiments) with a single exponential, are reported in table 3.3.

We performed the kinetic analysis by fitting the ratios between the toxin and control traces with a single exponential (in panel E the test potentials  $V_p = +30, 50, 70 mV$  are shown). At all potentials an unblock was observed. At negative potentials it is difficult to make a quantitative kinetic analysis because the difference between the closed and open state block is small. Furthermore the kinetics of activation of the channels have a similar time scale as the kinetics of toxin binding. Panel F shows the results of the kinetic analysis: the  $k_{on}$  has a mean value of  $121 \mu M^{-1} s^{-1}$ , while for positive potentials the  $k_{off}$  can be fitted with a single exponential ( $k_{off}(V) \cdot s = 22.4 \cdot \exp(V/46.2)$ ). The  $k_{off}$  values calculated for negative potentials are much higher than the values obtained with high  $[K]_O$ . In contrast, the  $k_{on}$  values are in the same range under those conditions. In table 3.3 are given the mean values for  $k_{off}$ ,  $k_{on}$  for outward currents for 10 patch experiments.

The responses to a double pulse protocol with a test potential of  $+40 mV$  for the same patch of fig 3.12 are shown in fig 3.13. In Panel B the early currents (average between the 50-75% of the activation in control) is plotted against the duration of the interpulse interval. The toxin equilibrates very fast with the closed state and 60 ms are enough to reach the equilibrium in 400 nM  $\kappa$ -PVIIA (time constant 20 ms), compared to seconds required in high external  $K^+$ . During the repolarization at  $V_H$  three processes take place: first, since the toxin potency in blocking open channels is higher at more negative potentials, the toxin has to re-equilibrate with the open channels at the new potential; second, deactivation occurs; third, the toxin equilibrates with the fraction of channels that are in the closed state. In high extracellular  $K^+$ , the last process has a much slower kinetics and therefore is easy to separate. In high extracellular  $Rb^+$ , firstly, the deactivation is slower, secondly the equilibration to the closed



states is faster. Therefore all the three processes have the same time scale and consequently a kinetic analysis of the reblock is not possible. We decided to investigate more in detail the closed channel block of  $\kappa$ -PVIIA in presence of increasing  $\text{Rb}^+$  concentrations. These experiments were performed with  $\text{Na}^+$  in the external bath but also few experiments were performed in a  $\text{Tris}^+$ -based solution where no difference was observed.

By using mostly the TEVC technique double pulse protocols eliciting outward currents were applied to estimate the properties of the closed channel binding. Since at  $[\text{Rb}]_0 \leq 60$  mM the equilibration of the toxin binding to the closed channels is faster than the deactivation process, we were able to measure also the kinetics parameters, that were not accessible in

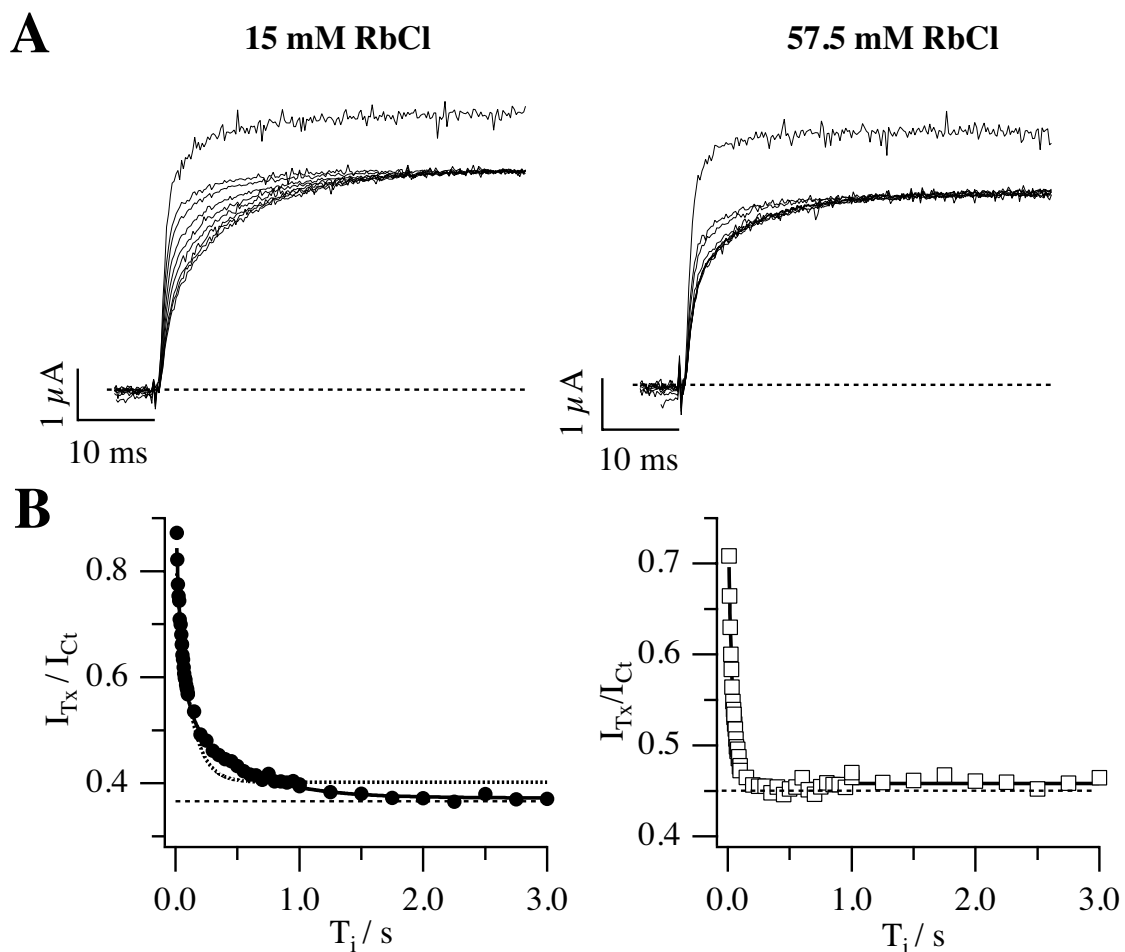


**Figure 3.14 Relaxation of  $\kappa$ -PVIIA-binding to closed *Shaker- $\Delta$* channels after a depolarizing pulse in  $[\text{Rb}]_0 = 15$  and  $57.5$  mM. **A)** Current responses to double pulse stimulation before and after the addition of  $200$  nM  $\kappa$ -PVIIA to the bath containing either  $15$  (left) or  $57.5$  (right) mM  $\text{RbCl}$ , performed in the same voltage clamp experiment. Each stimulation consisted of a conditioning  $100$ -ms pulse to  $40$  mV, followed by an identical test pulse with a variable pulse interval,  $T_i$  (shown  $10, 20, 50, 100, 200, 500$  ms and  $1, 3$  sec). In  $57.5$  mM  $\text{RbCl}$  after  $50$  ms the equilibrium is already reached. **B)** Amplitude of the second response at the half activation time of control normalized to the control current and plotted as a function of  $T_i$ . The relaxation is extremely fast in  $57.5$  mM  $\text{RbCl}$  and follows a single exponential decay with  $\tau = 33$  ms and an asymptotic value  $U^C$  of  $0.46$ , yielding to  $K^C = 163$  nM. Consequently we could evaluate  $k_{\text{off}}^C \cdot s = 17$  and  $k_{\text{on}}^C \cdot (\mu\text{M} \cdot s) = 81$  (eq.2.7). In  $15$  mM  $\text{RbCl}$  the relaxation can't be satisfyingly fitted with a single exponential, shown by the dotted line. The continuous line corresponds to the double exponential fit with  $\tau_{\text{Fast}} = 43$  ms and  $\tau_{\text{Slow}} = 450$  ms and an asymptotic  $U^C$  of  $0.37$ , corresponding to  $K^C = 117$  nM.**

$[Rb]_O = 115$  mM. The open channel properties were not investigated. In external 2.5 mM RbCl we observed a re-equilibration of the toxin with the closed channels in a time range similar to the one observed for NFR. Therefore, under these conditions, the counter cation  $Na^+$  seems to dominate the interaction between the channel and the toxin. Increasing  $Rb^+$  concentrations led to a decrease in the binding affinity of the toxin. In parallel a fast component is unmasked from the relaxation to the closed state. A double exponential behavior is observed for  $Rb^+$  between 5 and 30 mM. The amplitude of the fast component with respect to the slow component is increasing with the  $Rb^+$  concentration and at 57 mM only the fast component is observed. In some experiments only the fast component is present already at 30 mM  $Rb^+$ , depending on the toxin concentration applied.

Fig 3.14 shows a TEVC experiment performed with 15 mM and 57.5 mM external  $Rb^+$  and addition of 200 nM  $\kappa$ -PVIIA to the bath. Panel A shows the current responses to a double pulse protocol ( $V_H = -80$  mV,  $V_P = +40$  mV) in control and in 200 nM  $\kappa$ -PVIIA for the following interpulse intervals: 10, 20, 50, 100, 200, 500 ms and 1, 2, 3 s. In panel B the normalized early currents are plotted vs the interpulse duration  $T_i$ : in 15 mM RbCl the reequilibration develops with a double exponential law ( $\tau_{Fast} = 43$  ms;  $\tau_{Slow} = 450$  ms) and 2 s are needed to reach the equilibrium; in 57.5 mM RbCl the kinetics is much faster and exhibits a single exponential behavior with a time constant of 33 ms, close to the value of the fast

Table 3.4			single exp	fast kinetics		slow kinetics		
$[Rb]_O$ mM	$[Na]_O$ mM	$K^C$ nM	$k_{off}^C$ $s^{-1}$	$k_{on}^C$ $\mu M^{-1} s^{-1}$	A $s^{-1}$	B $\mu M^{-1} s^{-1}$	A $s^{-1}$	B $\mu M^{-1} s^{-1}$
0	115	$40 \pm 14$	$0.75 \pm 0.22$	$17 \pm 7$	-	-	-	-
2.5	112.5	$39 \pm 5$	$1.1 \pm 0.5$	$17 \pm 1$	-	-	-	-
5	110	$52 \pm 6$	$1.2 \pm 1.1$	$19 \pm 3$	$8 \pm 2$	$66 \pm 8$	$0.6 \pm 0.3$	$11 \pm 1$
15	100	$83 \pm 6$	-	-	$11 \pm 2$	$67 \pm 5$	$1.8 \pm 0.2$	$2.2 \pm 0.7$
30	85	$119 \pm 8$	$3 \pm 4$	$106 \pm 9$	$11 \pm 3.5$	$94 \pm 9$	No fit	No fit
57.5	57.5	$171 \pm 13$	$13 \pm 5$	$70 \pm 12$	-	-	-	-
115	0	$143 \pm 6$	-	-	-	-	-	-

**Table 3.4 Dependence of the  $\kappa$ -PVIIA-binding to closed *Shaker- $\Delta$*  channels on  $[Rb]_O$**

Best estimate for the parameters  $K^C$ ,  $k_{off}^C$  and  $k_{on}^C$  obtained from the fit of  $U^C$  and  $\tau$  with eq. 2.4 and 2.6 respectively. For the  $Rb^+$ -concentrations at which a double exponential relaxation was observed the dependence on  $[T]$  of the reciprocals of both the fast and slow time constants were fitted with a line:  $A+B \cdot [T]$ . Experiment were performed either with voltage or patch clamp technique, for each concentration number of experiments  $\geq 5$ , with 1-4 toxin application in each experiment.

component found in 15 mM KCl.

The closed state unblock probabilities from different experiments plotted against the toxin concentration for 2.5 and 15 mM RbCl are shown in panel A of fig. 3.15. The experimental data were fitted according eq 2.4. Panel B of fig. 3.15 shows a plot of the reciprocal of the relaxation time constants. A linear increase of those values with increasing toxin was observed as shown for 2.5 and 15 mM RbCl ( $\tau^{-1} = A + B \cdot [T]$ ).

In the presence of 30 mM KCl the slow component was not detected in all experiments.

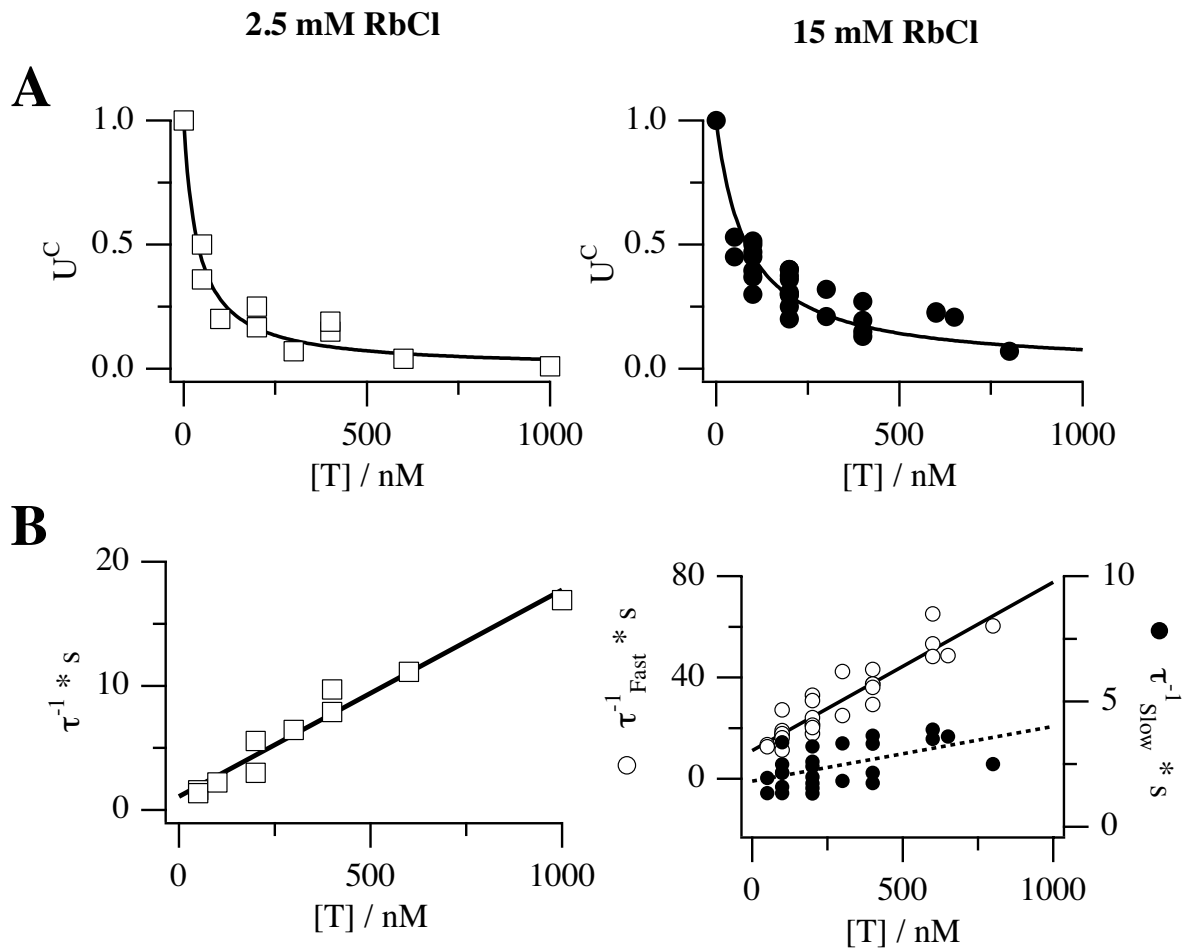


**Figure 3.15 Dose-response of  $\kappa$ -PVIIA effects on *Shaker- $\Delta$*  channels in  $[Rb]_O = 2.5$  and 15 mM. A)**  $[T]$ -dependence of  $U^C$  evaluated from different experiments in  $[Rb]_O = 2.5$  (left side) or 15 mM (right side). The solid line is the best fit with eq. 2.4, giving respectively  $K^C = 39 \pm 5$  nM and  $83 \pm 6$  nM. The error is the standard deviation evaluated from the fit, comparing the theoretical and the experimental values. **B)**  $[T]$ -dependence of the reciprocal of time constant  $\tau$  estimated by fitting the relaxation of the toxin block to closed channels with a single exponential for the data in 2.5 mM RbCl and with two exponentials in 15 mM RbCl (see fig. 3.14). The solid lines are the best fit with a line. For 2.5 mM RbCl the line fit corresponds to the reciprocal of the expression 2.6, yielding to  $k_{off}^C = 1.1 \pm 0.5$  s<sup>-1</sup> and  $k_{on}^O = 17 \pm 1$   $\mu$ M<sup>-1</sup>s<sup>-1</sup>; the ratio  $k_{off}^C / k_{on}^C$  gives  $K^C = 64$  nM in good agreement with the estimate obtained from the fit of  $U^C$  data in panel A. In 15 mM RbCl the line  $A + B \cdot [T]$ , gives for the fast component  $A = 11 \pm 2$  s<sup>-1</sup> and  $B = 67 \pm 5$   $\mu$ M<sup>-1</sup>s<sup>-1</sup>, for the slow component  $A = 1.8 \pm 0.2$  s<sup>-1</sup> and  $B = 2.2 \pm 0.7$   $\mu$ M<sup>-1</sup>s<sup>-1</sup>. The meaning of this fit will be discussed later.

Under these conditions the reciprocal of the time constant did not show any dependence on the toxin concentration. This is probably due to the low amplitude of the slow component, which makes a proper evaluation difficult. When a single exponential is sufficient to fit the relaxation process, the line intercept with the ordinate axis,  $A$ , would be the  $k_{\text{off}}$ , and the slope  $B$  the  $k_{\text{on}}$ , as in eq. 2.5. For the double exponential behavior the relationship between the association, dissociation rate and the experimental results is not straightforward and will be discussed in section 4.7.1. Table 3.4 reports the values for  $A$  and  $B$ .

### 3.5 Effect of intracellular cations

#### 3.5.1 Open channel block

It was shown that CTX ( $\alpha$ -KTx) block is very sensitive to the intracellular  $K^+$  concentration in the  $Ca^{2+}$ -dependent K-channels (MaxiK- or BK-channels; MacKinnon and Miller 1988; Park and Miller 1992). CTX block of both BK and *Shaker* (Goldstein and Miller 1992) channels is voltage dependent and, as we have shown for  $\kappa$ -PVIIA, the voltage dependence of the binding resides in the dissociation rate. Miller and coworkers (Anderson et al. 1988; MacKinnon and Miller 1988; Goldstein and Miller 1992) showed that CTX interacts electrostatically with a cation sitting in the pore. They found that substituting  $K^+$  with a not permeant cation the voltage dependence of toxin binding is completely lost in BK channels, and only reduced in *Shaker* channels. Because of the similarities between the two pore blockers CTX and  $\kappa$ -PVIIA, we investigated if the voltage dependence of  $\kappa$ -PVIIA block is modulated by the intracellular cations.

$K^+$  was either substituted completely by  $Rb^+$ ,  $Na^+$ ,  $Li^+$ ,  $NMG^+$  or  $Tris^+$  or the  $K^+$  concentration was lowered by exchanging it with another cation. The extracellular potassium was kept constant at 115 mM.

In fig. 3.16A current responses to an IV protocol from a holding potential of  $-100$  mV are shown. Test potentials are applied in 20 mV steps starting from  $-40$  mV. Currents were recorded from *outside-out* patches with 115 mM KCl in the bath and the pipette containing the cation indicated. Under these conditions only inward currents were recorded, except when  $Rb^+$  was in the pipette solution. This indicates that in presence of extracellular potassium the permeability of the cation tested is so small that the current is carried exclusively by potassium ions up to test potentials of  $+80$  mV. Because of the decreased driving force at high depolarizing potentials the current's amplitude is too small to allow the evaluation of the  $K^O$  from the ratio between the steady state currents of toxin and control traces. Therefore  $K^O$  was evaluated from the instantaneous tail current, as described in methods 2.5.1. We fitted the tail currents with a single exponential and extrapolated to the beginning of the repolarizing

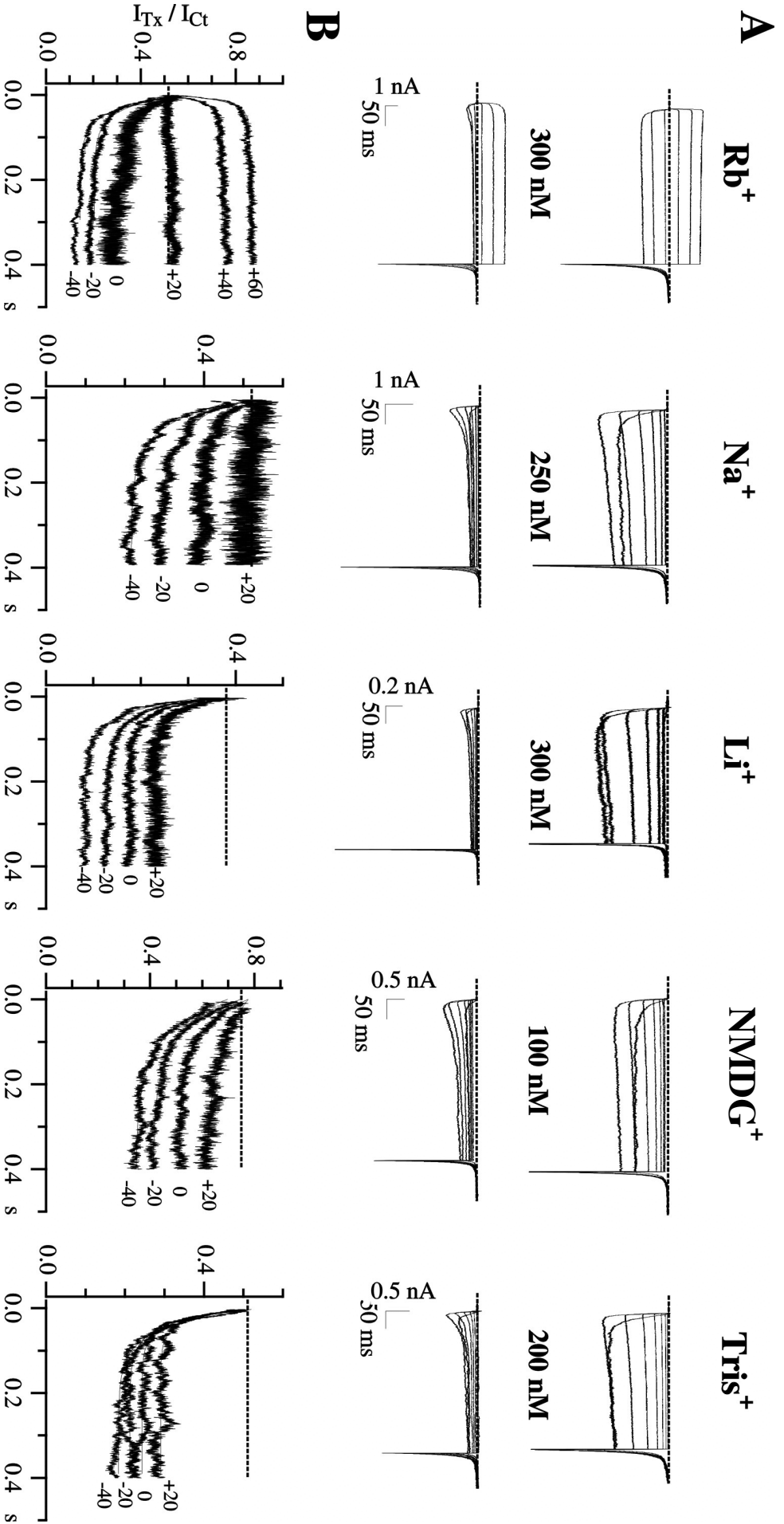


**Figure 3.16**  $\kappa$ -PVIIA-binding to *Shaker- $\Delta$*  channels with diverse intracellular monovalent cations. **A**) Current responses to an IV protocol ( $V_H = -100$  mV,  $V_p$  from  $-40$  mV, with  $20$  mV increment) recorded from *outside-out* patch clamp experiments with  $115$  mM KCl in the bath and the pipette containing the cation indicated ( $115$  mM). **B**) Toxin to control current ratios for voltage steps indicated. The dotted horizontal lines indicate the unblock probability relative to the closed state, yielding to a  $K^C$  of  $300$  nM in  $Rb^+$ ,  $270$  nM in  $Na^+$ ,  $184$  nM in  $Li^+$ ,  $300$  nM in  $NMDG^+$  and  $208$  nM in  $Tris^+$ .

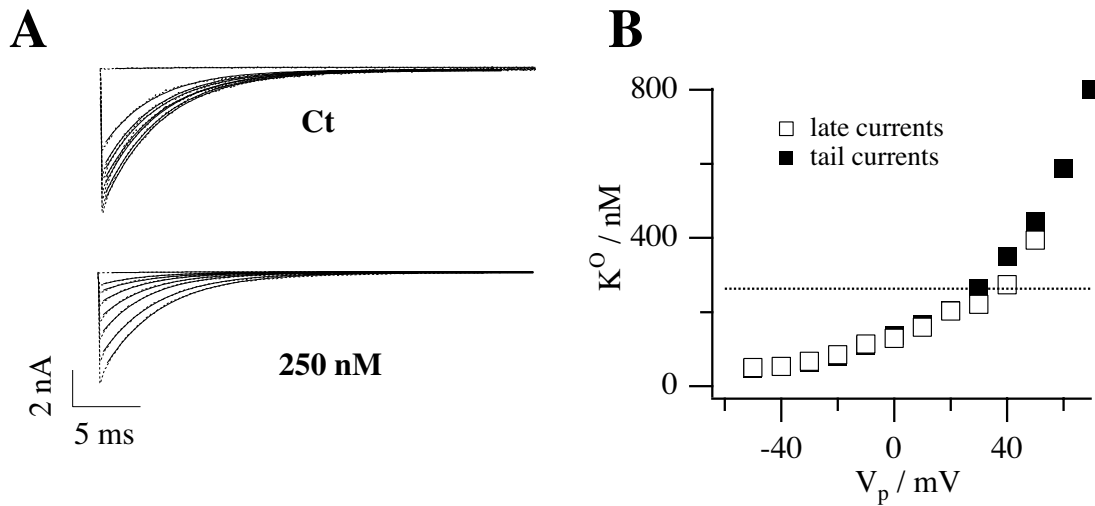


**Figure 3.17**  $K^O$  can be evaluated from the instantaneous tail currents. **A)** Tail currents at  $V_{Tail} = -100$  mV, following an IV protocol (shown potentials from -70 mV, with 20 mV increment; fig. 2.4 ). **B)** Comparison between the dissociation constant calculated from the late currents (  $\square$  ) or from the instantaneous tail currents (  $\blacksquare$  ). The horizontal line corresponds to  $K^C = 263$  nM and helps identifying the potential ( $V_{inv}$ ) at which  $K^O = K^C$ , in this experiment about 35 mV.

pulse plus the delay due to the filter (200  $\mu$ s). To improve the evaluation of  $K^O$ , in some experiments the tails were evaluated at a less negative potential, up to -60 mV, at which the deactivation is slower and therefore easier to fit. At the potentials at which it was possible to evaluate the  $K^O$  both from steady state and tail currents we did not observe any significant difference between these two methods. Fig 3.17A shows the tail currents ( $V_{Tail} = -100$  mV) with overlapped exponential fits in control and in toxin for the same IV protocols shown in fig 3.16 for intracellular  $Na^+$ . Panel B shows the dependence of the dissociation constant on the test potential for the open state evaluated from late currents (white squares) and instantaneous tail currents (black squares).

In fig. 3.18 we plot the equilibrium dissociation constants for all the intracellular cations tested at the various potentials. Data were collected from 3 to 6 different experiments, with globally 6 to 11 different toxin applications. Since the exact composition of the intracellular solution has to be known for the analysis, only the patch data were analysed for high intracellular  $K^+$ . The continuous lines represent single exponential fits to the experimental data, weighted with the reciprocal of the standard deviation (not shown for clarity). Estimates of the parameters  $K^O(0$  mV) and  $v_s$  are given in table 3.5.

The voltage dependence of the block is strongly reduced in presence of the impermeant cations  $Li^+$ ,  $NMDG^+$  and  $Tris^+$ , but surprisingly not in  $Na^+$ . Since the voltage dependence of the block is steeper in  $Rb^+$ , this cation seems more efficient in dislocating the toxin.

To establish which kinetic parameter is responsible for the reduction in the voltage dependence of the  $K^O$  value, the relaxation induced by the depolarizing steps was analysed by

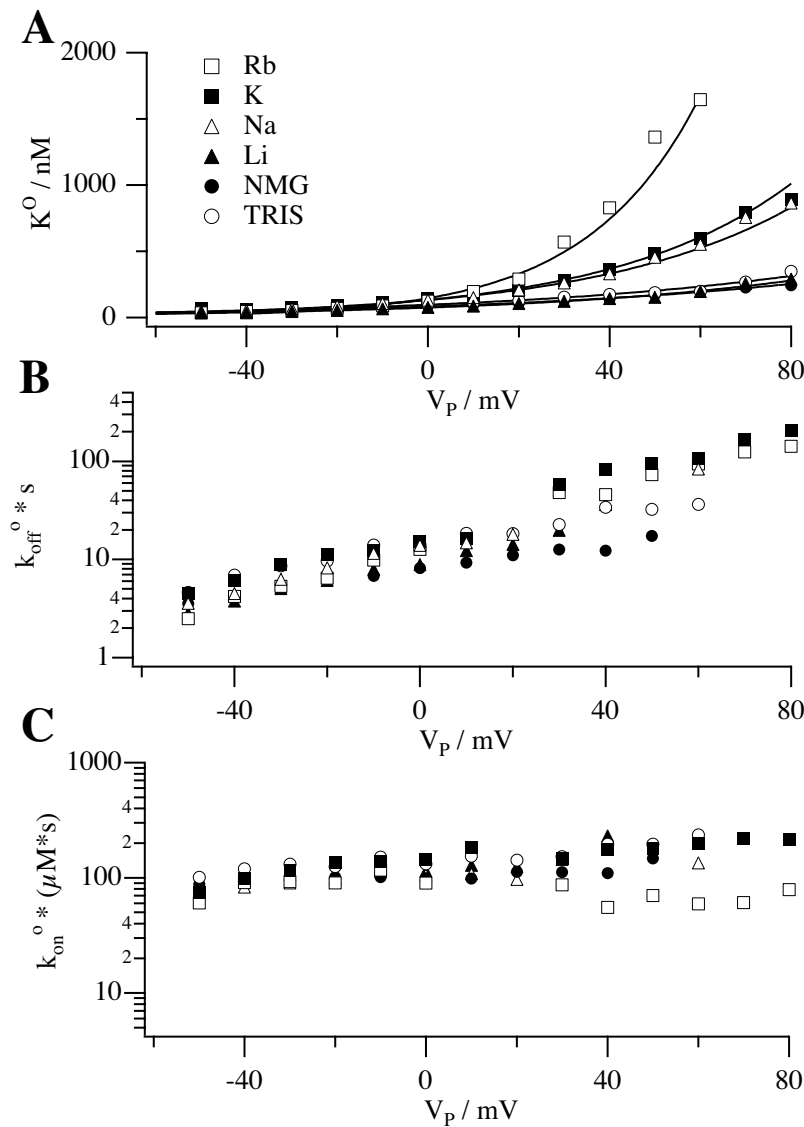


**Figure 3.18 Voltage dependence of  $\kappa$ -PVIIA-binding to open *Shaker- $\Delta$* channels with diverse intracellular monovalent cations.**

**A)** Plot of the mean values of dissociation constant of the toxin for the open channel vs the applied potential. The standard deviations are not shown for clarity. The continuous lines are the best exponential fits of the mean values of  $K^O$  weighted with the reciprocal of the standard deviation for the different intracellular cations. The values of the parameters  $K^O(0)$  and  $v_s$  are reported in table 3.5. **B and C)** Semi-logarithmic plot of the estimates of the first-order dissociation rate constant (**B**) and of the second-order association rate constant (**C**) against the applied potential. The Y scale used (2.5 decades) puts in evidence the strong voltage dependence of the dissociation rate in intracellular  $Rb^+$ ,  $K^+$  and  $Na^+$  respect to the almost constant association rate. The mean values are reported in table 3.5.

calculating the ratios between the toxin traces and the control traces, as shown in fig 3.16B. As in the presence of low extracellular potassium or symmetrical potassium the ratios under those conditions are well fitted with a single exponential. By applying the inverse relationship given by eq. 2.7.  $k_{off}^O$  and  $k_{on}^O$  for the open channel block were evaluated. For all ions tested the ratios show an increase in the block for test potentials below + 20 mV. For the impermeant ions at higher potentials the current is too small to allow to perform ratios. Therefore we used a tail protocol with variable prepulse duration, as described in methods 2.5.2 to study the relaxation of the block. Fig 3.19A shows the instantaneous tail currents measured in response to such a protocol ( $V_{Tail} = -100$  mV,  $V_p = +60$  mV) in function of the prepulse duration. The ratio between the instantaneous tail current in toxin and control (fig. 3.19B), allows to study the kinetics of the block of the open channel at  $V_p = +60$  mV.  $I_{Tx}/I_{Ct}$  can be well approximated with a single exponential (continuous line) with a time constant of 6.8 ms and a steady state value of 0.71, corresponding to  $k_{off}^O(+60 \text{ mV}) = 170 \mu M^{-1}s^{-1}$  and

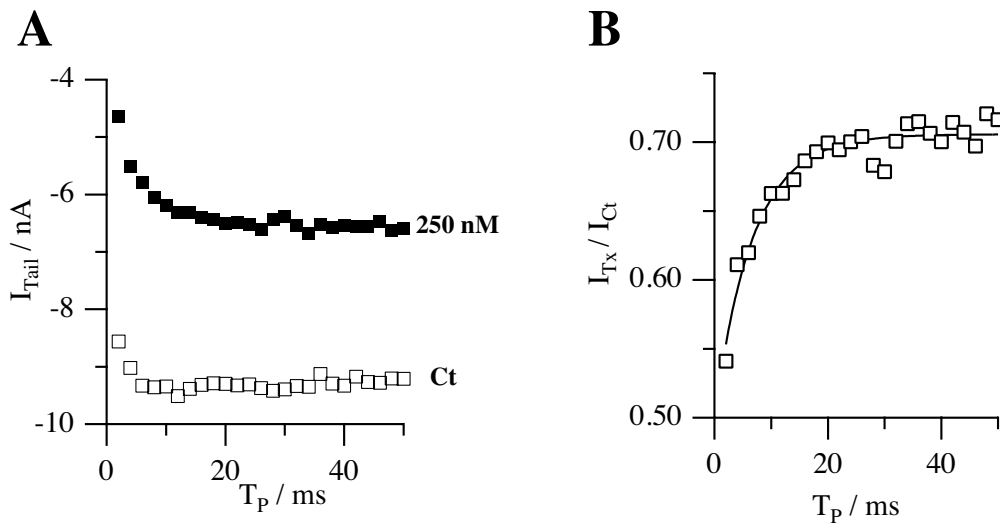


**Fig. 3.19 The kinetics of  $\kappa$ -PVIIA-binding to open channels can be determined from tail currents.** A) We evaluated the instantaneous tail current from a protocol with variable prepulse duration (see fig. 2.5) for the same experiment of fig. 3.16 and 3.17 with 115 mM NaCl in the pipette and 115 mM KCl in the bath. The instantaneous tail current in control and in 250 nM  $\kappa$ -PVIIA is plotted against the duration of the test pulse,  $T_P$ . The test potential  $V_p$  was +60 mV and was followed by a repolarization at  $V_{\text{Tail}} = -100$  mV. B) Ratio between the toxin and the control tail currents. The continuous line is the best exponential fit, with time constant of 6.8 ms and asymptotic value  $U^0 = 0.71$ , yielding to  $K^0 = 612$  nM,  $k_{\text{off}}^0 \cdot \text{s} = 104$  and  $k_{\text{on}}^0 \cdot (\mu\text{M} \cdot \text{s}) = 170$ .

$k_{\text{on}}^0(+60 \text{ mV}) = 100 \text{ s}^{-1}$ . With this method it was possible to measure the unblock process for intracellular  $\text{Na}^+$  at +60, +70 mV and for the other cations the reblock up to +60 mV.

In the presence of 115  $[\text{Rb}^+]_i$  the current reverses at +5 - +10 mV indicating that  $\text{Rb}^+$  is slightly less permeable than  $\text{K}^+$ . We therefore could evaluate well the relaxation for all potentials (except the reversal) with the ratio between the toxin and control traces. At +20 mV the open channel block is equal to the closed channel block, while for potentials  $> +20$  mV a decrease in the block is observed, as shown by the ratio traces in fig 3.16 panel C.

$k_{\text{on}}^0$  and  $k_{\text{off}}^0$  values evaluated from the same set of experiments used to obtain the equilibrium dissociation constant of fig 3.18A, are shown in fig. 3.18B and 3.18C. As in the case of high intracellular  $\text{K}^+$  the voltage dependence of the  $K^0$  is almost entirely due to the dissociation rate, except for  $\text{Rb}^+$ . Even if the  $k_{\text{on}}^0$  (mean values in table 3.5) shows a slight increase with the potential which is less than a factor of two in the potential range tested. In contrast to this within this potential range the  $k_{\text{off}}^0$  increases from a factor of about 5 in  $\text{Tris}^+$  and  $\text{NMDG}^+$  to a factor of about 40 in  $\text{K}^+$ .

The equilibrium dissociation constant (fig 3.18A) increases with the potential in the presence of 115 mM  $[\text{Rb}^+]_i$ , surprisingly not because of an increase in the dissociation rate  $k_{\text{off}}^0$  but a decrease in the association rate for positive potentials. The potentials at which the reduction in the  $k_{\text{on}}^0$  is observed correspond to an outward current carried by  $\text{Rb}^+$  ions: in fig 3.18C indeed the  $k_{\text{on}}^0$  values (white squares) at these potentials lay systematically below the others. This decrease in the  $k_{\text{on}}^0$  causes the reduction in toxin binding efficiency at depolarizing potentials. The dissociation rate  $k_{\text{off}}^0$ , (white squares in fig 3.18B), is indistinguishable from the one



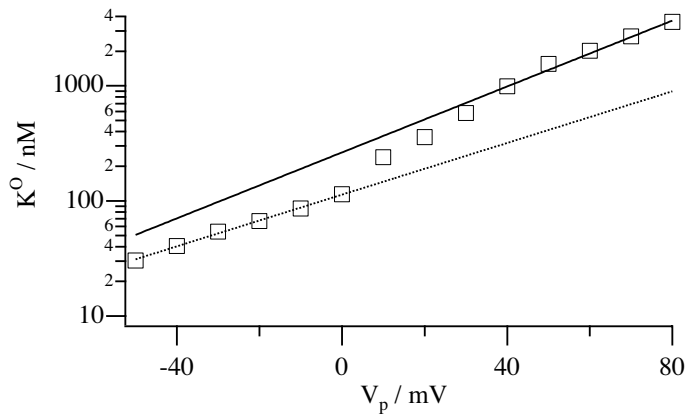


**Figure 3.20 Open channel block in  $[Rb]_i=115\text{mM}$  and  $[K]_o=115\text{mM}$ .** Semi-logarithmic plot of the dissociation constant of the toxin for the open channel block vs the applied potential for the same patch experiment shown in fig.3.16. The fit of the data with a single exponential (continuous line;  $247 \cdot \exp(V/30)$ ) is not satisfactory. The dotted line corresponds to the exponential fit of the data between  $-50$  and  $0$  mV, with  $113 \cdot \exp(V/39)$ . These values are in agreement with the estimates obtained in symmetrical  $115$  mM KCl.

observed in high intracellular  $K^+$  (black squares). Fig 3.20 shows the  $K^O$  calculated from the patch experiment in fig 3.16 with  $115 [Rb]_i$ . The semi-logarithmic scale demonstrates that the single exponential fit (continuous line;  $247 \cdot \exp(V/30)$ ) is not satisfyingly fitting the  $K^O$  data, leaving out the points recorded for negative potential steps. At the other side the fit of the data between  $-50$  and  $0$  mV (dotted line) gives an estimate of the parameters  $K^O(0) / \text{nM} = 113$  and  $v_s / \text{mV} = 39$  in agreement with the values estimated in intracellular high  $K^+$ .

From the direct comparison of the control records with the respective records under toxin which have been scaled by a factor corresponding to the open channel block, an increase or a decrease in the block during the pulse is observed. This change in toxin affinity depends on the applied potential and on the intracellular cation.

ion	open channel block				closed channel block			$V_{\text{Inv}}$ mV
	$K^O(0)^{\#}$ nM	$v_s^{\#}$ mV	$k_{\text{on}}^O$ $\mu\text{M}^{-1} \text{s}^{-1}$	$k_{\text{off}}^O(0)^{\#}$ $\text{s}^{-1}$	$K^C$ nM	$k_{\text{on}}^C^*$ $\mu\text{M}^{-1} \text{s}^{-1}$	$k_{\text{off}}^C^*$ $\text{s}^{-1}$	
Tris <sup>+</sup>	$97 \pm 8$	$68 \pm 9$	$150 \pm 40$	$14 \pm 2$	$216 \pm 14$	$1.7 \pm 1.0$	$0.8 \pm 0.1$	>70
NMDG <sup>+</sup>	$84 \pm 7$	$70 \pm 10$	$101 \pm 23$	$7.6 \pm 0.6$	$279 \pm 68$	$2.3 \pm 0.1$	$0.7 \pm 0.1$	>70
Li <sup>+</sup>	$76 \pm 7$	$61 \pm 8$	$125 \pm 41$	$9.6 \pm 1.5$	$230 \pm 66$	$1.6 \pm 0.3$	$0.5 \pm 0.1$	$61 \pm 6$
Na <sup>+</sup>	$133 \pm 6$	$44 \pm 3$	$99 \pm 17$	$14.3 \pm 0.9$	$260 \pm 58$	$2.7 \pm 0.6$	$0.9 \pm 0.6$	$39 \pm 6$
K <sup>+</sup>	$150 \pm 15$	$44 \pm 5$	$150 \pm 40$	$18 \pm 2$	$223 \pm 55$	$1.9 \pm 0.5$	$0.6 \pm 0.3$	$28 \pm 3$
Rb <sup>+</sup>	$150 \pm 10$	$26 \pm 1$	$90 \pm 18$	$13 \pm 1$	$274 \pm 129$	$2.7 \pm 0.6$	$0.9 \pm 0.1$	$21 \pm 2$

**Table 3.5 Dependence on the intracellular solution composition of  $\kappa$ -PVIIA-binding to *Shaker*- $\Delta$  channels.** Patch-clamp experiments performed in the *outside-out* configuration, number of experiments  $\geq 5$ , with 1-3 toxin applications for experiment. Mean values ( $\pm$  SD), otherwise best estimate ( $\pm$  SD) obtained from the fit of the experimental data with a single exponential ( $\#$ ) or with eq. 2.6 ( $*$ ).

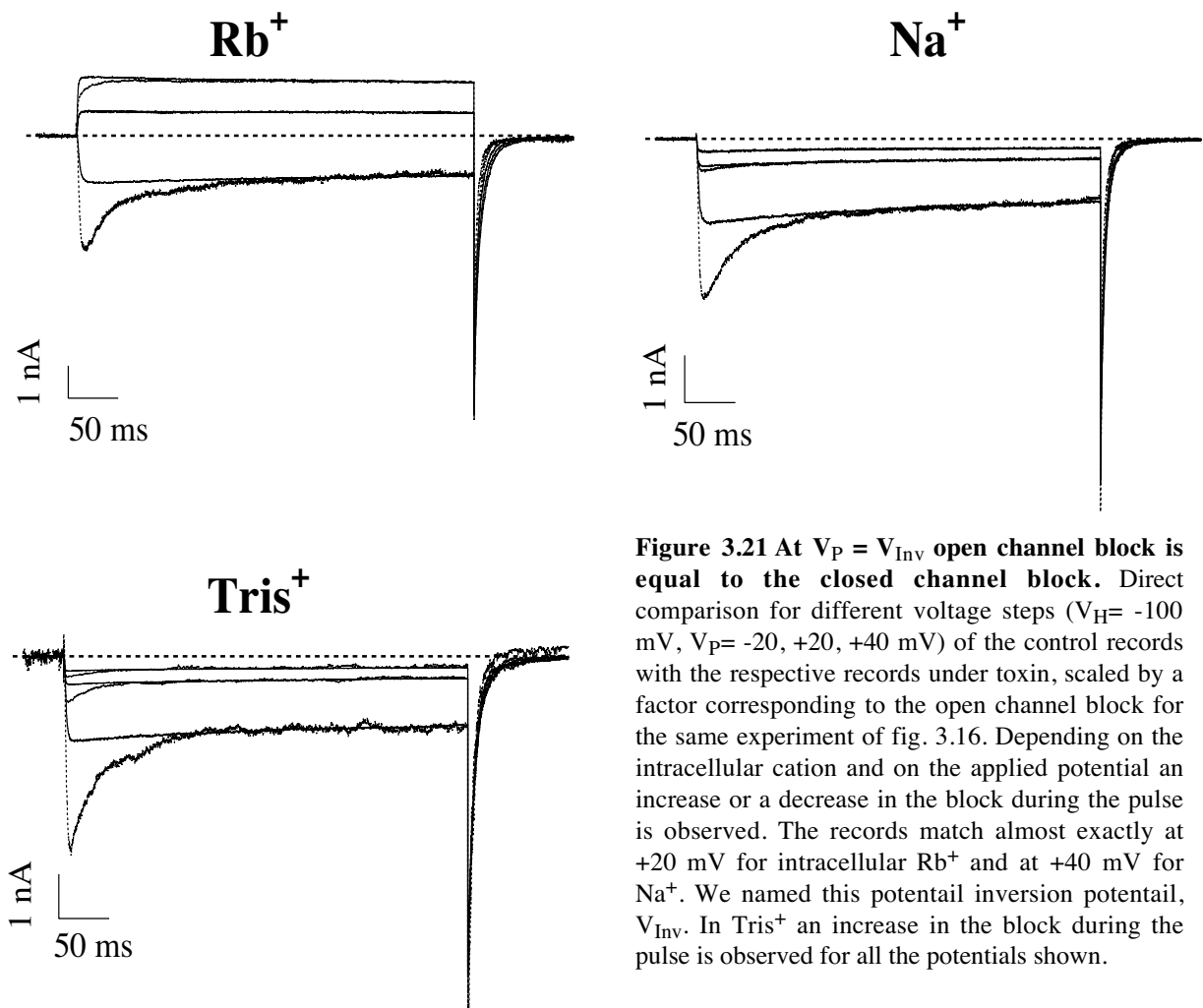


**Figure 3.21** At  $V_P = V_{Inv}$  open channel block is equal to the closed channel block. Direct comparison for different voltage steps ( $V_H = -100$  mV,  $V_P = -20, +20, +40$  mV) of the control records with the respective records under toxin, scaled by a factor corresponding to the open channel block for the same experiment of fig. 3.16. Depending on the intracellular cation and on the applied potential an increase or a decrease in the block during the pulse is observed. The records match almost exactly at  $+20$  mV for intracellular  $Rb^+$  and at  $+40$  mV for  $Na^+$ . We named this potential inversion potential,  $V_{Inv}$ . In  $Tris^+$  an increase in the block during the pulse is observed for all the potentials shown.

The unblock or reblock during the test pulse is determined by a smaller or bigger block of open channels at the applied potential with respect to the equilibrium dissociation constant for the closed channels.

In fig 3.21 control traces and scaled toxin traces for different voltage steps are shown ( $V_H = -100$  mV,  $V_P = -20, +20, +40$  mV; same experiments of fig.3.16) with intracellular  $Rb^+$  (A)  $Na^+$  (B) and  $Tris^+$  (C). The records match almost exactly at a test potential of  $+20$  mV for intracellular  $Rb^+$  (A) and  $+40$  mV for  $Na^+$  (B). At this potentials the dissociation constant of the open channel block is identical to the closed channel block. An increase in the block during the pulse was observed in  $Tris^+$  (C) for all the potentials shown. This direct comparison is possible only during patch recordings with a high current density ( $> 1$  nA) with a good signal to noise ratio. Otherwise it is only possible to have an estimate of this “inversion” potential looking at which potential equilibrium dissociation constant for the closed channel crosses equilibrium dissociation constant of the open channel. This is shown in fig 3.17 by the continuous horizontal line for the same experiment of fig 3.17 and 3.21 with  $Na^+$  in the intracellular solution. Mean values of the “inversion” potential for the different ion

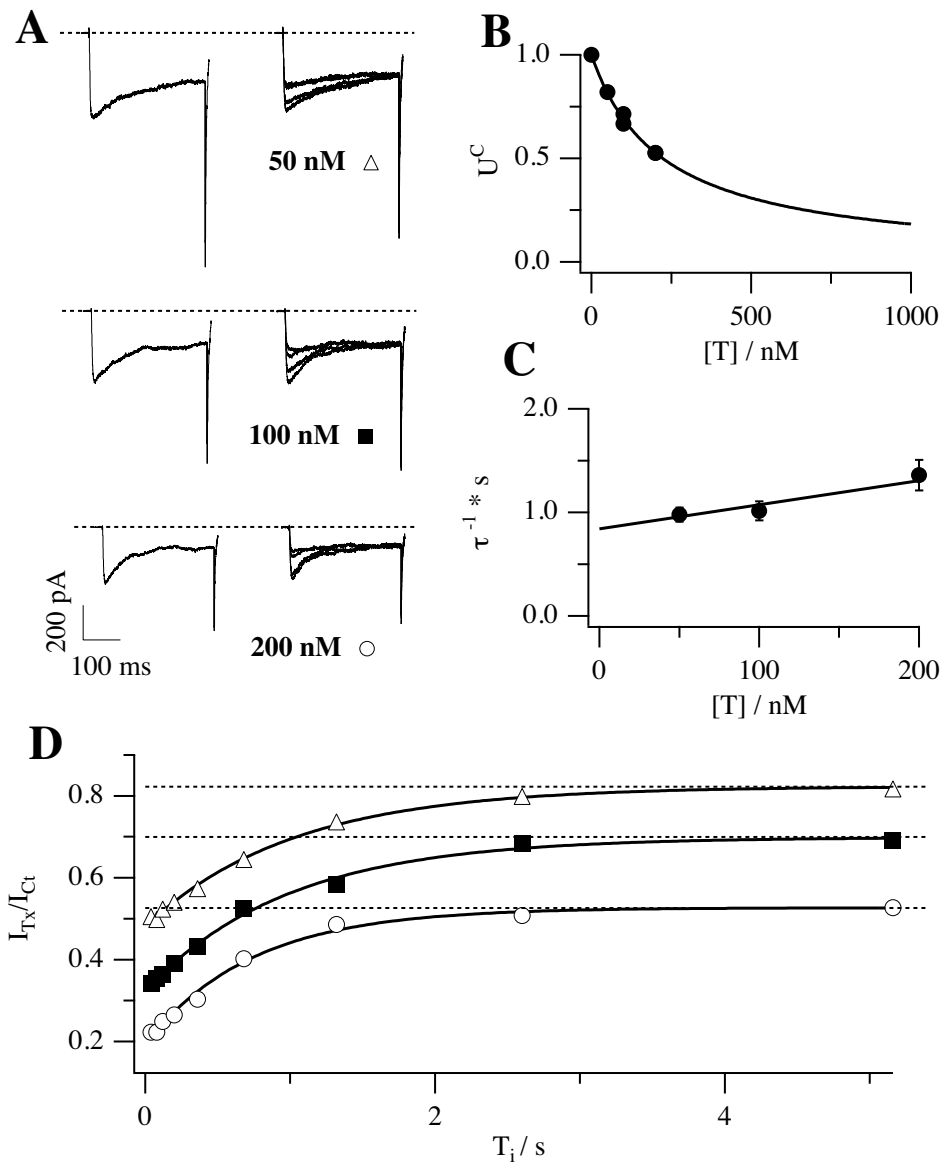


**Fig. 3.22 Relaxation of  $\kappa$ -PVIIA-binding to closed *Shaker- $\Delta$*  channels after a depolarizing pulse in high intracellular  $\text{Tris}^+$ .** **A)** Superimposed records of responses to double pulse stimulation in 50, 100 and 200 nM  $\kappa$ -PVIIA to the 115 mM KCl bath, with 115 mM TrisCl in the pipette. Each stimulation consisted of a conditioning 300 ms pulse to -20 mV, followed by an identical test pulse with a variable pulse interval,  $T_i$  (shown 120, 340 ms and 1, 5 s) spent at  $V_H = -100$  mV. **B)**  $[T]$ -dependence of  $U^C$  for the same experiment shown in panel A. The solid line is the best fit with eq. 2.4, giving  $K^C = 223 \pm 7$  nM. The error is the standard deviation evaluated from the fit, by comparing the theoretical and the experimental values. **C)**  $[T]$ -dependence of the reciprocal of time constant  $\tau$  estimated by fitting with a single exponential the relaxation of the toxin block to closed channels (panel D). The solid line is the best fit with the expression 2.3, giving  $k_{\text{off}}^C = 0.8 \pm 0.1 \text{ s}^{-1}$  and  $k_{\text{on}}^O = 2 \pm 1 \mu\text{M}^{-1}\text{s}^{-1}$ ; the ratio  $k_{\text{off}}^C / k_{\text{on}}^C$  gives an estimate of  $K^C = 365 \pm 200$  nM in agreement with the estimate obtained from the fit of  $U^C$  data in panel B. **D)** Amplitude of the early current normalized to the control response and plotted as a function of  $T_i$  for the diverse toxin concentrations. The dotted horizontal lines correspond to the asymptotic value  $U^C$ . The continuous lines are the best single exponential fits with  $\tau = 0.97$  s and  $U = 0.8$  in 50 nM  $\kappa$ -PVIIA ( $\Delta$ ),  $\tau = 1.0$  s and  $U = 0.7$  in 100 nM ( $\blacksquare$ ) and  $\tau = 1.36$  s and  $U = 0.72$  in 200 nM  $\kappa$ -PVIIA ( $\circ$ ).

tested are given in table 3.5. In case the properties of the closed channel are not modified by the composition of the intracellular solution (see below, section 3.5.2), the potential at which the open channel block is equal to the closed channel block can be used to estimate the

relative efficiency of the different cations in destabilizing the toxin. Table 3.5 yields the following scale:  $\text{Rb}^+ \geq \text{K}^+ > \text{Na}^+ > \text{Li}^+ > \text{NMDG}^+ \approx \text{Tris}^+$ .

### 3.5.2 Closed channel block

The block of early current during depolarizing test potentials was evaluated in all the experimental conditions shown in paragraph 3.5.1. Double pulse protocols were performed to evaluate the kinetic parameters of the toxin block to closed channels.

The toxin block to closed channels measured with 115 mM  $[\text{Tris}^+]_i$  (fig. 3.22) and 115 mM  $[\text{Rb}^+]_i$  (fig. 3.23) strongly resembles the one observed under symmetrical potassium. The conditioning pulse induces an increase of toxin block that appears as a reproducible peak in the first response, while in the second response the peak is present only for long  $T_i$ . In the experiment shown in fig. 3.22 we performed a double pulse protocol at  $V_p = -30$  mV with three different toxin concentrations. Successive stimulations were separated by interpulse intervals of 5 s at a holding potential of -100 mV. At higher toxin concentrations we observed an increase in the block and a faster recovery of tonic block of  $\kappa$ -PVIIA to closed channels.

Panel C shows the ratio of the currents between toxin and control for the conditioning responses as a function of the interpulse duration  $T_i$ . The steady state values of the  $I_{\text{Tx}} / I_{\text{Ct}}$  ratios correspond to the block under tonic conditions and are plotted against the toxin concentrations in panel B. The continuous line corresponds to the fit with a dose response

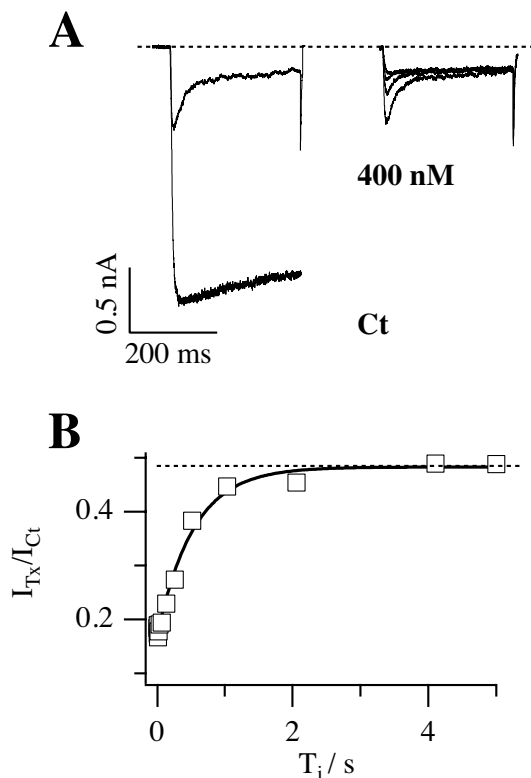


**Fig. 3.23 Relaxation of  $\kappa$ -PVIIA-binding to closed *Shaker- $\Delta$*  channels after a depolarizing pulse in high intracellular  $\text{Rb}^+$ .** A) Superimposed records of responses to double pulse stimulation before and after the addition of 400 nM  $\kappa$ -PVIIA to the 115 mM KCl bath, with 115 mM RbCl in the pipette. Each stimulation consisted of a conditioning 300 ms pulse to -30 mV, followed by an identical test pulse with a variable pulse interval,  $T_i$  (shown 10, 74, 266 ms and 1s) spent at  $V_H = -100$  mV. B) Amplitude of the early current normalized to the control response and plotted as a function of  $T_i$ . The dotted horizontal line corresponds to the asymptotic value  $U^C$ , giving  $K^C = 369$  nM. The continuous line is the best single exponential fit with  $\tau = 0.53$  s, corresponding to  $k_{\text{on}}^0 = 2.4 \mu\text{M}^{-1}\text{s}^{-1}$  and  $k_{\text{off}}^0 = 0.94 \text{ s}^{-1}$ .

function (eq. 2.4), that gives an estimate for the closed state equilibrium dissociation constant of  $223 \pm 7$  nM. The relaxation plotted in panel C is well fitted by a single exponential. The reciprocal of the time constants is plotted in panel D against the toxin concentrations. The intercept with the ordinate axis and the slope of the line fit gives an estimate of the off rate ( $0.8 \pm 1$ ) and of the on rate ( $2.3 \pm 1$ ) respectively. The values obtained are in agreement with the mean values observed for symmetrical  $K^+$ . Fig. 3.23 shows a similar experiment with 115 mM  $Rb^+$  in the pipette and with 400 nM  $\kappa$ -PVIIA in the bath containing 115 mM KCl. According to the inverse expressions given by eq. 2.7 the  $k_{on}^C$  and the  $k_{off}^C$  can be evaluated from the steady state unblock probability and from the time constant of the relaxation:  $k_{on}^C = (2.35 \pm 0.23) \mu M^{-1} s^{-1}$  and  $k_{off}^C = (0.94 \pm 0.09) s^{-1}$ .

Table 3.5 shows the estimates found for  $K^C$ ,  $k_{on}^C$  and  $k_{off}^C$  for all the conditions tested. From the table it becomes clear that these parameters are independent from the ionic composition of the intracellular solution, but are determined by the extracellular  $[K^+]_O$  which in all experiments was equal to 115 mM.

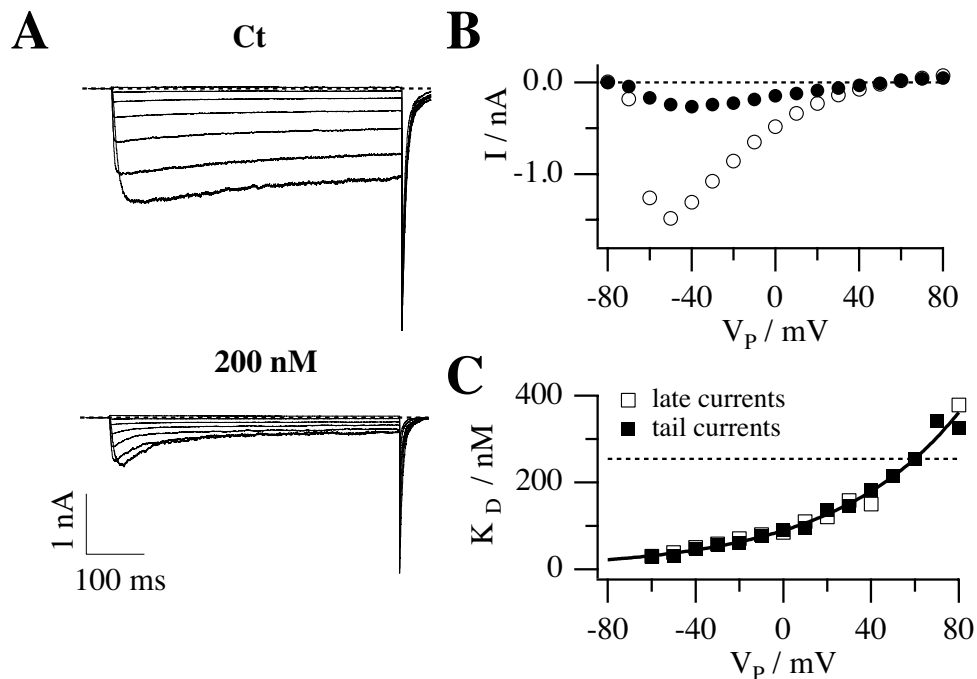


**Figure 3.24** Effect of  $\kappa$ -PVIIA on *Shaker- $\Delta$*  currents in  $[K]_i=10$  mM. **A)** *Outside-out* patch experiment performed in  $[K]_i=10$  mM in a Tris<sup>+</sup>-based solution and  $[K]_O=115$  mM. Currents records in response to an IV-protocol, before (top) and after (bottom) the addition to the bath of 200 nM  $\kappa$ -PVIIA ( $V_H = -100$  mV;  $V_P$  from  $-50$  mV, every 20 mV). **B)** Plot of the late currents (O control, ● 200 nM  $\kappa$ -PVIIA) in function of the applied potential.  $V_{rev} = +50$  mV. **C)** Plot of the dissociation constant calculated from the late currents (panel B, □) or from the instantaneous tail currents (■) as described in par. 2.5.1. The continuous line correspond to the exponential fit of the data,  $K^O/nM = 89 \cdot \exp(V/57mV)$ . The horizontal dotted line corresponds to  $K^C = 254$  nM. At  $V_P = V_{Inv} = 60$  mV,  $K^C = K^O$ .

### 3.5.3 Intermediate $[K]_i$

Additional experiments to test sensitivity of  $\kappa$ -PVIIA to ion occupancy in the pore were performed. The  $K^+$  concentration in a  $TRIS^+$  based intracellular solution was increased while the extracellular potassium was kept constant at 115 mM.

Concentrations of few mM intracellular  $K^+$  did not modify the binding parameters compared to the pure  $TRIS^+$  solution. Panels A of fig 3.24 and 3.25 show current responses to an IV protocol recorded in *outside-out* patches with respectively 10 and 20 mM  $K^+$  in the pipette. The presence of  $K^+$  on the intracellular side of the membrane lowers the reversal potential, to +50 mV in 10 mM KCl and +35 mV in 20 mM KCl, as shown by the plot of the steady state currents in panels B. The  $K^O$  values, plotted in panels C, were calculated from the tail currents or also with the steady state currents (fig. 3.24). Fits with a single exponential resulted a voltage sensitivity of  $\kappa$ -PVIIA block of 57 mV in 10 mM  $K^+$  and 44.7 mV in 20 mM  $K^+$ . The inversion potential decreases gradually for increasing  $K^+$  concentrations. This might indicate an increasing repulsion of the toxin by a higher probability of  $K^+$  ions in the vestibule of the ion channel pore. In the two experiments shown  $V_{Inv} = +60$  mV in 10 mM KCl and +50 mV

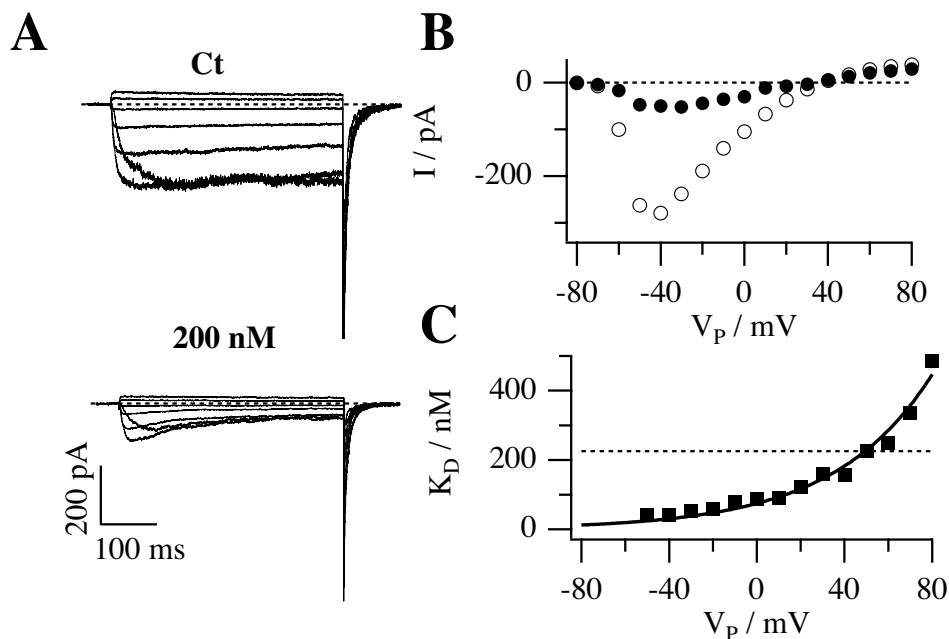


**Figure 3.25** Effect of  $\kappa$ -PVIIA on *Shaker- $\Delta$*  currents in  $[K]_i=20mM$ . **A)** *Outside-out* patch experiment performed in  $[K]_i=20$  mM in a  $Tris^+$ -based solution and  $[K]_o=115mM$ . Superimposed records of currents in response to an IV-protocol, before (top) and after (bottom) the addition to the bath of 200 nM  $\kappa$ -PVIIA ( $V_H = -100$  mV;  $V_p$  from  $-50$  mV, every 20 mV). **B)** Plot of the late currents (  $\circ$  control,  $\bullet$  200 nM  $\kappa$ -PVIIA) in function of the applied potential.  $V_{Rev}=+35$  mV. **C)** Because of the small amplitude of the current at potential close to the reversal, we evaluated the dissociation constant calculated from the instantaneous tail currents (  $\blacksquare$ ; par. 2.5.1).The continuous line correspond to the exponential fit of  $K^O$  vs  $V_p$ ,  $K^O / nM = 75 * \exp(V / 45 \text{ mV})$ . The horizontal dotted line corresponds to  $K^C = 225$  nM. At  $V_p = V_{Inv} = 50$  mV,  $K^C = K^O$ .

in 20 mM which is higher than the 28 mV found for the 115 mM K<sup>+</sup> solution.

These values indicate that the repulsion of  $\kappa$ -PVIIA by K<sup>+</sup> ions is still smaller than in the high K<sup>+</sup> solution and might indicate the presence of a low affinity K<sup>+</sup>-binding site

### 3.6 Effects of toxin binding on "tail currents"

The instantaneous tail currents elicited by an IV protocol are proportional to the steady state current values, therefore under control conditions they reflect the activation properties of the channel. If the tail currents in the presence of toxin with the ones obtained under control conditions are compared, a reduction of the current, an increase of the instantaneous current in toxin for higher depolarizing prepulses, and a faster deactivation are observed (see fig. 3.26).

The first two features are straightforward consequences of the voltage dependence of the toxin block: the currents in toxin are reduced because of the blocking action, and they do not reach a steady state value because the toxin block is reduced for increasing depolarizing steps. Therefore this current can be used to evaluate the unblock probability and the K<sup>0</sup> in steady state conditions (see methods 2.5.1). Tail currents are well fitted by a single exponential (see

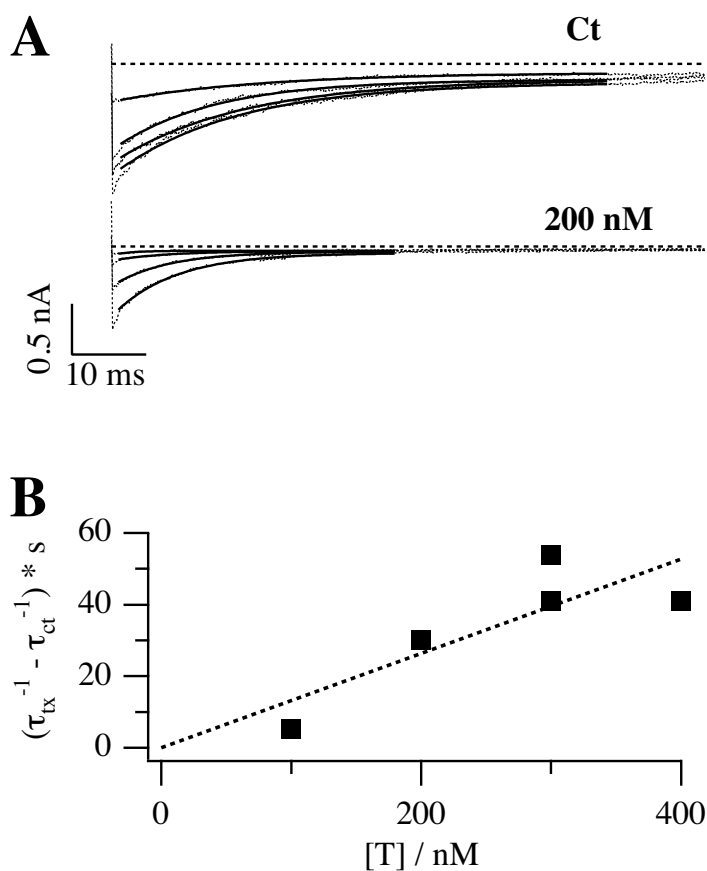


**Figure 3.26  $\kappa$ -PVIIA accelerates deactivation.** **A)** Tail currents (dotted traces) measured before (top) and after (bottom) the addition to the bath of 200 nM  $\kappa$ -PVIIA at  $V_{Tail} = -60$  mV and following a pulse of  $-50$ ,  $-20$ ,  $+20$  and  $+60$  mV (fig. 2.4). The *outside-out* patch experiment was performed in symmetrical 115 mM KCl. The tail currents in control and in toxin were fitted with a single exponential, shown by the continuous lines. **B)** In the same experiment shown in panel A, diverse [T] were used. The difference between the reciprocals of the time constant of deactivation in toxin and in control,  $(\tau_{Tx}^{-1} - \tau_{Ct}^{-1})$ , is plotted vs [T]. The linear fit has a slope of  $132 \mu M^{-1} s^{-1}$ , which is an estimate of the second order association rate (see discussion, 4.6).

fig. 2.4). In the presence of  $\kappa$ -PVIIA we observed a systematic decrease in the deactivation time constants of the currents, which could be quantified only for higher toxin concentrations, because under these conditions the tails are faster and the difference with the control is bigger. Interestingly a slowing of the tail currents in the presence of  $\kappa$ -PVIIA was observed for test potentials from  $-100$  mV up to  $-50$  mV. In two experiments performed in symmetrical 115 mM KCl, one with  $V_{\text{Tail}}=-60$  mV, the second with  $V_{\text{Tail}}=-100$  mV, the deactivation time constant for several toxin concentrations was measured. Fig 3.26 A shows tails currents in control and in the presence of 400 nM  $\kappa$ -PVIIA measured for the experiment with  $V_{\text{Tail}}=-60$  mV, with a prepulse to  $-50$ ,  $-20$ ,  $+20$  and  $+60$  mV. In fig 3.26 B the differences between the reciprocals of the time constants of deactivation in toxin and in control,  $(\tau_{\text{Tx}}^{-1}-\tau_{\text{Ci}}^{-1})$ , are plotted against the toxin concentrations and fitted with a line (dotted line) with a slope of  $132 \mu\text{M}^{-1}\text{s}^{-1}$ . In the discussion (4.6) it will be shown that this slope is a measure of the  $k_{\text{on}}^{\text{O}}$  at the potential at which the deactivation is measured.

### 3.7 Effect of symmetrical $[\text{Rb}]_{\text{O}}$

The sections 3.4. and 3.5.1 have shown that the toxin interaction with the channel might depend on the permeating cation type, even if  $\text{K}^+$  and  $\text{Rb}^+$  are quite similar and usually treated as identical. To investigate further the difference between these two cations, patch clamp experiments in symmetrical 115 RbCl were performed.

Fig 3.27 A shows the responses to an IV protocol ( $V_{\text{H}}=-100$  mV,  $V_{\text{P}}$  from  $-50$  mV, every 20 mV) in control conditions and with 500 nM  $\kappa$ -PVIIA in the bath. The reversal potential is  $+3$  mV. The block of the evoked currents by  $\kappa$ -PVIIA is very small (late currents are shown in panel B) and the toxin traces do not present the typical hump present in the presence of high external  $\text{K}^+$ . As a matter of fact the ratio between toxin and control traces shows a fast increase in the unblock probability at every potential tested, as shown in panel C for  $V_{\text{P}}=-30$ ,  $-10$ ,  $+30$  and  $+50$  mV. Panel D shows that the equilibrium dissociation constant which was calculated from the steady state currents increases roughly linearly with the applied potential: at 0 mV the  $K^{\text{O}}$  is  $1.2 \mu\text{M}$  and the linear slope is  $0.018 \mu\text{M}/\text{mV}$ , corresponding to a variation of 1.4 % per mV. The equilibrium dissociation constant for the open channel is always higher than for the closed channel. We estimated the  $k_{\text{off}}^{\text{O}}$  and  $k_{\text{on}}^{\text{O}}$  from the single exponential fit of the ratios ratio between toxin and control currents, shown by the continuous line in panel C. As shown in Panel E,  $k_{\text{on}}^{\text{O}}$  is fairly constant, with an average value of  $102 (\mu\text{M}\cdot\text{s})^{-1}$ , while the  $k_{\text{off}}^{\text{O}}$  has the same linear voltage dependence of the equilibrium dissociation constant, with  $k_{\text{off}}^{\text{O}}(0 \text{ mV})=134 \text{ s}^{-1}$  and a linear slope of  $1.8 (\text{s}\cdot\text{mV})^{-1}$ , corresponding to a variation of 1.4 % per mV. The mean values for 4 experiments and 7 toxin applications are shown in table 3.3.



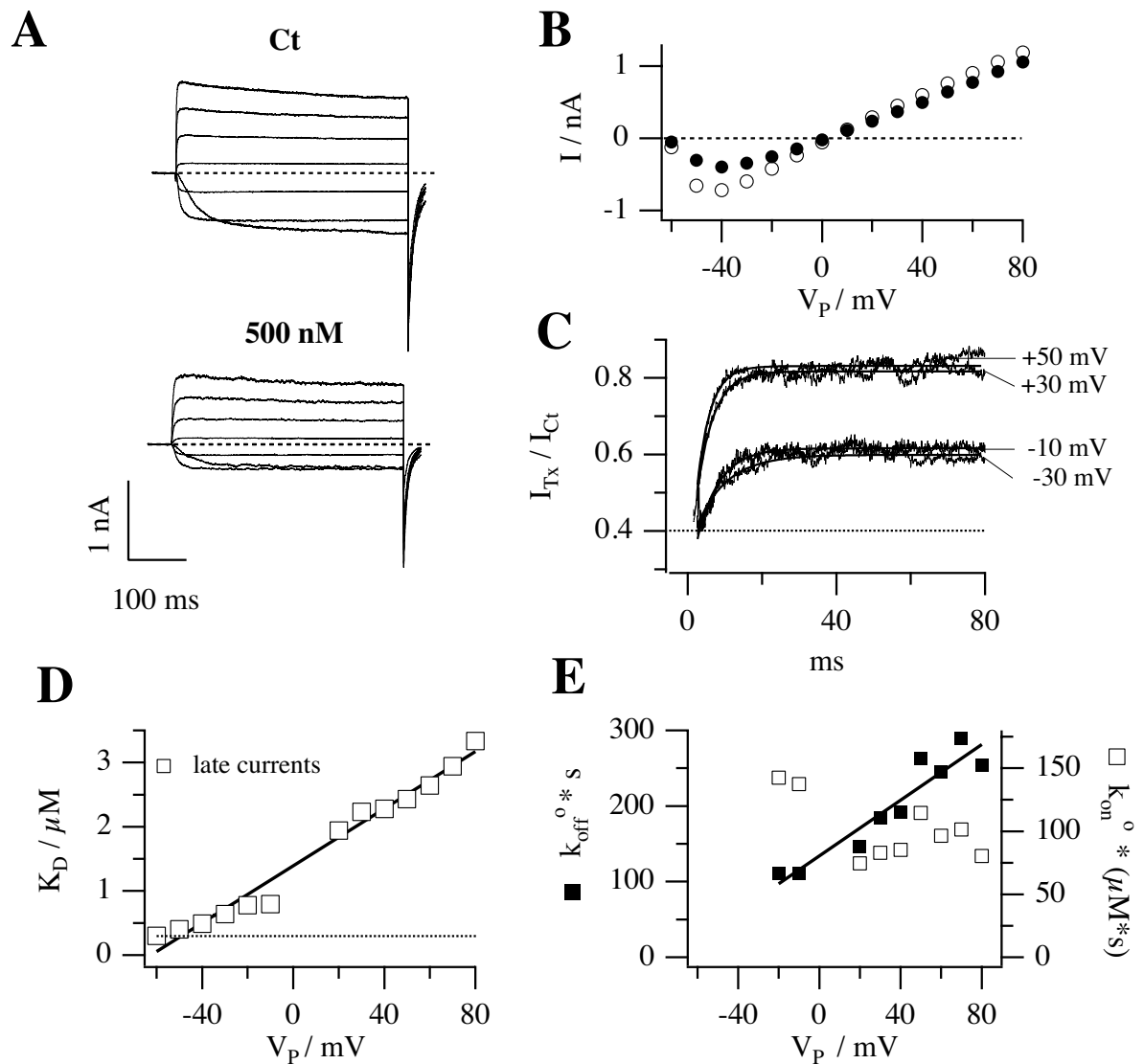


**Figure 3.27**  $\kappa$ -PVIIA-binding to *Shaker-Δ*channels in symmetrical high  $\text{Rb}^+$ . **A**) Current records of responses to an IV protocol in symmetrical 115 mM  $\text{RbCl}$ , before and after the addition of 500 nM  $\kappa$ -PVIIA to the bath ( $V_H = -100$  mV;  $V_P$  from  $-50$  mV, every 20 mV). **B**) The plot of the late currents ( $\circ$  control,  $\bullet$  500 nM  $\kappa$ -PVIIA) shows that block at  $V_P > -20$  mV is very low. **C**) Ratios between toxin and control currents (shown for voltage steps of  $-30$ ,  $-10$ ,  $+30$  and  $+50$  mV) show at every potential tested a decrease in the block that is well fitted by a single exponential (smooth lines). **D**) Plot of the dissociation constant calculated from the late currents. The continuous line corresponds to the linear fit to the data,  $K_D^O / \mu\text{M} = 1.2 + 0.018 \cdot V/\text{mV}$ , corresponding to a variation of 1.4 % per mV. The horizontal dotted line corresponds to the closed state dissociation constant, equal to 290 nM. **E**) Plot of the estimates of the  $k_{\text{off}}^O$  and  $k_{\text{on}}^O$ , calculated from the exponential fit of the ratios between toxin and control currents, shown in panel C. The continuous line is the linear fit of the  $k_{\text{off}}^O$  ( $k_{\text{off}}^O \cdot \text{s} = 134 + 1.8 \cdot V/\text{mV}$ ) with an increase of 1.3 % per mV. The  $k_{\text{on}}^O$  is fairly constant with a mean value of  $102 \mu\text{M}^{-1} \cdot \text{s}^{-1}$ .

Thus in presence of symmetric  $\text{Rb}^+$ , the toxin block is at 0 mV about 10 times less efficient than in symmetrical  $\text{K}^+$  and the voltage sensitivity of the block appears to be much smaller. In fig. 3.28 the dissociation constants (A) and the dissociation rates (B) for open channel block are plotted in function of the test potential in symmetrical  $\text{K}^+$  and symmetrical  $\text{Rb}^+$  and in addition in intracellular  $\text{Rb}^+$ , extracellular  $\text{K}^+$  and intracellular  $\text{K}^+$ , extracellular  $\text{Rb}^+$ .

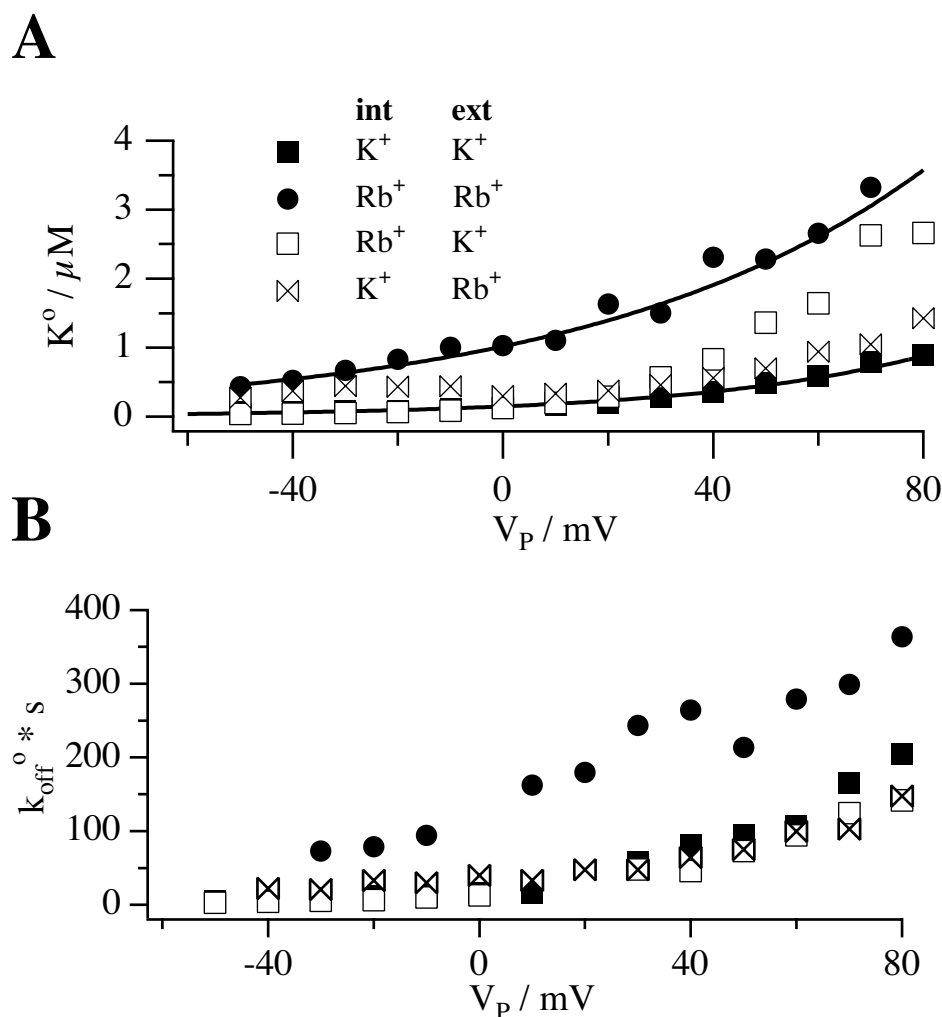


**Figure 3.28 Comparison of the  $\kappa$ -PVIIA efficiencies in Rb<sup>+</sup>-based or K<sup>+</sup>-based solutions.** **A)** Plot of the mean values of dissociation constant vs  $V_P$  for monocationic solutions of either Rb<sup>+</sup> or K<sup>+</sup>. The continuous lines correspond to the single exponential fit for the experiments performed in symmetrical K<sup>+</sup> ( $K^0/nM = 149 \cdot \exp(V_P/45mV)$ ) and symmetrical Rb<sup>+</sup> ( $K^0/\mu M = 1.02 \cdot \exp(V_P/63mV)$ ). **B)** Plot of the  $k_{off}^0$  vs  $V_P$ . In symmetrical high Rb<sup>+</sup> the toxin is maximally destabilized. Also in int K<sup>+</sup>- ext Rb<sup>+</sup>, when inward currents are driven, the toxin results to be more destabilized respect to the symmetrical 115 mM KCl case.

Fig. 3.28A shows that  $\kappa$ -PVIIA efficiency is strongly reduced whenever Rb<sup>+</sup> current is driven. Surprisingly this pattern is not completely confirmed by the plot of the dissociation rates (panel B; fig. 3.18). In fact an increase of the destabilization is observed in symmetrical Rb<sup>+</sup> (black circles), in intracellular K<sup>+</sup> and extracellular Rb<sup>+</sup> for inward currents (white double triangles) but not in intracellular Rb<sup>+</sup> and extracellular K<sup>+</sup> for inward currents (white squares). These findings are a strong indication that the interaction of the toxin with Rb<sup>+</sup> ions in the ion channel pore is different with respect to the K<sup>+</sup> and probably is related to multiple occupancy of the pore by these ions.

Such a diverse interaction of the toxin with these two permeable cations is quite surprising because Rb<sup>+</sup> and K<sup>+</sup> have similar radius, can both readily enter the channel, as shown by the reversal potential, and they are believed to interact in almost equivalent ways with the channel.

## 4 Discussion

In this study the binding of  $\kappa$ -PVIIA to the different conformational states of the *Shaker* K<sup>+</sup> channels has been investigated. We showed that the interaction between the toxin and the channel protein is bimolecular (fig. 3.2; Terlau et al. 1999), therefore one molecule is enough to occlude the channel. We focused our research on the modulation of this interaction by the electrical potential and by the composition of the intracellular and extracellular milieus.

### 4.1 $\kappa$ -PVIIA is a pore blocker

$\kappa$ -PVIIA binds to the extracellular mouth of the ion pore of *Shaker* K<sup>+</sup> channels blocking the flow of K<sup>+</sup> currents (Shon et al. 1998; Terlau et al. 1999). Phenomenologically the effect of the toxin on the currents mediated by the wild type *Shaker* K<sup>+</sup> channels, or by mutant channels that lack the N-type inactivation domain appears quite different (fig. 3.1). For the inactivating channel the main observed effect of the toxin is the inhibition of the K<sup>+</sup> current, while in the non-inactivating channels it seems to be a voltage-dependent modification of the rate of activation. However, a more careful analysis shows that this modification of the gating is only apparent and that our results are consistent with the hypothesis that the most prominent effect of toxin-channel association is the block of the channel conductance. Indeed, a substantial modification of channel gating properties, as observed for example in the case of the spider venom toxin Hanatoxin (Swartz and MacKinnon 1997), cannot account for the [T]-dependence of the currents shown in fig. 3.2A as a change in the fraction of channels that have a toxin-modified activation. On the contrary, the analysis illustrated in panels B, C and D of the same figure shows that the toxin-dependent modification of the currents has all the characteristics expected for the relaxation of a bimolecular binding reaction following a step change of the reaction parameters. Moreover, in response to a double pulse stimulation with a short interpulse interval, the current elicited by the second pulse in presence of toxin has “normal” activation kinetics and is merely reduced by a constant factor with respect to the control (fig 3.4).

### 4.2 $\kappa$ -PVIIA-block is state-dependent

We have shown that  $\kappa$ -PVIIA binds to both open and closed channel with a 1:1 stoichiometry (fig. 3.2). The fact that the binding parameters are different for open or closed channels cannot be attributed solely to the voltage dependence of the reaction rates.

On the one hand, while the value of  $k_{\text{off}}^{\text{C}}$  could be thought as the extrapolation of the  $k_{\text{off}}^{\text{O}}(\text{V})$  to hyperpolarizing potentials, the independence of  $k_{\text{on}}^{\text{O}}$  on voltage and  $[\text{K}]_{\text{O}}$  is in disagreement

with the 6-fold or 90-fold lower estimates of  $k_{on}^C$ , respectively at  $[K]_O = 2.5$  and  $115$  mM. On the other hand, our observation that the relaxation of the closed-channel block is independent of the holding potential in the range of  $-60$  to  $-120$  mV shows that, in sharp contrast to the case of open channels, the binding of  $\kappa$ -PVIIA to closed channels is fairly insensitive to the transmembrane voltage. Indeed, the fact that inactivation protects significantly depolarized *Shaker-wt* channels from toxin unbinding is an indication for a similar binding of  $\kappa$ -PVIIA to any non-conducting state of the channel at any voltage.

An important consideration that justifies a posteriori most of our experimental analysis is that the relaxations of toxin binding to open or closed channels occur on very different time scales. The mean properties that we expect from flickering between open and closed states are weighted for each state in direct proportion to the probability of that state, and in inverse proportion to the time constant of the binding relaxation in that state. Since the binding kinetics for closed channels is at least 10 times slower than for open channels, the relative weight of the open state in *Shaker-Δ* channels that do not inactivate would be  $> 0.9$  for any open-probability,  $P_O > 0.5$ . Therefore, it is reasonable to assume that during depolarizations of non-inactivating channels we are essentially measuring the binding to the open channels. The situation is less favorable for *Shaker-wt* channels were  $P_O \sim 0.1$ . In this case we expect that the relative weight of the open state would be  $\sim 0.53$  which is indeed fairly consistent with our finding that the  $K_{app}^O$  measured for *Shaker-wt* channels in NFR is  $\sim 0.6 K^O$ . Our finding that the toxin is much less efficient in blocking the late currents in high extracellular  $K^+$  respect to NFR suggests that the non conductive inactivated state of *Shaker-wt* channels is analogous to the closed state, and that the high  $K_{app}^O$  values are due to the contribute of the closed channel that are less efficiently blocked in high  $[K]_O$  than in NFR.

### 4.3 $\kappa$ -PVIIA block of open channels is voltage dependent

As shown in the Results (for example figs. 3.1F, 3.3A) the efficiency of  $\kappa$ -PVIIA in blocking *Shaker* open channels decreases exponentially with the applied potential. We calculated the affinity of the toxin for the channel by comparing either the late currents or the instantaneous tail currents in control and in presence of toxin. We have shown that the two methods give identical results (section 3.2.2 and figs. 3.12D and 3.17). The plot of the instantaneous tail currents as a function of the potential (see for example fig. 3.7D for an experiment in high symmetrical  $K^+$ ) has almost a linear behavior, in apparent contrast with the exponential voltage dependence of  $K^O$ . The instantaneous tail current under control conditions is proportional to the open probability and can be fitted with a Boltzmann function, with mid-voltage  $V_{1/2}$  and e-fold slope  $s$  as parameters (eq. 2.1, fig.3.7D). The currents in the presence

of the toxin is proportional to the product of the open probability times the unblock probability. Due to the exponential voltage-dependence of  $K^O$ ,  $K^O(V) = K^O(0) \cdot \exp(V/v_s)$ , the unblock probability has a Boltzmann-like behavior, characterized by the mid-voltage  $V_T = v_s \cdot \ln([T]/K^O(0))$  and by the e-fold slope  $v_s$ . In most of the conditions explored in our experiments the voltage range tested does not allow to see the saturation of toxin unblock and the data around  $V_T$  appear like a linear increase of tail currents with slope  $0.25 \cdot v_s^{-1}$ .

Which is the mechanism that renders the toxin less efficient in blocking the open channels at high depolarizations?

The presence of positive charges in the toxin could eventually confer an intrinsic voltage dependence to the peptide: in this case the protruding Lysine 7 would sense part of the potential drop at the edges of the membrane.

Is any other mechanism possible? For the scorpion toxin CTX, the voltage dependence of the K-channel block was shown to be due to the interaction of the toxin with the permeant ions in the pore. Can such a mechanism be applied also to  $\kappa$ -PVIIA?

In the next sections, 4.4 and 4.5, these questions will be addressed.

#### 4.4 Analogy between $\kappa$ -PVIIA and CTX

Both, the structural similarity of  $\kappa$ -PVIIA to the scorpion toxins of the Charybdotoxin (CTX) family (Scanlon et al. 1997) and the strong effect on  $\kappa$ -PVIIA sensitivity of mutations of some amino acid residues that are believed to shape the outer pore vestibule (Shon et al. 1998), indicate that  $\kappa$ -PVIIA acts, such as CTX, by obstructing the extracellular mouth of the ion pore. Besides showing that the binding occurs with a 1:1 stoichiometry, the results demonstrate that CTX and  $\kappa$ -PVIIA share also other strong similarities in their mechanism of block.

As for the case of CTX block of BK channels (MacKinnon and Miller 1988) or *Shaker* channels (Goldstein and Miller 1993),  $\kappa$ -PVIIA block is strongly decreased during channel opening with a voltage dependence conferred exclusively by the dissociation rate constant and not by the association rate of toxin binding (fig. 3.3). Furthermore an increase in the extracellular  $K^+$  concentration leads to a reduction in the affinity to the closed state which is mainly due to a reduction in the association rate, but has little effect on the open state (table 3.1 and 3.2, figs. 3.3, 3.8). Accordingly, the mechanism of the  $K^+$  inhibition of the toxin block cannot be of competitive nature because such a mechanism would demand a reduction association rate of the blocker. For CTX the amino group of the side chain of Lys-27 has been proposed to interact intimately with the  $K^+$ -permeation pathway by occluding the pore. Jacobsen et al. (2000) proposed a similar role for the Lysine in position 7 of  $\kappa$ -PVIIA.

Likewise, the state-dependency of  $\kappa$ -PVIIA-binding is qualitatively very similar to that reported for the binding of CTX to BK channels, which occurs with a 7 to 8-fold lower rate of association when the channels are fully closed (Anderson et al. 1988).

The only clear difference besides the actual orientation in the pore (Jacobsen et al. 2000) between CTX and  $\kappa$ -PVIIA appears to be that the latter has faster binding kinetics due to a higher dissociation rate constant.

Nevertheless, it has been observed that several CTX variants block open *Shaker* channels with relatively fast kinetics (Goldstein and Miller 1993; Goldstein et al. 1994). It is interesting to notice that nearly all of the more than 60 variants of CTX characterized by Goldstein et al. (1994) have second-order association rate constants close to the wild type toxin, and in the same range ( $\sim 150 \mu\text{M}^{-1}\text{s}^{-1}$ ) of our estimates for  $\kappa$ -PVIIA (table 3.1), in agreement with a diffusion limited toxin binding. None of the CTX variants was studied in a way that would allow a clear separate characterization of closed- and open-channel binding, because slow toxins were studied with multi-pulse protocols that characterize the binding to closed channels, whereas fast toxins were tested for open-channel block with wash-in/wash-out measurements during long depolarizations. Therefore, there is no direct evidence that CTX block of *Shaker* channels is state-dependent. However, one variant, CTX-R25Q, was studied with both protocols, although with different  $[\text{K}]_{\text{O}}$  conditions (2 mM vs 100 mM), and the results of the two measurements were quite different, the fast protocol yielding a 5-times larger  $k_{\text{on}}$ , and 10-times larger  $k_{\text{off}}$ . Although the authors suggest a different explanation related to the different  $[\text{K}]_{\text{O}}$  conditions, we notice that this result is in fact consistent with CTX block having the same state-dependency of  $\kappa$ -PVIIA block.

A simple model was proposed for CTX (scheme 4.1), describing the destabilization of the toxin by intracellular  $\text{K}^+$  (MacKinnon and Miller 1988). A channel with CTX bound can be occupied by a  $\text{K}^+$  ion at some other site ( $\text{Tx}:\text{K}^+:\text{C}$  or  $\text{Tx}:\text{C}$ ). The basic idea is that CTX dissociation from the  $\text{K}^+$ -occupied channel is faster than that from the  $\text{K}^+$  unoccupied channel ( $k_{-1}^{(0)} \ll k_{-1}^{(\text{K})}$ ). The site from which  $\text{K}^+$  is interacting with the toxin equilibrates with the ion at higher rates than CTX does with its site. Consequently, the observed dissociation rate for CTX is simply a mixture of  $k_{-1}^{(\text{K})}$  and  $k_{-1}^{(0)}$ , weighted by the probabilities that the site would or would not be occupied by a  $\text{K}^+$  ion.

Furthermore, the voltage dependence originates from the fact that depolarization renders  $\text{K}^+$  more effective in accelerating the toxin dissociation and it is not due to an inherent voltage dependence of the toxin. The authors proposed that the only voltage dependent parameter in the interaction of CTX with  $\text{K}^+$  is the equilibrium dissociation constant for  $\text{K}^+$ . According to a Woodhull model (Woodhull 1973) the site at which  $\text{K}^+$  exerts its effect on CTX dissociation

is assumed to be located at an electrical distance  $\delta$  across the transmembrane voltage drop, as measured from the inside, with  $\delta = 25/v_s$ . Hence, the voltage dependence is included in the probability terms and the dissociation rate would follow the expression

$$k_{\text{off}}^{\text{O}} = k_{-1}^{(0)} + \frac{(k_{-1}^{(\text{K})} - k_{-1}^{(0)})[\text{K}]_{\text{I}}}{[\text{K}]_{\text{I}} + K_{\text{K}}^{(\text{Tx})}(0)\exp(-V/v_s)} \quad \text{eq. 4.1}$$

where  $k_{-1}^{(0)}$  and  $k_{-1}^{(\text{K})}$  are respectively the minimum and maximum dissociation rates,  $v_s$  is the voltage dependence and  $K_{\text{K}}^{(\text{Tx})}(0)$  is the dissociation constant for  $\text{K}^+$  at 0 mV.

The model predicts some features of CTX block. First, as  $[\text{K}]_{\text{I}}$  increases the CTX dissociation rate rises from a minimum value of  $k_{-1}^{(0)}$ , and tends to saturate at a maximum value  $k_{-1}^{(\text{K})}$ . Second, lowering the intracellular concentration of the permeating ion reduces the measured  $k_{\text{off}}$  at all voltages, which may apparently result in a lower apparent voltage dependence of the CTX dissociation rate. Third, as voltage is made more negative the CTX dissociation rate approaches the same value approached at  $[\text{K}]_{\text{I}} = 0$ .

MacKinnon and Miller (1988) could show in a single channel study measuring  $\text{Ca}^{2+}$ -activated  $\text{K}^+$  channels reconstituted in lipid bilayers that the  $\text{K}^+$ -binding tends to saturate at higher  $[\text{K}]_{\text{I}}$  by using values of  $[\text{K}]_{\text{I}}$  up to 700 mM. Similar experiments cannot be performed by using the oocyte expression system because hypertonic solution leads to shrinkage of the cells.

In addition, they could obtain an estimate of the finite lower limit of  $k_{-1}^{(0)}$  by adjusting the internal  $[\text{Ca}^{2+}]$ , in order to maintain channel open at hyperpolarized potentials. From their data it is possible to estimate  $K_{\text{K}}^{(\text{Tx})}(0)$  values in the range of 1 to 3 M,  $k_{-1}^{(\text{K})} / k_{-1}^{(0)}$  ratios (in their terminology  $\beta_{\text{max}} / \beta_{\text{min}}$ ) in the range of 20 to 50, and a value of  $\delta$  close to 1.

Interestingly, while in BK channels the voltage dependence of CTX block was completely lost with  $\text{Na}^+$  and  $\text{Li}^+$  as intracellular cations, Goldstein and Miller (1993) reported that for *Shaker* channels (with the mutation F425G that increases 1000 times the affinity, Goldstein and Miller 1992) the voltage dependence is reduced, but not abolished. The authors used a mutant toxin (Y36A) with a rapid off rate to study the kinetic of block within a single pulse. This is not possible with the wild type toxin due to the slow dissociation rate. Since the extracellular TEA binding is voltage dependent in  $\text{K}^+$  but not in  $\text{Li}^+$ , Goldstein and Miller stated that the residual voltage dependence of CTX observed with intracellular  $\text{Li}^+$  would be inherent to the toxin. This corresponds to about the 20% of the potential applied compared to the 53% and the 39% of the potential measured in high  $\text{K}^+$  and in high  $\text{Na}^+$ , respectively.

#### 4.5 A model for the state-dependency of $\kappa$ -PVIIA-block

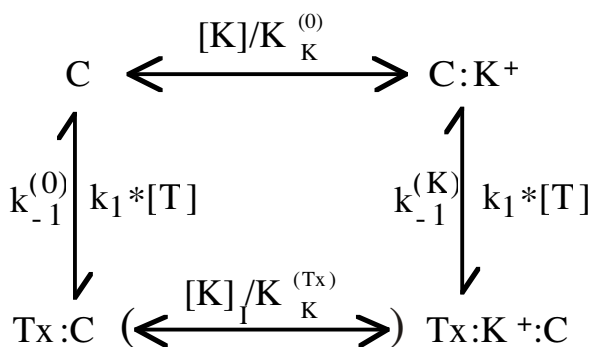
Despite the fact that we cannot exclude that a  $\kappa$ -PVIIA molecule bound to an open channel senses a significant fraction of the transmembrane electric field, the analogies with CTX and the antagonizing action of high- $K^+$  solutions on tonic  $\kappa$ -PVIIA block suggest that the unblock observed upon opening the channels in low external  $K^+$  may largely arise from the destabilization of toxin-binding by internal  $K^+$  as it has been reported for CTX (MacKinnon and Miller 1988).

The data collected with different cations in the intracellular solutions support the hypothesis that the toxin is destabilized by internal  $K^+$ . However, the effect of  $K^+$  is significantly emulated not only by the permeant  $Rb^+$ , but also by  $Na^+$ . We observe a clear reduction of the absolute value and voltage-dependence of the dissociation rate of the toxin when substituting  $K^+$  with  $Li^+$ , and the larger cations  $NMDG^+$  and  $Tris^+$  (fig. 3.18).

Our findings of a marked difference between the toxin-binding properties to the open versus closed channels and of a strong  $[K]_O$ -dependence of closed-channel binding can have a simple explanation in the context of a model, similar to the one proposed by MacKinnon and Miller (1988) for CTX, described in scheme 4.1.

In this model the major factor that influences the toxin binding is the state of occupancy of a  $K^+$ -binding site within the channel permeation pathway. So far no hypothesis has been made about the fact that this binding site is the same for the open and closed channel.

The scheme assumes that the  $K^+$ -binding is in fast equilibrium and is governed by different dissociation constants,  $K_K^{(Tx)}$  or  $K_K^{(0)}$ , depending on whether or not there is a toxin molecule bound to the outer pore vestibule. While a bound toxin is blocking the extracellular access,  $K^+$ -binding to the pore is assumed to be in equilibrium only with the cytoplasmic  $K^+$ -concentration  $[K]_I$ , and the parenthesis in the transition  $Tx:C \leftrightarrow Tx:K^+:C$  indicate that such event can occur only when the channel is open.  $[K]$  stands for the extracellular  $K^+$ -



**Scheme 4.1**



concentration provided that the channel is closed and not blocked by  $\kappa$ -PVIIA, whereas when the channel is open  $[K]$  is determined either by the extracellular solution or by the flux of ions in the pore. When  $K^+$  is the only permeant ion present in the extracellular solution, the binding site would be occupied in any case by  $K^+$ , since it is the only ion that has access to the site and that can be pushed further into the pore by the toxin binding to the extracellular side. This justifies our first finding that the open channel block is not affected by the external solution composition when  $K^+$  is the only permeant cation. We will discuss later the role of other permeant ion species in the interaction with the toxin.

For a better description the open and closed channel block will be discussed separately.

#### 4.5.1 Dependence of the open channel block on the solution composition

For the open channel the scheme 4.1 is reduced to the simple two-state, scheme 4.2, where we identify  $k_{on}^O$  with  $k_1$  and  $k_{off}^O$  with an average of  $k_{-1}^{(K)}$  and  $k_{-1}^{(0)}$ , weighted according to the relative probabilities of states Tx:K+:C and Tx:C.



For  $K_K^{(Tx)}$  was assumed a voltage-dependence associated with the charge translocation occurring along the pore in the transition Tx:C  $\leftrightarrow$  Tx:K+:C, following the approach used to describe CTX block.

Notice that scheme 4.2 leads to the conclusion that our voltage-independent estimates of  $k_{on}^O$  provide a direct measurement of the true rate constant of  $\kappa$ -PVIIA association to open channels. We can express the dissociation constant for open channels,  $K^O$ , using eq 4.1 for the dissociation rate constant, as:

$$K^O = \frac{1}{k_1} \left( k_{-1}^{(0)} + \frac{(k_{-1}^{(K)} - k_{-1}^{(0)})[K]_I}{[K]_I + K_K^{(Tx)}(0) \exp(-V/v_s)} \right) \quad \text{eq. 4.2}$$

where  $K_K^{(Tx)}(0)$  is the dissociation constant at 0 mV for the binding site from which  $K^+$  is destabilizing the toxin and  $v_s$  is the voltage dependence that can be equivalently expressed by the fraction of transmembrane voltage  $\delta = 25/v_s$  (with  $v_s$  expressed in mV) through which the ion moves. In case of a concerted movement of more ions, as seems to be the case for K-channel permeation, these parameters describe just a mean behavior, where  $K_K^{(Tx)}(0)$  is the concentration at which the probability of the binding site to be occupied by a  $K^+$  at 0 mV is 0.5 and  $\delta$  reflects the fraction of transmembrane voltage altogether traversed by the ions.

It is important to notice that eq.4.2 and the condition  $k_{on}^O = k_1$  bear no reference to the extracellular solution conditions, a strong prediction of scheme 4.1 that was verified in our experiments performed with different  $[K]_O$  (fig.3.3) but valid only when  $K^+$  is the only permeant cation.

For large values of the ratio  $k_{-1}^{(K)} / k_{-1}^{(O)}$  the voltage dependence of  $k_{off}^O$  behaves in an exponential manner (increasing e-fold/ $v_s$ ) in the wide voltage-range

$$\ln\left(\frac{K_K(0)}{[K]_I} \times \frac{k_{-1}^{(O)}}{k_{-1}^{(K)}}\right) < \frac{V}{v_s} < \ln\left(\frac{K_K(0)}{[K]_I}\right) \quad \text{eq. 4.3}$$

Imposing the consistency of our data recorded in  $[K]_I = 115$  mM with eq. 4.1 and 4.2 yields only lower estimates for  $K_K^{(Tx)}(0)$  and  $k_{-1}^{(K)}$  and a good estimate of  $v_s$ . With  $k_{-1}^{(K)} \gg 200$  s<sup>-1</sup>, the measured value of  $k_{off}^O$  at 80 mV, and for a voltage sensitivity of 40 mV, with  $[K]_I = 115$  mM we get  $K_K^{(Tx)}(0) \gg 0.8$  M and  $K_K(0) / M < 0.03 k_{-1}^{(K)} \cdot s$ .

Eq. 4.1 and 4.2 predict a sigmoidal dependence of  $k_{off}^O$  and  $K^O$  on voltage, a decrease at every potential when  $[K]_I$  is decreased, and a total loss of the voltage dependence in  $[K]_I = 0$ .

The first prediction cannot be observed because the voltage range measurable with the oocyte system is limited and because in any case the voltage dependence of the gating properties of the *Shaker* channel drives them to the closed state at hyperpolarizing potentials.

In contrast with what has been reported for CTX, the voltage dependence of the block of  $\kappa$ -PVIIA is not completely lost when the intracellular  $K^+$  is substituted by impermeant cations. In particular, intracellular  $Na^+$  was found almost as efficient as  $K^+$  in destabilizing the toxin binding to the open channels (fig. 3.18). At first sight this suggest that the site that is mediating the interaction should not be much more selective for  $K^+$  over  $Na^+$ . This idea is supported by the finding that the  $K^+$  concentration required to restore completely the maximal voltage dependence observed is relatively high,  $> 20$  mM (fig. 3.25).

The model proposed by MacKinnon and Miller cannot explain the voltage dependence of the toxin binding observed in the presence of non permeant cations such as  $Tris^+$ ,  $NMDG^+$  and  $Li^+$  (fig.3.18). There are at least two possible explanations for the voltage dependence of the toxin binding. Firstly the positively charged toxin might be capable of feeling part of the potential drop. Secondly the voltage dependence might still be conferred by a cation moving in the electric field, but in the case of an impermeant cation the movement would be restricted to the area within the cavity of the pore known to be present at the intracellular side (fig. 1.3; Doyle et al. 1998). This movement could in turn push a  $K^+$  present in the pore toward an outer site where it repels efficiently the toxin.

According to the first hypothesis, the voltage dependence of the toxin in presence of impermeant intracellular ions would be intrinsic ( $v_i = 70$  mV) and corresponds to a fraction of electrical distance  $\delta$  of 0.36.

Thus, with our experimental data,  $K^O$  and  $k_{\text{off}}^O$ , can be described with the same eq 4.1 and 4.2 but with an additional voltage dependence factor included in the dissociation rate terms:

$$k_{-1}^{(O)}(V) = k_{-1}^{(O)}(0) \cdot \exp(V / v_i) \quad \text{and} \quad k_{-1}^{(K)}(V) = k_{-1}^{(K)}(0) \cdot \exp(V / v_i) \quad \text{eq. 4.4}$$

with  $k_{-1}^{(O)}(0 \text{ mV}) = 14 \text{ s}^{-1}$  and  $v_i = 70 \text{ mV}$  (table 3.5).

The channels without a  $K^+$  interacting with the toxin would contribute to the voltage dependence with an e-fold slope  $v_i$  while the others with  $(v_s^{-1} - v_i^{-1})^{-1}$ .

The voltage range accessible to our measurements falls in the exponential region, defined by eq. 4.3 and therefore the description of our experimental data eq.4.2 is reduced to the simpler form

$$K^O = \frac{1}{k_1} \left( k_{-1}^{(O)} + \frac{(k_{-1}^{(K)} - k_{-1}^{(O)})}{K_K^{(Tx)}(0)} \cdot [K]_I \cdot \exp(V / v_s) \right) \quad \text{eq. 4.5}$$

where  $k_{-1}^{(K)}$  and  $k_{-1}^{(O)}$  contain the intrinsic voltage dependence as expressed in eq.4.4.

We fixed  $k_{-1}^{(O)}(0)$  and  $v_i$  to the values obtained from the data with intracellular 115 mM Tris<sup>+</sup>, 14.4 s<sup>-1</sup> and 70 mV respectively. The approximation of the data recorded in intracellular high  $K^+$ , (weighted with the inverse of the square of the standard deviation) with eq. 4.5 gave  $v_s = 50$  mV, corresponding to an electrical distance  $\delta$  of 0.5. Unfortunately the fit cannot give a unique evaluation of  $k_{-1}^{(K)}(0)$ , but it is sensitive only to the ratio between  $(k_{-1}^{(K)}(0) - k_{-1}^{(O)}(0))$  and  $K_K^{(Tx)}$  that was found to be 0.06 s<sup>-1</sup>mM<sup>-1</sup>. Assuming a  $K_K^{(Tx)}$  of 1 M, we get an estimate for  $k_{-1}^{(K)}(0)$  of about 70 s<sup>-1</sup>.

In fig. 4.1 the results of the fit with eq 4.5 (thick dotted line) of the experimental data recorded in high  $[K]_I$  (black squares) are shown together with the theoretical values for intermediate  $[K]_I$ , 5, 20 and 50 mM, (dotted lines), calculated for the best estimates of the parameters obtained above. In agreement with our experimental data (fig. 3.24 and 3.25) the voltage dependence increases gradually with  $[K]_I$ .

Which is the rationale of the second hypothesis for the voltage dependence of toxin binding? The KcsA crystal structure revealed the presence of three ions in the conduction pathway (Doyle et al. 1998). One  $K^+$  ion, presumably surrounded by water molecules, was detected in a large water filled cavity (roughly 10 Å in diameter) at the center of the pore near the cytoplasmic end of the selectivity filter. Jiang and MacKinnon suggested that this could be the low affinity and low selectivity internal lock-in site that impedes  $Ba^{2+}$  to leave the channel

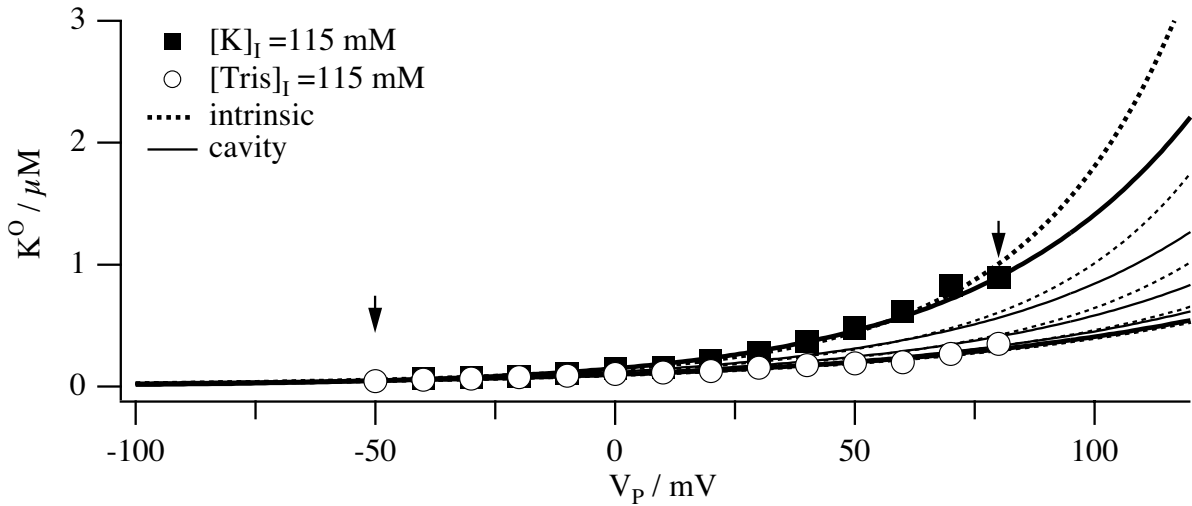


**Figure 4.1 Voltage dependence of the open channel block.** Plot of the dissociation constant  $K^O$  vs the membrane potential in intracellular 115 mM KCl (■) and 115 intracellular TrisCl (○) with 115 mM extracellular KCl. The vertical arrows correspond to the potential range accessible in our measurements.

- Intrinsic voltage dependence: fit of the experimental data (thick dotted lines) with eq. 4.5, containing the intrinsic voltage dependence contribute. The thin dotted lines correspond to the previsions for  $[K]_I=5, 20$  and 50 mM.
- Ion moving in the cavity: the thick lines are the exponential fit to the experimental data with a single exponential, while the thin lines are the previsions according to eq. 4.9 for  $[K]_I=5, 20$  and 50 mM.

Both models can account for our experimental data (section 4.5)

into the intracellular medium (Jiang and MacKinnon 2000; fig.4.5, see below section 4.8). An ion that traverses the cavity feels about 30% of the electric field corresponding to a voltage dependence of 80 mV for a monovalent cation. A cation traversing the cavity could confer slight voltage dependence to the toxin block, probably stabilizing the more internal permeable cation in the pore in an outer position. In case the cavity ion is permeable, it can push the last ion to a more external binding site, resulting in a steeper voltage dependence. Therefore a molecule of toxin bound to the channel finds a  $K^+$  in the pore and a  $K^+$ , a  $Tris^+$  or no ion in the cavity. The presence of a  $K^+$  or a  $Tris^+$  in the cavity increases the probability of the inner  $K^+$  to “jump” in an outer position from which it destabilizes the toxin.

We tested this hypothesis by approximating our experimental data recorded in the two extreme conditions  $[K]_I=115$  mM and  $[Tris]_I=115$  mM with

$$K^O(V) = \frac{1}{k_{on}^O} * \left[ k_{-1}^{(0)} p_{cav}(0) + k_{-1}^{(K)} (p(K,K) + p(K,Tris)) \right] \quad \text{eq. 4.6}$$

where  $p(K,K) = p(K/K) \cdot p_{cav}(K)$  is the probability to have a  $K^+$  both in the pore and in the cavity, while  $p(K,Tris) = p(K/Tris) \cdot p_{cav}(Tris)$  is the probability to have a  $K^+$  in the pore and a  $Tris^+$  in the cavity.  $p(K/K)$  and  $p(K/Tris)$  are the conditional probabilities that a  $K^+$  is in the outer position if respectively a  $K^+$  or a  $Tris^+$  is in the cavity.  $p_{cav}(0)$ ,  $p_{cav}(K)$  and  $p_{cav}(Tris)$  are

the probabilities that the cavity is empty, occupied by a  $K^+$  or occupied by a  $Tris^+$ . These probabilities can be expressed by

$$p_{cav}(0) = \frac{1}{1 + [K]_I / K_K + [Tris]_I / K_{Tris}}; p_{cav}(K) = \frac{[K]_I / K_K}{1 + [K]_I / K_K + [Tris]_I / K_{Tris}}$$

$$p_{cav}(Tris) = \frac{[Tris]_I / K_{Tris}}{1 + [K]_I / K_K + [Tris]_I / K_{Tris}} \quad \text{eq. 4.7}$$

$K_K$  and  $K_{Tris}$  are the concentrations at which the probability that the cavity is occupied by a  $K^+$  and a  $Tris^+$  is 0.5. Since the cavity is within the electric field,  $K_K$  and  $K_{Tris}$  could depend on the membrane potential, but we neglected this contribution. We will make the further approximation that  $K_K = K_{Tris}$  and that they are small relatively to the concentrations used, therefore the probabilities will have the simpler form

$$p_{cav}(0) \approx 0; p_{cav}(K) \approx \frac{[K]_I}{[K]_I + [Tris]_I}; p_{cav}(Tris) \approx \frac{[Tris]_I}{[K]_I + [Tris]_I} \quad \text{eq. 4.8}$$

Unfortunately we do not know the exact behavior of the conditional probabilities  $p(K/K)$  and  $p(K/Tris)$ : they would tend to 0 at hyperpolarizing potentials and to 1 for high positive potentials. Nevertheless we can describe this behavior with a Boltzmann curve, with characteristic parameters  $V_{K,K}$  and  $v_{K,K}$  for  $p(K/K)$  and  $V_{K,Tris}$  and  $v_{K,Tris}$  for  $p(K/Tris)$ .  $V_{K,K}$  and  $V_{K,Tris}$  represent the potential at which the probability of the last site to be occupied by a  $K^+$  is 0.5, with either a  $K^+$  or a  $Tris^+$  in the cavity.

Because under our experimental conditions the binding sites are far from saturation of the ion we can approximate the Boltzmann with a single exponential.

Therefore  $K^O$  at divers  $[K]_I$  can be approximated by

$$K^O(V) = \frac{k_{-1}^{(K)}}{k_{on}^O} \cdot \left[ \frac{[K]_I}{[K]_I + [Tris]_I} \cdot e^{\frac{V - V_{K,K}}{v_{K,K}}} + \frac{[Tris]_I}{[K]_I + [Tris]_I} \cdot e^{\frac{V - V_{K,Tris}}{v_{K,Tris}}} \right] \quad \text{eq. 4.9}$$

where  $v_{K,K}$ ,  $v_{K,Tris}$ ,  $k_{-1}^{(K)} \cdot \exp(-V_{K,K}/v_{K,K})$  and  $k_{-1}^{(K)} \cdot \exp(-V_{K,Tris}/v_{K,Tris})$  are evaluated by the experiments performed in monocationic intracellular solutions and assume the following values:

$$v_{K,K} = 44.5 \text{ mV}, v_{K,Tris} = 70 \text{ mV}, k_{-1}^{(K)} \cdot \exp(-V_{K,K}/v_{K,K}) = 22 \text{ s}^{-1} \text{ and } k_{-1}^{(K)} \cdot \exp(-V_{K,Tris}/v_{K,Tris}) = 15 \text{ s}^{-1}.$$

The continuous lines in fig 4.1 show the theoretical values obtained by eq. 4.8 for intermediate  $[K]_I$ , 5, 20 and 50 mM together with a single exponential fit of the data in  $[K]_I=115$  mM (black squares; thick continuous line) and  $[Tris]_I=115$  mM (white circles; thick continuous line).

Similarly to the case of intrinsic voltage dependence hypothesis and in agreement with our experimental data (fig. 3.24 and 3.25), we found that the steepness of the voltage dependence increases gradually with  $[K]_i$ .

Is there a good way to decide which hypothesis fits our data best?

According to the intrinsic voltage dependence hypothesis the  $K^O$  would increase indefinitely for increasing voltage, and no saturation of the block would be observed. With the second model we would expect saturation when 100% of the channels are occupied by a  $K^+$  ion. Unfortunately, this behavior would occur at potentials far away from the voltage range that can be investigated under our experimental conditions and therefore we cannot draw conclusions from the data by using the oocyte expression system.

Actually  $K^O$  increases steeper as a function of the potential in case of intrinsic voltage dependence, shown in fig. 4.1 by the dotted lines that are far above the continuous lines corresponding to the same  $[K]_i$ , but only for potential above 70-80 mV, (which are at the limit of our experimental range, highlighted in fig. 4.1 by the two vertical arrows).

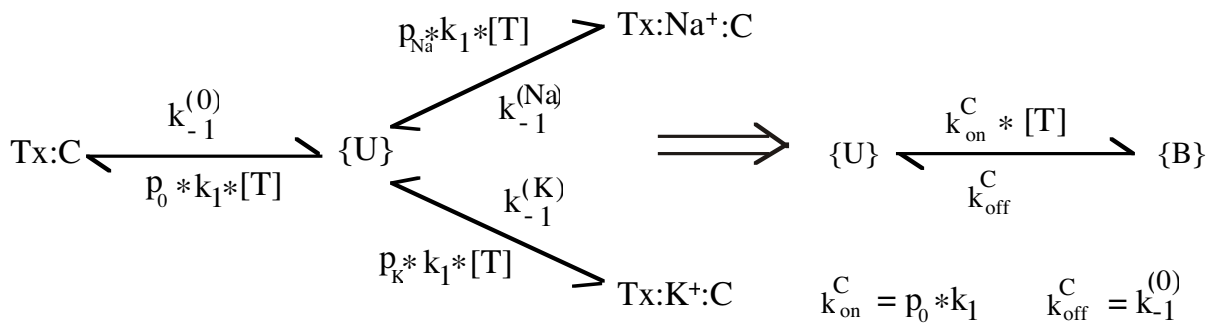
The second difference in the predictions of the two models regards the asymptotic value of  $K^O$  or  $k_{off}^O$  reached at large hyperpolarizing potentials. In the case of the intrinsic voltage dependence we expect the first order dissociation rate and  $K^O$  to approach zero. The second model predicts an asymptotic value for  $k_{off}^O$  equal to the closed channel dissociation rate. With an association rate of  $150 \mu M^{-1}s^{-1}$  it would result in a  $K^O$  between 5 and 10 nM. Without making any model-based hypothesis, in our analysis we fitted the experimental data with a single exponential fixing to zero the asymptotic value for  $V \rightarrow -\infty$ , ( $K^O$  in  $K^O + K^O(0) \exp(V/v_S)$ ). The good agreement with the experimental data unfortunately does not allow to state that the intrinsic voltage dependence hypothesis is correct. In fact the asymptotic values expected from the two models do not differ so much between each other and are quite small with respect to the values obtained at higher voltages.

In conclusion, the potential range of our experiments does not allow us to decide which of the two hypotheses is correct but we showed that both can qualitatively account for our findings.

#### 4.5.2 Closed channel block vs $[K]_o$

The predictions of scheme 4.1 for the binding of  $\kappa$ -PVIIA to closed channels will be discussed in the following. As already anticipated, the most important difference with respect to the binding of  $\kappa$ -PVIIA to the open channel is the absence of  $Tx:C \leftrightarrow Tx:K^+:C$  transitions. An additional important difference is the fact that  $C: \leftrightarrow C:K^+$  transitions involve only a very fast equilibration with the extracellular  $K^+$ .

Compared with open-channel properties both the association and the dissociation rates of  $\kappa$ -



Scheme 4.3

Scheme 4.4

PVIIA-binding to closed channels in physiological conditions are much slower (see table 3.1). The about 4-fold higher value of  $K^{\text{O}(0)}$  relative to  $K^{\text{C}}$  results from the combination of an increase of the rate of  $\kappa$ -PVIIA dissociation by a factor of  $\sim 20$  and an increase of the association rate by a factor of  $\sim 5$ . The most important conclusion from these measurements is that, while the low value of  $k_{\text{off}}^{\text{C}}$  could be thought as an extrapolation to hyperpolarized potentials of the voltage-dependence of  $k_{\text{off}}^{\text{O}}$ , the 5-fold lower value of  $k_{\text{on}}^{\text{C}}$  is incompatible with the voltage-independence of  $k_{\text{on}}^{\text{O}}$  (fig. 3.3B). This finding indicates that closed channels have indeed different toxin-binding properties.

Scheme 4.3 illustrates the interaction of the toxin with the closed channels.

One assumption implied in the model is that the toxin can bind to whatever state of the channel with the same second-order-association rate constant,  $k_1$ , whereas its first-order-dissociation rate constant is  $k_{-1}^{(\text{X})}$  or  $k_{-1}^{(0)}$  depending on whether or not the pore outermost binding site is occupied by a cation of species X. All the rate constants are assumed to be voltage-independent.  $\{U\}$  indicates the set toxin-free states with probability  $p_X$  of having the pore outer site occupied by a cation X this occupancy is determined by a very fast equilibrium with the extracellular cation concentration.

We found that the affinity of the toxin for the channel is higher by a factor of two when Tris<sup>+</sup> replaces Na<sup>+</sup> as the only extracellular monovalent cation (section 3.3). This suggest that also Na<sup>+</sup> and not only K<sup>+</sup> might bind to the cation binding site and moreover that in the presence of 115 mM NaCl half of the channels are occupied by Na<sup>+</sup>. When the channel is closed and not blocked by  $\kappa$ -PVIIA, the cation binding-site would be in equilibrium only with the extracellular solution, and the toxin can bind to a cation-free pore-mouth forming a Tx:C complex, or to a cation occupied pore, forming a Tx:K<sup>+</sup>:C or Tx:Na<sup>+</sup>:C complex.  $\{U\}$  lumps together the unblocked states C, Na<sup>+</sup>:C and K<sup>+</sup>:C. The scheme assumes that Na<sup>+</sup> and K<sup>+</sup>-binding is in fast equilibrium and the occupancy of the site is determined by the dissociation constants  $K_{\text{Na}}$  and  $K_{\text{K}}$ . Direct transitions between the states Tx:C and Tx:K<sup>+</sup>:C or Tx:Na<sup>+</sup>:C

are not allowed because they require preliminarily that the channel opens or that the toxin dissociates from the channel.

The apparent affinity of the toxin for the closed state, i.d. the inverse of  $K^C$ , is the sum of the affinities of the channel for the empty or occupied channel, weighted by the respective probabilities,  $p_0$ ,  $p_K$  and  $p_{Na}$ :

$$K^C = [p_0 \cdot A_0 + p_K \cdot A_K + p_{Na} \cdot A_{Na}]^{-1} \quad \text{eq. 4.10}$$

with  $p_0 = 1 / (1 + [K]_O / K_K + [Na]_O / K_{Na})$ ,  $p_K = ([K]_O / K_K) / (1 + [K]_O / K_K + [Na]_O / K_{Na})$  and  $p_{Na} = ([Na]_O / K_{Na}) / (1 + [K]_O / K_K + [Na]_O / K_{Na})$ .

Since  $\text{Tris}^+$  is a cation which is much bigger than  $\text{Na}^+$  and  $\text{K}^+$  we can reasonably assume that it does not bind to the outer site of the pore (this working hypothesis is commonly assumed for  $\text{Tris}^+$  and  $\text{NMDG}^+$ , among others Neyton and Miller 1988b, Harris et al. 1998). Therefore, the affinity measured with  $\text{Tris}^+$  as the only monovalent cation in the extracellular solution can be assumed as the affinity of the toxin for the empty channel ( $K_0 = A_0^{-1}$ ). We expect that the toxin binds better to the channel when the  $\text{K}^+$  or  $\text{Na}^+$  are not in the pore, and since the hydrated  $\text{Na}^+$  has a larger size than the hydrated  $\text{K}^+$  we expect  $A_{Na} \ll A_K \ll A_0$ . If the terms  $p_K A_K$  and  $p_{Na} A_{Na}$  are much smaller than  $(1 - p_K - p_{Na}) A_0$ , then we would expect a linear dependence of  $K^C$  on the cation concentrations,

$$K^C = \frac{1}{p_0 A_0} \left[ 1 + \frac{[Na]_O}{K_{Na}} + \frac{[K]_O}{K_K} \right] \quad \text{eq. 4.11}$$

At intermediate or high  $[K]_O$  we can consider only the  $\text{K}^+$  contribution: the linear approximation would be valid only when  $A_K/A_0 \ll K_K / 115 \ll K_K/[K]_O$ , where 115 mM is the maximal  $[K]_O$  that we used. For example if  $A_K/A_0 = 1/100$ , the validity of linear approximation requires  $K_K \gg 1.15$  mM.

In fig. 4.2 the equilibrium dissociation constant (black squares) is plotted against  $[K]_O$ : the fit with a line, eq. 4.11, shown by the dotted line, is not satisfactory, because the data points of the intermediate concentrations are systematically above the fit.

We therefore fitted the experimental data with the eq. 4.10, shown by the continuous line in fig.4.2. A first fit was done keeping the following parameters fixed:  $K_0^{\text{Tx}} = A_0^{-1} = 20$  nM, corresponding to the affinity in Tris,  $K_{Na} = 115$  mM and  $K_{Na}^{\text{Tx}} = A_{Na}^{-1} = 4000$  nM (8 times the value estimated for potassium). With this choice of parameters  $\text{Na}^+$  has some probability of binding to the site in no or very low  $\text{K}^+$ . Nevertheless under these conditions  $\text{Na}^+$  contributes very little to the total affinity because the toxin binds with an almost zero affinity. The best fit corresponded to the following values of the free parameters:  $K_K^{\text{Tx}} = A_K^{-1} = 570$  nM,  $K_K = 5.4$



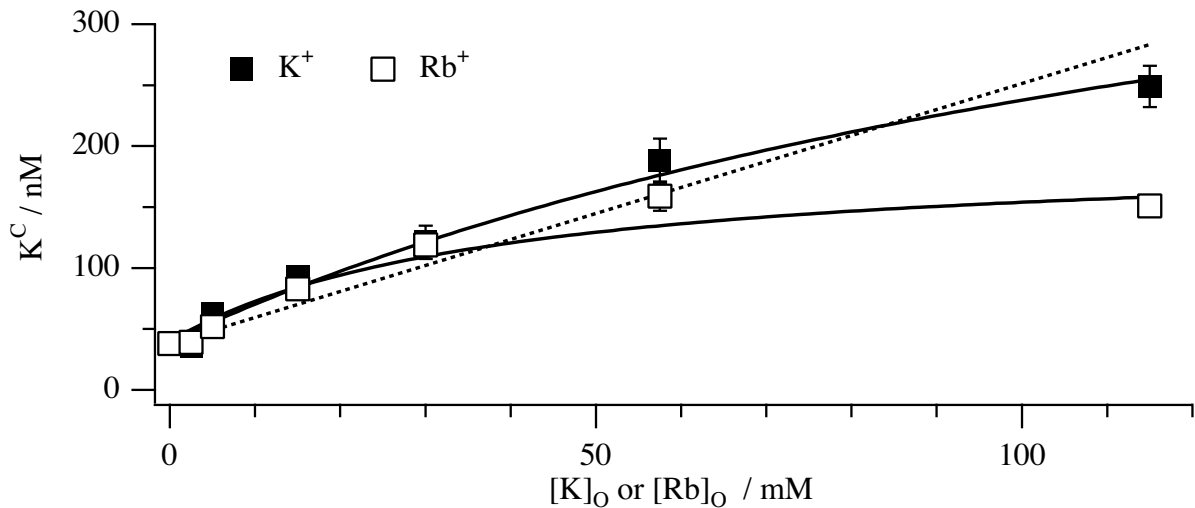


**Figure 4.2 Dependence of  $K^C$  on  $[K]_O$  and  $[Rb]_O$ .** Plot of the dissociation constant  $K^C$  vs the concentration of the extracellular permeant cation, either  $K^+$  (■) or  $Rb^+$  (□). Data were approximated with eq. 4.10, considering the contribute of the channels empty or trapping a  $Na^+$ , a  $K^+$  or a  $Rb^+$ . From the fit we could evaluate  $K_K^{Tx} = A_K^{-1} = 570$  nM,  $K_K = 5.4$  mM and  $K_{Rb}^{Tx} = A_{Rb}^{-1} = 203$  nM,  $K_{Rb} = 3.7$  mM. The dotted line shows the attempt of approximating the data in potassium with a line.

mM. These values of the parameters did not satisfy the above requirement for the linear approximation, because  $A_K/A_0 = 1/28$ .

Therefore, the experimental data fit with the presence of a cationic binding site that is about 20 times more selective for  $K^+$  with respect to  $Na^+$ . The toxin can also bind trapping a cation and the probability for this to occur increases with  $[K]_O$ . This most likely leads to the saturation of  $K^C$  at high  $[K]_O$ .

According to scheme 4.3 the relaxation following a perturbation of the equilibrium, measured with a double pulse protocol, should in principle contain 2 or 3 exponential terms when one or two species of competing cations are present. In practice at all  $[K]_O \geq 2.5$  mM we observed only a single exponential relaxation, with a time constant that increased with  $[K]_O$ . This suggests that in presence of external  $K^+$  scheme 4.3 reduces to scheme 4.4. The change of the kinetic behavior is due to a decrease in the dissociation rate with increasing  $[K]_O$ , while the association rate is constant, supporting a competition effect between the toxin and the cation sitting in the pore.

This simplification can be easily explained if we consider that the off rate of a bound toxin trapping either a potassium or a sodium ion is much higher than its off rate from an empty channel. Even if these states may be significantly occupied, the kinetics is too fast to be measured. In scheme 4.4  $k_{off}^C = k_{-1}^{(0)}$  is the off-rate from the empty channel and  $k_{on}^C = p_0 \cdot k_1$ , where  $k_1$  is the association rate for the open channels, where the trapping phenomenon is avoided because  $K^+$  can escape through the intracellular side of the pore. We found (table 3.2)

that  $k_{\text{off}}^{\text{C}}$  is independent of  $[\text{K}]_{\text{O}}$  and  $k_{\text{on}}^{\text{C}}$  decreases upon increasing  $[\text{K}]_{\text{O}}$ : both findings are consistent with the above interpretation.

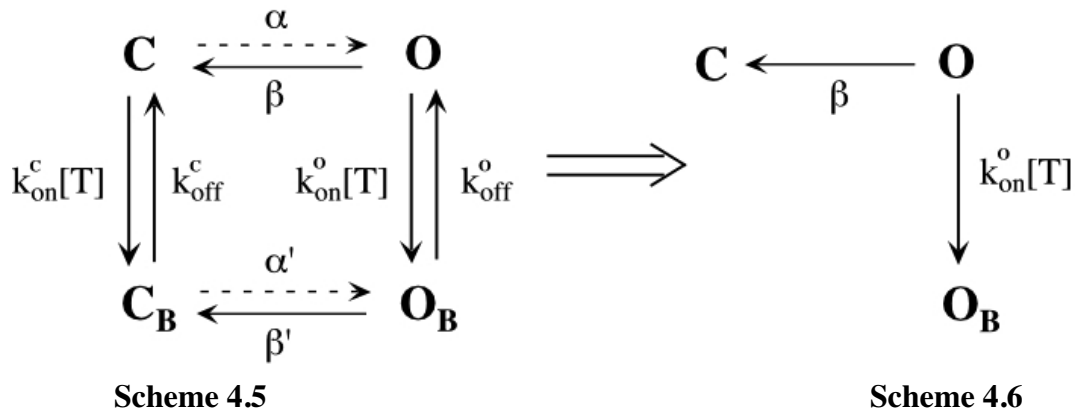
#### 4.5.3 Closed channel block does not depend on the intracellular solution

The results shown in table 3.5 demonstrate that the binding of  $\kappa$ -PVIIA to closed channels does not depend on the intracellular solution composition.

For the CTX block of BK channels it has been reported that only the rate of association (Anderson et al. 1988), but not the dissociation rate, depends on the open channel probability. As in our case of  $\kappa$ -PVIIA, the association rate was found to be sensitive to the extracellular composition of the solution and the dissociation rate depended on the intracellular milieu. However, in contrast to our findings for  $\kappa$ -PVIIA the dissociation rate was found to be the same in the open and in the closed state. This difference of behavior can be explained as follows: a CTX molecule binds to the channel on average for several seconds, so that even “mostly closed “ channels ( $> 98\%$  of the time) will open many times during an average CTX block event. If the channel has a chance to open while it is blocked by a CTX, the  $\text{K}^+$ - binding site would presumably equilibrate with the intracellular solution on a sub-microsecond time scale, comparable with the permeation time. This might account for the observation that internal  $\text{K}^+$  is not more effective for CTX-BK interactions when a channel is open most of the time than when it is mostly closed (MacKinnon and Miller 1988). In contrast  $\kappa$ -PVIIA binds to *Shaker* channels for a much shorter time particularly when trapping an external cation. The largest dwell time with no cation trapped is estimated to be about 1 sec. At hyperpolarizing potentials the probability that a channel opens at least once in 1 sec is  $\sim 10^{-2}$ - $10^{-3}$ , so that the influence of these openings on  $\kappa$ -PVIIA binding is negligible.

#### 4.6 Effects of toxin binding on "tail currents"

Further support for our interpretation that the toxin blocks the channel conductance in a state-dependent way, with almost no intrinsic effect on channel gating, comes from the analysis of deactivation kinetics. The toxin modifies the deactivation of the  $\text{K}^+$ -currents, by making them faster, this effect being more prominent at higher concentrations (see section 3.6). Can we interpret this effect in terms of the kinetic parameters that regulate the binding of the toxin to the channel? Scheme 4.5 describes the binding of the toxin to both open and closed channels: the greek letters indicate the activation and deactivation rates, while for the binding parameter the usual nomenclature was used. O, C and  $\text{O}_\text{B}$ ,  $\text{C}_\text{B}$  indicate the channel in the open and in the closed conformation respectively free or blocked by the toxin. The dashed lines indicate transitions that do not contribute significantly under our experimental conditions: at negative



potentials  $\alpha$ ,  $\alpha'$  are much smaller than  $\beta$  and  $\beta'$ . For simplicity we also assume that  $\beta = \beta'$  for these steps. Furthermore the equilibration of the toxin with closed channels in the presence of any  $[K]_O$  tested is a much slower process than tail deactivation, therefore scheme 4.5 can be reduced to scheme 4.6. In this approximation the probability to be in the state O varies with time according to  $\dot{p}_O = -(\beta + k_{on}^o \cdot [T]) \cdot p_O$ . In response to a repolarizing voltage step  $p_O$  would decrease in the presence of toxin with time according to an exponential law with a time constant

$$\tau = (\beta + k_{off} + k_{on}[T])^{-1}, \quad \text{eq. 4.12}$$

where  $\beta = \tau_{Ct}^{-1}$ .

In two experiments, where more than one toxin concentration was applied, the reciprocal of  $\tau$  increases linearly with  $[T]$  as expected from the above. At the potentials tested  $k_{off} \ll k_{on}[T]$ , therefore an estimate of  $k_{on}$  at the test potential of the tail current,  $V_{Tail}$ , can be obtained from the expression:

$$k_{on}^O(V_{Tail}) = \frac{(\tau_{Tx}^{-1} - \tau_{Ct}^{-1})}{[T]} \quad \text{eq. 4.13}$$

where  $\tau_{Tx}$  and  $\tau_{Ct}$  are the time constants, respectively, in toxin and control.

Unfortunately several sources of potential errors make the results of this analysis only qualitative and not quantitative. 1) The difference between the two time constants measured in control and in toxin is not very big (depending on the concentration from 10% to 20 %) and can be well estimated only at high concentrations or when the tail currents are slower, like at less negative potentials or in presence of external  $Rb^+$  which leads to a slowing of the deactivation kinetics (Swenson and Armstrong 1981; Matteson and Swenson 1986). 2) In some experiments we observed that the kinetics of the tail currents may get spontaneously faster with time. This observation may be due to a shift in the activation / inactivation curve during the time course of the experiment. To minimize this error the deactivation time

constant of the current in the presence of the toxin was compared to the time constants of corresponding measurements for control and wash. 3) Another source of error can arise from incomplete or insufficient voltage clamp of the tail currents or from contamination from endogenous currents present in the oocyte under investigation. Experiments which showed appreciable contamination were discarded for this analysis. From experiments performed in the presence of 115 mM external KCl or 115 mM external RbCl, with deactivation test potentials between  $-100$  and  $-50$  mV, the  $k_{on}$  was evaluated by using the expression eq. 4.13 which was  $200 \pm 26$  in the presence of 115 mM KCl ( $n=22$ ; mean  $\pm$  sdm) and  $127 \pm 24$  in the presence of 115 mM RbCl ( $n=10$ ).

Considering the above mentioned sources of error, this result is quite consistent with the  $k_{on}^O$  evaluated at more depolarizing potentials. First, these findings confirm a low or no voltage-dependence of the  $k_{on}^O$ , even in a voltage range that had not been explored before. Second, these findings exclude the possibility that the low  $k_{on}$  observed for the closed channel is actually the  $k_{on}$  corresponding to the open channel at hyperpolarized potentials, because association rates in the range measured for closed channels would not be expected to affect significantly the deactivation time constant.

#### 4.7 $\kappa$ -PVIIA destabilization by $Rb^+$

The data obtained in presence of  $Rb^+$  are compatible with a state dependent block but they also show that the interaction of the toxin with the channel is different with  $Rb^+$  present in the ion channel pore compared to  $K^+$ . Such a different interaction of the toxin with these two permeable cations is quite surprising because  $Rb^+$  and  $K^+$  have similar radius, can both readily enter the channel, as shown by a very similar reversal potential, and they are believed to interact in almost equivalent ways with the channel.

##### 4.7.1 Closed channel block vs $[Rb]_O$

Similarly to what was found for extracellular  $K^+$ , the affinity of the toxin for the channel decreases with increasing  $[Rb]_O$  (see table 3.4). Fig. 4.3 shows the dependence of the closed state equilibrium dissociation constant (empty squares) versus  $[Rb]_O$ : a saturation of the antagonism of external  $Rb^+$  for  $\kappa$ -PVIIA binding seems to be reached already at  $\sim 60$  mM. Furthermore the largest dissociation constant for  $\kappa$ -PVIIA binding to closed channels is about 1.8 times smaller than in high extracellular  $K^+$  (150 nM vs 265 nM), indicating that the toxin can tolerate much better the presence of a trapped  $Rb^+$  than of a  $K^+$ . We can apply the kinetic scheme 4.3 also to this situation where the state  $Tx:K^+:C$  would be replaced by  $Tx:Rb^+:C$ . Also in this case the approximation of the dependence of  $K^C$  on  $[Rb]_O$  with a line is not

possible as one can see clearly in fig. 4.2 from the saturating behavior that is already present at  $[Rb]_O \sim 60$  mM.

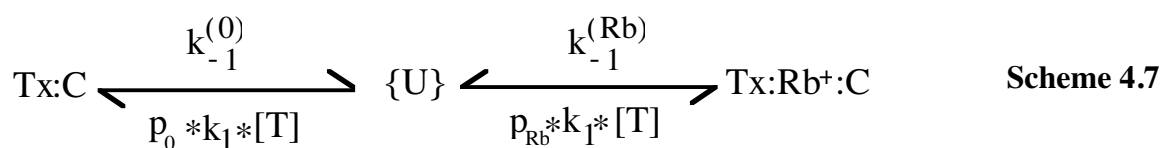
We therefore fitted the experimental data with eq 4.10, where we substituted  $p_K$  with  $p_{Rb}$  and  $K_K$  with  $K_{Rb}$ , keeping constant  $K_O^{Tx} = A_O^{-1} = 20$  nM, corresponding to the affinity measured in Tris,  $K_{Na} = 115$  mM and  $K_{Na}^{Tx} = A_{Na}^{-1} = 4000$  nM. The best fit corresponded to the following values of the free parameters:  $K_{Rb}^{Tx} = A_{Rb}^{-1} = 203$  nM,  $K_{Rb} = 3.7$  mM.

These estimates, compared to the values obtained for  $K^+$  (see 4.5.2), indicate that the toxin can bind to the channel 2-3 times better if a Rb ion rather than a K ion is trapped, and that  $Rb^+$  binds to the outer site of the pore slightly better than  $K^+$  (1.5 times).

When we measure the re-equilibration of the binding of  $\kappa$ -PVIIA to closed channels with a double pulse protocol, we find that for a wide intermediate range of  $[Rb]_O$  values, the binding relaxation contains two contributions. Therefore the direct conclusion that the increase in the  $K^C$  with  $[Rb]_O$  is due to a decrease in the association rate with a constant dissociation rate, like shown for  $K^+$ , cannot be drawn as easily.

For  $[Rb]_O = 2.5$  mM, or  $[Rb]_O \geq 60$  mM a single exponential relaxation is observed upon stimulation with a double pulse protocol. In these cases scheme 4.3 can be reduced, as done for the  $[K]_O$  data, to scheme 4.4 and the relaxation time constant interpreted according to the expression:  $\tau^{-1} = k_{off}^C + k_{on}^C \cdot [T]$ . With 2.5 mM  $[Rb]_O$  the binding kinetics were similar the those observed in high  $Na^+$  or in NFR (table 3.2 and 3.4), mainly reflecting the equilibration process with the empty channels, with  $k_{off}^C = k_{-1}^{(0)}$  and  $k_{on}^C = (1 - p_{Na} - p_{Rb}) \cdot k_1$ . In high  $[Rb]_O$  the binding kinetics observed are 1-2 order of magnitude faster (table 3.4, fig. 3.14), both the dissociation and the association rates being significantly higher. We interpret these high rates as reflecting the interaction of the toxin with channels that have a high probability of having  $Rb^+$  occupying the outer side of the pore. This is consistent with the fact that the toxin can bind almost 3 times better in the presence of extracellular  $Rb^+$  ( $A_{Rb}/A_K = 2.8$ ) than in  $K^+$ . Therefore in this case the rates of the binding reaction would be interpreted as:  $k_{off}^C = k_{-1}^{(Rb)}$  and  $k_{on}^C = p_{Rb} \cdot k_1$  and  $k_{on}^C$  would approach the open channel second order association rate  $k_1$  at high  $[Rb]_O$ , where  $p_{Rb}$  tends to 1.

This suggests that under these conditions scheme 4.3 can be reduced to the three states scheme 4.7. At intermediate  $[Rb]_O$  both a slow and a fast component are present. Indeed the finding that no significant difference was found in the binding of the toxin between 5 and 15 mM KCl in  $Na^+$ -based and  $Tris^+$ -based solutions validates the assumption that the contribution due to  $\kappa$ -PVIIA binding to the  $Na^+$ -occupied channels is negligible.



According to the scheme 4.7 the relaxation rate constants,  $\lambda_F$  and  $\lambda_S$  experimentally measured (F stands for fast, S for slow), are expected to be related to the kinetic parameters through the following expressions:

$$\lambda_S \cdot \lambda_F = P = k_1 \cdot [\text{T}] \cdot \left( (1 - p_{\text{Rb}} - p_{\text{Na}}) k_{-1}^{(\text{Rb})} + p_{\text{Rb}} k_{-1}^{(0)} \right) + k_{-1}^{(\text{Rb})} \cdot k_{-1}^{(0)} \quad \text{eq. 4.14}$$

$$\lambda_S + \lambda_F = S = (1 - p_{\text{Na}}) \cdot k_1 \cdot [\text{T}] + k_{-1}^{(\text{Rb})} + k_{-1}^{(0)} \quad \text{eq. 4.15}$$

with

$$\lambda_{F,S} = \frac{S \pm \sqrt{S^2 - 4P}}{2} \quad \text{eq. 4.16}$$

where S is the sum of the rate constants and P the product. A first prediction of the scheme 4.7 and eqs. 4.14 and 4.15 is that both S and P depend linearly on [T]. Second the steepness of the dependence of P on [T] should decrease with [Rb]<sub>0</sub>. Third, since in the Rb<sup>+</sup> concentration range where the fast component is measurable  $p_{\text{Na}}$  changes of only a 25%, we expect the slope of S vs [T] to be fairly constant (between 75%  $k_1$  and 100%  $k_1$ ).

The dependence on [T] of both the fast and the slow component could be well approximated by a straight line (chapter 3.4.2, fig. 3.15, table 3.4). Because  $\lambda_F$  and  $\lambda_S$  differ about one order of magnitude,  $\lambda_F$  would be a good approximation of S and  $\lambda_S$  would be roughly equal to P/S. Thus a rough estimate of the slope of  $\lambda_S$  vs [T] is given by the ratio of the slopes of the P and S dependencies on [T], which is expected to be closed to  $k_{-1}^{(\text{Rb})}$ .

Indeed the linear fit of  $\lambda_F$  vs [T] at any [Rb]<sub>0</sub> ≥ 5 mM did not show a clear dependence on [Rb]<sub>0</sub> giving within the error [Rb]<sub>0</sub>-independent values for the intercept with the Y axis, A, and the slope, B (table 3.4, with  $\lambda = A + B \cdot [\text{T}]$ ). In contrast, the slope of the slow component was clearly decreasing with [Rb]<sub>0</sub>, while A was fairly constant (table 3.4).

These findings support the validity of scheme 4.7 in the interpretation of our data.

We used measurements of  $\lambda_F$  and  $\lambda_S$  performed at different [T] and [Rb]<sub>0</sub> to evaluate the kinetic parameters  $k_{-1}^{(\text{Rb})}$  and  $k_1$  fixing  $p_{\text{Rb}}$  and  $p_{\text{Na}}$  to the values estimated assuming respectively  $K_{\text{Rb}} = 3.7$  and  $K_{\text{Na}} = 115$  mM and fixing  $k_{-1}^{(0)}$  to the value measured in low [Rb]<sub>0</sub> and low [K]<sub>0</sub> (1 s<sup>-1</sup>).

We fitted the sum,  $S = \lambda_F + \lambda_S$ , at [Rb]<sub>0</sub> = 5 and 15 mM and only the fast components at 30 and 57.5 mM with eq. 4.15 and the product  $P = \lambda_F \cdot \lambda_S$ , at [Rb]<sub>0</sub> = 5 and 15 mM with eq 4.14.

We estimated the values of the parameters  $k_{-1}^{(\text{Rb})}$  and  $k_1$  that could best approximate our experimental data by minimizing the global error of the fit, estimated to be proportional to the square root of  $(\lambda_{\text{S,theo}} - \lambda_{\text{S,exp}})^2 / (\lambda_{\text{S,exp}})^2 + (\lambda_{\text{F,theo}} - \lambda_{\text{F,exp}})^2 / (\lambda_{\text{F,exp}})^2$ . The best fit was obtained for the following values:  $k_{-1}^{(\text{Rb})} = 12 \text{ s}^{-1}$  and  $k_1 = 90 \mu\text{M}^{-1}\text{s}^{-1}$ .

The above values support once more the model assumption that  $k_1$  is the intrinsic rate of association to the channel outer vestibule, expected to be independent on the conformational state of the channel and on the occupancy of the pore by cations. On the contrary, the dissociation rate of the toxin is about 10-20 times larger when the association results in the trapping of  $\text{Rb}^+$  in the pore.

#### 4.7.2 Simulation of closed channel block in $[\text{K}]_0$ or $[\text{Rb}]_0$

We could describe the binding of  $\kappa$ -PVIIA to closed channels with a two state scheme in extracellular  $\text{K}^+$  (section 4.5.2; scheme 4.4) and with a three state scheme in extracellular  $\text{Rb}^+$  (section 4.7.1; scheme 4.7). Actually in both cases the toxin can block the channel by trapping or not trapping an ion. A  $\text{K}^+$  destabilizes the toxin more efficiently than a  $\text{Rb}^+$ , therefore we can observe the state  $\text{Tx}:\text{K}^+:\text{C}$  only indirectly, as a group of “missing” channels. In fact for increasing concentrations of  $[\text{K}]_0$  we observe a reduction of the association rate of the toxin due to the decrease of the number of channel that are blocked by the toxin and empty.

When in the extracellular solution  $\text{Rb}^+$  is present in some cases we can directly observe the relaxation of the channels that are in the state  $\text{Tx}:\text{Rb}^+:\text{C}$ .

We have found that the dissociation rate of the toxin from the channel is about  $1 \text{ s}^{-1}$  if no ion is trapped, about  $10 \text{ s}^{-1}$  in case a  $\text{Rb}^+$  is trapped. The actual association rate is the same measured for the open channels. For the dissociation rate of the toxin from a channel with a  $\text{K}^+$  in the pore we do not have any direct estimate because the kinetic is too fast to be measured. Assuming the same association rate, by comparing the dissociation constant  $K_{\text{K}^+}^{\text{Tx}}$  and  $K_{\text{Rb}^+}^{\text{Tx}}$ , we expect a dissociation rate 2-3 times higher when a  $\text{K}^+$  instead of a  $\text{Rb}^+$  is trapped.

In fig. 4.3 we show the predicted unblock probability for the indicated concentrations of extracellular  $\text{K}^+$  or  $\text{Rb}^+$ . They were obtained by calculating the amplitudes of the states of scheme 4.7 in the two cases ( $X_0$  for  $\{\text{U}\}$ ,  $X_{\text{S}}$  for  $\text{Tx}:\text{C}$ , and  $X_{\text{F}}$  for  $\text{Tx}:\text{K}^+:\text{C}$  or  $\text{Tx}:\text{Rb}^+:\text{C}$ ) and for simplicity we neglect the contributions of the channels that trap a  $\text{Na}^+$  ion:

$$U^{\text{C}} = X_0 + X_{\text{F}} \cdot \exp(-t \cdot \lambda_{\text{F}}) + X_{\text{S}} \cdot \exp(-t \cdot \lambda_{\text{S}}) \quad \text{eq. 4.17}$$

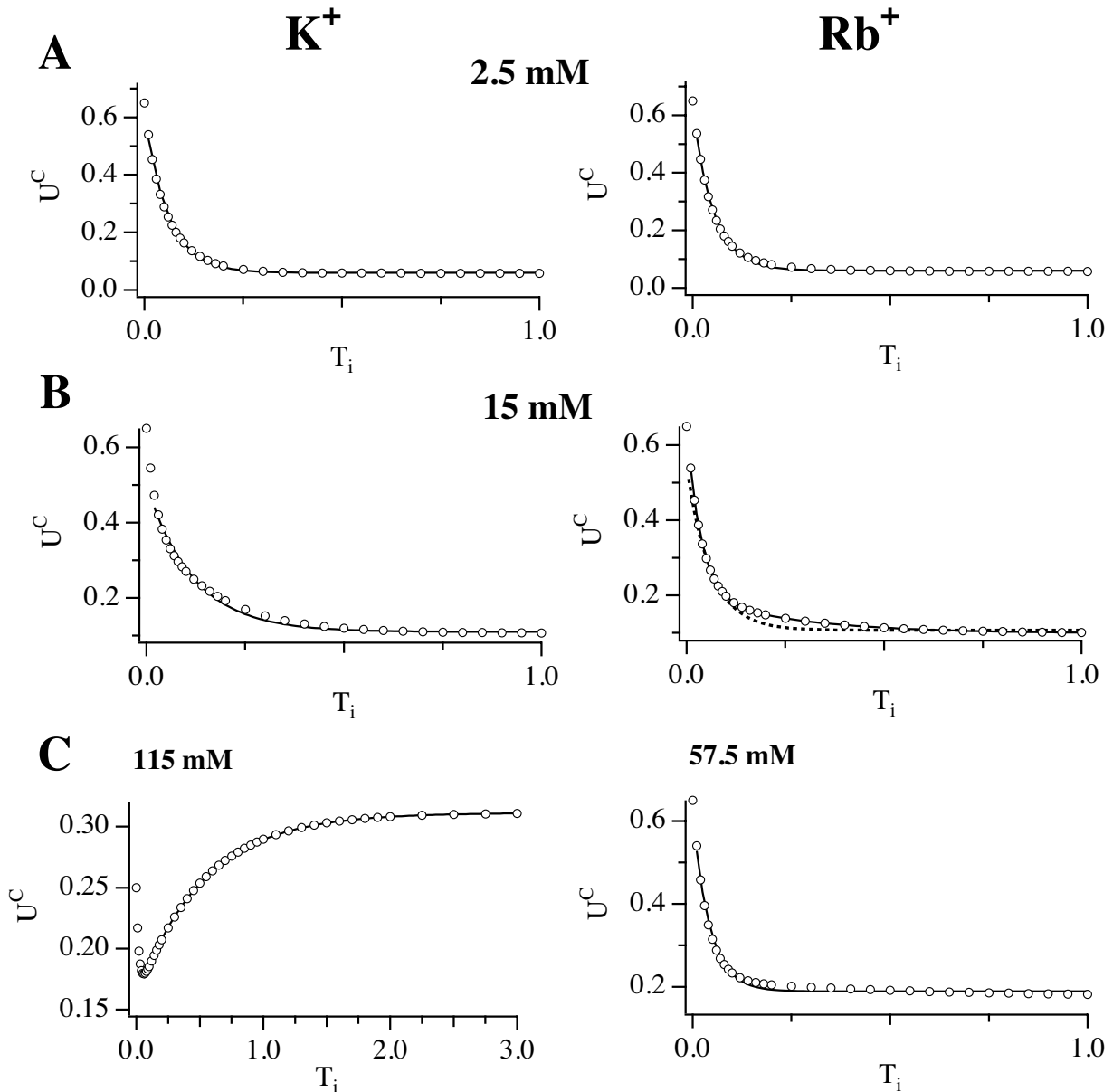


**Figure 4.3 Simulation of  $\kappa$ -PVIIA relaxation to closed channels in extracellular  $K^+$  (left) and  $Rb^+$  (right).** The starting unblock probability reflects our typical experimental conditions with 150 nM  $\kappa$ -PVIIA in the extracellular solution:  $U = 0.65$ , corresponding to a depolarizing pulse was used in all cases except for 115 mM KCl (panel C, left) where  $U = 0.25$ , corresponding to a pulse of about  $-20$  mV. The parameters assumed the following values:  $k_{-1}^{(0)} = 1 \text{ s}^{-1}$ ,  $k_{-1}^{(Rb)} = 10 \text{ s}^{-1}$ ,  $k_{-1}^{(K)} = 30 \text{ s}^{-1}$ ,  $k_1 \cdot [T] = 20 \text{ s}^{-1}$  and  $K_K = K_{Rb} = 5 \text{ mM}$ . The thick lines correspond to a single exponential fit with time constants: 60 ms in 2.5 mM KCl, 120 ms in 15 mM, 510 ms in 115 mM KCl; 53 ms in 2.5 mM RbCl, 43 ms 57.5 mM RbCl. In 15 mM RbCl the continuous line corresponds to a double exponential fit with time constants 270 ms and 35 ms. The dotted line to the single exponential fit with time constant 61 ms.

These amplitudes depend on  $k_{-1}^{(0)}$ ,  $k_{-1}^{(Rb)}$ ,  $k_{-1}^{(K)}$ ,  $k_1 \cdot [T]$ ,  $p_K$  or  $p_{Rb}$  and on the initial conditions. We assumed  $k_{-1}^{(0)} = 1 \text{ s}^{-1}$ ,  $k_{-1}^{(Rb)} = 10 \text{ s}^{-1}$  and  $k_{-1}^{(K)} = 30 \text{ s}^{-1}$ , and  $k_1 \cdot [T] = 20 \text{ s}^{-1}$ . Because we are interested in showing just roughly the consequences of a different destabilization of the toxin by  $K^+$  and  $Rb^+$ , we fixed  $K_K$  and  $K_{Rb}$  to the same value of 5 mM. The amplitudes of the states  $Tx:C$ ,  $Tx:K^+:C$  and  $Tx:Rb^+:C$  depended on the above parameters and on the starting



conditions. We used for  $U^C$  starting conditions corresponding to typical experiments: 0.65, corresponding to the unblock probability at the end of a depolarizing pulse in all cases except for 115 mM KCl, where we used 0.25, corresponding to a pulse to about  $-20$  mV with 150 nM  $\kappa$ -PVIIA in the extracellular solution ( $k_1 \cdot [T] = 20 \text{ s}^{-1}$ ). The predicted unblock probability ( $\circ$ ) as a function of time (in 115 mM KCl between 0-3 s, in the other cases between 0 and 1 s), is shown in the left panels for extracellular  $K^+$  and in the right panels for extracellular  $Rb^+$ . In the analysis of our experimental data we considered only the points corresponding to  $T_i$  at which the deactivation was complete. Consequently we fitted the simulated data as well with a single exponential, therefore skipping the first points. The fit is satisfactory for all the conditions, except  $[Rb]_O = 15 \text{ mM}$ . Depending on the initial condition the amplitudes change and both fast and slow component can contribute significantly to the relaxation also at other concentrations. Interestingly in 115 mM KCl, the two amplitudes have opposite sign and the slow component is preceded by a faster one (fig. 4.4C, left). In our experiments we occasionally observed this behavior, but since it occurred in a similar time scale of the kinetics of the deactivation at the test potentials investigated, we skipped these points from our analysis. In addition the initial unblock probability that we observed in such experiments, measured usually at  $T_i \sim 50 \text{ ms}$  was systematically lower than the unblock probability measured at the end of the first test pulse. In fact in fig. 3.8 the unblock probability at the end of the first pulse at  $-20 \text{ mV}$  is 0.23, while after  $T_i = 80 \text{ ms}$  at  $V_H = -100 \text{ mV}$  it is 0.19. This last observation supports the validity of the proposed kinetic schemes in interpreting the interaction of  $\kappa$ -PVIIA with K-channels.

#### 4.7.3 Open channel block vs $[Rb]_O$

Our data indicate that the toxin block of open channels is quite complex when  $Rb^+$  is in the extracellular solution.

Since both  $Rb^+$  and  $K^+$  are permeant, the kind of ion that occupies or not the outer site in the pore, thus affecting the interaction of the toxin with the channel, may depend either on the composition of the extracellular solution or on the direction of the current. We have seen above that for extracellular solutions where  $K^+$  was the only permeant ion, this site was always occupied by a  $K^+$ , independently on the  $[K]_O$  and on the current direction. We will show that to explain the data collected in  $Rb^+$  at least two ions in the pore must be involved in the process.

The first question to be answered is if the occupancy of the most external binding site is determined by the extracellular solution or by the ion species carrying the current. If cations present in the extracellular solution have free access to the more external binding site, we

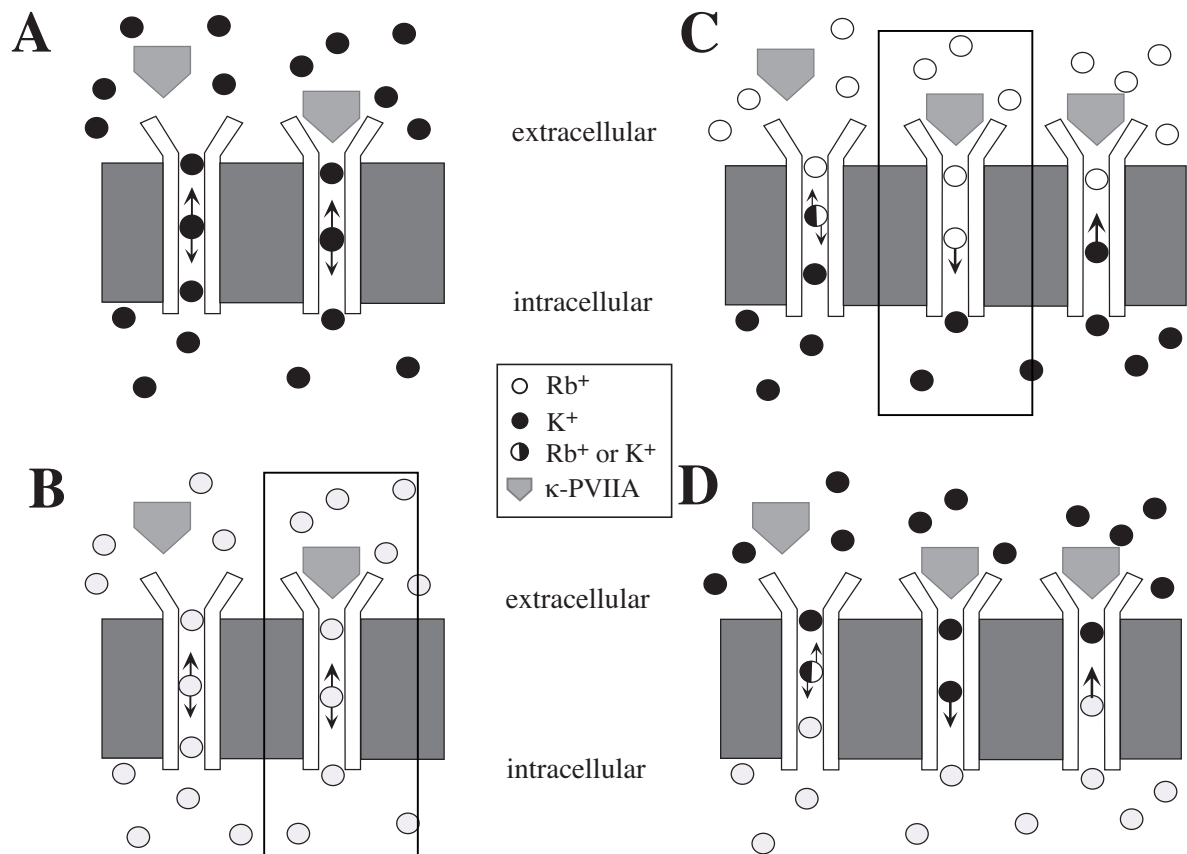


**Figure 4.4** Cartoons showing  $\kappa$ -PVIIA binding to *Shaker* channel in presence of  $K^+$  or  $Rb^+$ .

In control conditions the outer binding site is occupied by the ion in the extracellular solution. This ion is pushed and trapped inside the pore when the toxin binds. The central ion is determined by the ion species that carries the current. In symmetrical solutions, KCl (A) or RbCl (B), the two or more ions in the pore are of the same type. In not symmetrical solutions (C and D) the configuration of the pore is determined by the direction of the current, indicated by the arrows.

Eventually a third ion can occupy the pore and its species would be determined by the composition of the intracellular solution.

The configurations corresponding to the maximal destabilization of the toxins are highlighted by the box and correspond to two  $Rb^+$  in the pore.

expect that the number of ions that can reach the binding site per second is about  $10^8$ - $10^9$ . This estimate can be derived, following Hille (Hille 1992), by calculating the number of ions captured by a hemispherical sink whose radius,  $r_p$ , is the pore radius. We neglected the contribution of negative charges in the sink that would increase the number of ions captured. The number of diffusing ions per second would be equal to  $2\pi r_p D_K [K]_O$ , where  $D_K = 2 \cdot 10^{-5} \text{ cm}^2/\text{s}$  is the diffusion coefficient for potassium ions (Robinson and Stokes 1965).

Do all the ion that reach the pore permeate? The channels conductance, about 10 pS, produces a flux of  $6 \cdot 10^6$  ions per second with a driving force of 100 mV. Consequently not every ion arriving at the pore mouth will pass through the pore itself and therefore the occupancy of the most external binding site would be essentially determined by the extracellular solution.

When the toxin binds, it pushes this ion, if permeable, deeper in the pore. This ion would face from one site the toxin, and from the other another ion, eventually separated by a molecule of

water. This second ion would be the last ion that permeates and therefore its species would be determined by the direction of the current.

The cartoons in fig. 4.4 schematize the pore occupancy in the 4 different situations that we studied with monocationic solutions containing either the permeant  $K^+$  or  $Rb^+$ . When the solutions are symmetrical, two ions of the same specie are present in the pore, while when different cations are present the pattern of occupancy depends on the direction of the current. Considering just the dissociation rate, our results indicate that the toxin is much more destabilized in two cases: first, when  $Rb^+$  is present in both intracellular and extracellular solution (figs. 3.27, 3.28), second when  $Rb^+$  is in the extracellular solution,  $K^+$  in the intracellular solution and inward currents are driven (figs. 3.12, 3.28). According to our cartoons these cases correspond to the presence of two  $Rb^+$  in the pore (indicated by the box in fig. 4.4).

With respect to the dissociation rate, intracellular  $Rb^+$ , with extracellular  $K^+$ , is as efficient as  $K^+$  in repelling the toxin (fig. 3.18C). This case corresponds to an occupancy of the pore of either  $K^+$  and  $Rb^+$  or  $K^+$  and  $K^+$ , depending on the direction of the current. These two configurations repel equally well the toxin. Surprisingly, when we look at the dissociation constant, we observe for outward currents, carried by  $Rb^+$ , a steeper voltage dependence, due to a decrease of the second order association rate (fig 3.18B, 3.20). Even if we have no straightforward interpretation for this finding, we observe that when the toxin arrives at the channel mouth, it finds various patterns for pore occupancy that can influence differently the ability of toxin to bind. As pure speculation we add that the ion type may influence also the number of ions that may be accommodated at the same time in the pore.

The presented experimental findings show unequivocally how toxins like  $\kappa$ -PVIIA can be used as a probe of pore permeation.

#### **4.8 $K^+$ channels have 3 - 4 $K^+$ -binding sites**

Our results show that  $\kappa$ -PVIIA block of potassium channels is strongly affected by the composition of the solutions. Indeed the cations in the extracellular solution interfere competitively with the block of closed channels, while the intracellular cations modify the block of the open channels by pushing off the toxin with different efficiencies, depending on the permeability of the cation species.

These interactions are mediated by one or more binding sites in the pore region. In addition, the data recorded in presence of  $Rb^+$  rise the possibility that the distribution of the ions might depend on the ion species and be influenced by the presence of a bound toxin.

Can we identify our “putative” binding sites with the ones described in the literature?

Which are the analogies and the differences between  $K^+$  and  $Rb^+$ ?

$K^+$  channels have been described as a multi ion pores, with ability to conduct ions with great selectivity and yet at high rates achieved also thanks to the inter-ion repulsion (Hille and Schwarz 1978). The structural data of the pore region of the  $K^+$  channel from *Streptomyces lividans* (Doyle et al. 1998) revealed that the conduction pathway could indeed contain up to three ions, two in the selectivity filter and one in the intracellular cavity (fig. 4.5). As anticipated by electrophysiological data,  $Ba^{2+}$ , that has the same crystal radius as  $K^+$ , can fit in the selectivity filter (Jiang and MacKinnon 2000), but its charge apparently causes it to bind too tightly. Detailed studies on the properties of  $Ba^{2+}$  block showed that  $Ba^{2+}$  inhibition is sensitive to the presence of  $K^+$  in the pore of the  $K^+$  channels under investigation (for BK channels Neyton and Miller 1988a; b; Vergara et al. 1999, in *Shaker* Harris et al. 1998). Low external  $K^+$  concentrations tended to prevent  $Ba^{2+}$  to exit from the extracellular side, while higher concentrations caused  $Ba^{2+}$  to dissociate more rapidly to the internal side as if it could be pushed through. These phenomena were attributed to the presence of two  $K^+$  ion sites located between the blocking  $Ba^{2+}$  ion and the external solution. The presence of  $K^+$  at the first of these sites, termed the external lock-in site, would obstruct barium's outward movement. Occupancy of both sites by  $K^+$  (the site closest to  $Ba^{2+}$  was termed the enhancement site) would destabilize  $Ba^{2+}$  and speed its exit to the inside. The proposed positions of these sites (Neyton and Miller 1988a) compared with the crystallographic

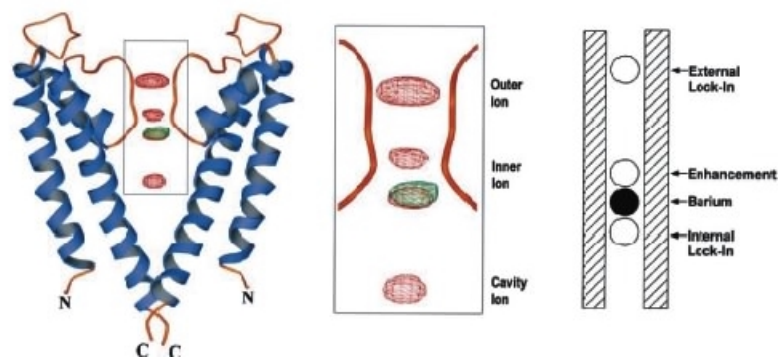


**Figure 4.5 Visualization cations binding sites in the KcsA K-channel by X-ray crystallography and in a Ca-activated K-channel by analysis of single channel function** (from Jiang and MacKinnon 2000) Left panel: ribbon picture of the KcsA K-channel (blue and orange) showing the positions of  $Rb^+$  (red mesh) and  $Ba^{2+}$  (green mesh) in the pore by difference in electron densities.  $Rb^+$  instead of  $K^+$  is reported because it is more electrondense. The magnification of the boxed region in KcsA channel (middle) is compared to the diagram proposed by Neyton and Miller (1988a) for the relative locations of  $Ba^{2+}$  and  $K^+$  or  $Rb^+$  sites in the pore of  $Ca^{2+}$ -activated K-channel (external lock-in, enhancement, and internal lock-in) as determined by examination of single-channel records. The ions are positioned according to their electrical distance across the membrane potential difference. In the KcsA channel (middle panel) the three ion positions are labeled outer, inner, and cavity. The inner ion shows two peaks reflecting alternative positions.  $Ba^{2+}$  is located at the innermost position of the inner ion.

structure (Doyle et al. 1998; Jiang and MacKinnon 2000) are shown in fig 4.5, as described in Jiang and MacKinnon (2000). By evaluating a series of different ions, the lock-in and enhancement sites were shown to be highly selective for alkali metal ions that permeate K<sup>+</sup> channels such as K<sup>+</sup> and Rb<sup>+</sup>, and weakly for Na<sup>+</sup>. The lock-in site in *Shaker* channels has an affinity of 0.75 mM for K<sup>+</sup> and feel the 35% of the potential drop (Harris et al. 1998). Quite interestingly the pore occupancy by an ion seems to be determined by the concentration of permeant ions: the enhancement site indeed become significantly occupied only at high K<sup>+</sup> concentrations.

In BK channels an additional monovalent ion site, termed the internal lock-in site, was hypothesized to be located between the position of Ba<sup>2+</sup> and the internal entry of the ion channel pore; this site became occupied with an affinity constant of about 10 mM. In contrast to the sites which are located external to Ba<sup>2+</sup>, the internal lock-in site was not very selective for K<sup>+</sup> when compared with Na<sup>+</sup> (Neyton and Miller 1988a). So far it is not known if a similar site does exist in the pore lining of *Shaker* channels.

Within the pore lining several binding sites for cations have been identified for which the binding of the cation interferes with channel gating, like inactivation and deactivation.

It has been shown that the presence of permeant cations as K<sup>+</sup> and Rb<sup>+</sup> in the external solution slow the closing of K<sup>+</sup> channels, leaving the activation kinetics unaffected (Swenson and Armstrong 1981; Matteson and Swenson 1986). In this case the presence of a permeant ion near the inner end of the channel is thought to prevent closing probably by binding near the inner surface of the membrane. Rb<sup>+</sup>, which enters equally well the channel but binds more tightly, has a larger effect on the closing rate than the more loosely bound K<sup>+</sup>. The dissociation constant of Rb<sup>+</sup> with its site of action is 5.4 mM in squid (Matteson and Swenson 1986).

Additionally also the rate of C-type inactivation is determined by the occupancy of a binding site near the external mouth of the pore (López-Barneo et al. 1993). This site is strongly selective for K<sup>+</sup> over Na<sup>+</sup>, even if an acceleration of the kinetic of inactivation is observed with NMDG<sup>+</sup>: in *Shaker* the affinity for K<sup>+</sup> is about 2 mM (Baukrowitz and Yellen 1995 and Baukrowitz and Yellen 1996). This value is quite similar to that found for the external lock-in site, suggesting that it may be the same site (Harris et al. 1998). This hypothesis is supported by the finding that for BK channels, which do not show C-type inactivation in nominally K<sup>+</sup>-free solution, the external lock-in site has an affinity for K<sup>+</sup> in the micromolar range. In presence of a K<sup>+</sup>-chelator in the bath, these channels show long closing events (Vergara et al. 1999).

The presence of K<sup>+</sup> is important for the normal functioning of some K<sup>+</sup> channels: in fact the

total removal of  $K^+$ , i.e. from both the internal and the external side, exerts some effect, like spontaneous and irreversible run down or complete loss of the ionic currents of the channel (Pardo et al. 1992). In contrast some channels remain stable and even conduct  $Na^+$  after the total removal of  $K^+$  (Korn and Ikeda 1995). Furthermore *Shaker* channels that undergo fast C-type inactivation in absence of  $K^+$  conduct  $Na^+$  or  $Li^+$  when they are in the C-type inactivated state (Starkus et al. 1997; Starkus et al. 2000). This demonstrates that channels are capable of conducting normally impermeant cations after the total removal of internal  $K^+$ . The permeation of these ions can be blocked by submillimolar concentrations of internal  $K^+$ , suggesting the presence of a high affinity  $K^+$  binding site at the internal surface of the permeation pathway, where  $K^+$  binding contributes to the blockade of apparently impermeant ion species.

A similar feature was observed in  $Ca^{2+}$ -selective channels that in absence of extracellular  $Ca^{2+}$  become freely permeable to divalent as well as monovalent cations, such as  $K^+$  and  $Na^+$ . Apparently the selectivity of the channel depends on the occupancy by  $Ca^{2+}$  of a specific site of high affinity (in the  $\mu M$   $Ca^{2+}$  -concentration range; McCleskey and Almers 1985).

The occupancy of cation binding sites can interfere also with the blocking ability of intracellular and extracellular compound, like TEA. Thompson and Begenisich (2000) found that in *Shaker* channels external TEA antagonizes the effectiveness of internal TEA only when  $K^+$  ions are in the intracellular and extracellular solution. On the contrary when  $Rb^+$  is the permeant ion, external TEA is entirely ineffective in protecting the channels from block by internal TEA, even if external TEA binds slightly more efficiently in the presence in the extracellular solution of  $Rb^+$  than of  $K^+$ . The apparent interaction between external and internal TEA seems to depend on the identity of the permeant ion and is not likely to be mediated by a through-space electrostatic repulsion mechanism. The authors used a 4-barrier-3-site model with symmetrical barrier shapes to simulate their results and assuming simply a larger second energy maximum in  $Rb^+$  than in  $K^+$ . In this way they could predict the elimination of the internal and external TEA antagonism in presence of  $Rb^+$ . The addition of TEA causes probably a different redistribution of the ions, depending on the ion species.

The inward rectifier ROMK1  $K^+$ -channel exhibits different degrees of rectification when different alkali metal ions are present in the extra- and intracellular solutions. It has been shown that the binding to an external ion site of various alkali metal ions can be altered by the binding of different permeating ions at an internal site (Spassova and Lu 1999). This mechanism seems not to be of electrostatic nature. The external and internal ion-binding sites in the ROMK1 pore appear to have different ion selectivity: the external site selects strongly against the smaller  $Na^+$ , but only modestly among the three larger ions,  $K^+$ ,  $Rb^+$  and  $Cs^+$ ,

whereas the internal site interacts quite differently with  $K^+$  and  $Rb^+$ .

With respect to the data presented in this work, literature shows indeed that ion permeability is not absolute, but actually depends on the “ionic-environment” and on some extent even on the conformation of the channel (C-type inactivated state). Moreover the pore appears to host several binding sites with different ion-selectivity scales, in particular an outer binding site highly discriminating between  $K^+$  or  $Rb^+$  and  $Na^+$  and an inner binding site poorly selective between  $K^+$  and  $Na^+$ , but discriminating against the less permeant cations as  $NMDG^+$  and  $Tris^+$ . These binding sites could eventually be involved in the interaction of  $\kappa$ -PVIIA with the *Shaker* channel, accounting respectively for the dependency on the extracellular and intracellular solution composition.

Finally, as a pure speculation, we can add that the data of Thompson and Begenisich (2000) arise the possibility of a different redistribution of the ions depending on the species and also on the presence or not of a “perturbation”, represented in their case by TEA and in our by  $\kappa$ -PVIIA.

## 4.9 Summary

$\kappa$ -PVIIA blocks  $K^+$  channels by interacting with the outer pore mouth without modifying the gating apparatus. When the toxin is bound it interacts intimately with the ion(s) sitting in the pore as shown by the dependence of the block on the solution composition and on voltage.

$\kappa$ -PVIIA blocks differently the channel in the conductive or non-conductive state, which is either the closed or N-type inactivated state. This ability can be due to a different interaction of the toxin either with the conformational states of the protein or with ions in the pore. Our data support the last hypothesis.

The interaction of  $\kappa$ -PVIIA with the channel depends on the identity of the permeant ion.

When  $K^+$  is the only permeant ion the destabilization of the toxin bound to the open channel is independent of the extracellular  $K^+$  concentration, while for closed channels the efficiency of the block decreases at higher extracellular  $K^+$  concentrations.

The removal of intracellular permeant ions reduces, but does not eliminate completely the voltage dependence of the block.  $Na^+$ , which is permeable in absence of  $K^+$ , mimics its destabilizing action.

The study of the interaction of  $\kappa$ -PVIIA with the channel in presence of  $Rb^+$  instead of  $K^+$  as a permeant ion, showed a complex interaction between the toxin and the channel, mediated by at least two ions in the pore when the channel is in the open conformation. The destabilization of the toxin is much higher when two  $Rb^+$  are present in the pore. In contrast, the toxin that binds to the channel in the closed conformation is less destabilized by a trapped  $Rb^+$  than by a

K<sup>+</sup>.

Such a different interaction of the toxin with two similar cations suggests that there might be a different occupancy of the pore by these ions, either in number of ions and maybe positions. This different occupancy depends on the solution composition and eventually on the state of the channel.

Therefore  $\kappa$ -PVIIA can be successfully used as a probe for understanding channel functioning and could help to correlate electrophysiological and structural data.



## Abbreviations

cRNA	complementary RNA (ribonucleic acid)
CTX	Charybdotoxin ( $\alpha$ -KTx)
EGTA	Ethylenglycol-bis( $\beta$ -aminoethylether-)N,N,N',N'-Tetra acetic acid
Hepes	N-2-Hydroxyethylpiperazine-N'-2-ethane-sulfonic acid
$I_C$	capacitive current
$I_G$	gating current
$I_L$	leakage current
$I_{ION}$	ionic current
$IC_{50}$	half maximal inhibitory dose
$K_D$	dissociation constant
$K^O, K^C$	dissociation constant for the open and closed channel
$K_{app}^O$	apparent dissociation constant for the open channel
$k_{off}^O, k_{off}^C$	dissociation rate for the open or closed channel
$k_{on}^O, k_{on}^C$	2 <sup>nd</sup> order association rate for the open or closed channel
$\kappa$ -PVIIA	$\kappa$ -conotoxin PVIIA
NFR	normal frog Ringer
NMDG	N-Methyl-D-Glucamine
<i>Shaker-wt, Shaker-<math>\Delta</math></i>	<i>Shaker</i> wild type, <i>Shaker-<math>\Delta</math>6-46</i>
TEA	Tetraethylammonium
TEVC	Two electrode voltage clamp
$T_i$	interpulse interval
Tris	Tris(hydroxymethyl)aminomethane
$U^O, U^C$	unblock probability for open and closed channel
$v_s$	e-fold slope for toxin block voltage sensitivity
$V_{1/2}$	half activation potential
$V_H$	holding potential
$V_{Inv}$	inversion potential
$V_P$	test potential
$V_{Rev}$	reversal potential
$V_{Tail}$	tail potential
X-Ringer	Ringer solution with ion X
$[X]_I, [X]_O$	intracellular and extracellular concentration of the ion of species X
[T]	toxin concentration

## References

- Adams, M. E. and Olivera, B. M. 1994. Neurotoxins: overview of an emerging research technology. *Trends Neurosci.* **17**: 151-155.
- Anderson, C. S., MacKinnon, R., Smith, C. and Miller, C. 1988. Charybdotoxin block of single Ca<sup>2+</sup>-activated K<sup>+</sup> channels. Effects of channel gating, voltage and ionic strength. *J. Gen. Physiol.* **91**: 317-333.
- Armstrong, C. M. 1971. Interaction of tetraethylammonium ion derivatives with the potassium channels of giant axons. *J. Gen. Physiol.* **58**: 413-437.
- Armstrong, C. M. and Bezanilla, F. 1977. Inactivation of the sodium channel. II. Gating current experiments. *J. Gen. Physiol.* **70**: 567-590.
- Armstrong, C. M. and Hille, B. 1998. Voltage-gated ion channels and electrical excitability. *Neuron* **20**: 371-380.
- Barry, P. H. and Lynch, J. W. 1991. Liquid junction potential and small cells effects in patch-clamp analysis. *J. Membr. Biol.* **121**:101-117.
- Baukrowitz, T. and Yellen, G. 1995. Modulation of K<sup>+</sup> current by frequency and external [K]: a tale of two inactivation mechanism. *Neuron* **15**: 951-960.
- Baukrowitz, T. and Yellen, G. 1996. Use-dependent blockers and exit rate of the last ion from the multi-ion pore of a K<sup>+</sup> channel. *Science* **271**: 653-656.
- Baumgartner, W., Islas, L. and Sigworth, F. J. 1999. Two-microelectrode voltage clamp of *Xenopus* oocytes: voltage errors and compensation for local current flow. *Biophys. J.* **77**: 1980-1991.
- Bontems, F., Roumestand, C., Gilquin, B., Ménez, A. and Toma, F. 1991. Refined structure of charybdotoxin: common motifs in scorpion toxins and insects defensins. *Science* **254**: 1521-1523.
- Chen, J., Avdonin, V., Ciorba, M. A., Heinemann, S. H. and Hoshi, T. 2000. Acceleration of P/C-type inactivation in voltage-gated K<sup>+</sup> channels by methionine oxidation. *Biophys. J.* **78**: 174-187.
- Choi, K. L., Aldrich, R. W. and Yellen, G. 1991. Tetraethylammonium blockade distinguishes two activation mechanisms in voltage-activated K<sup>+</sup> channels. *Proc. Natl. Acad. Sci. USA* **88**: 5092-5095.
- Cushman, S. J., Nanao, M. H., Jahng, A. W., Derubeis, D., Senyon, C. and Pfaffinger, P. J. 2000. Voltage dependent activation of potassium channels is coupled to T1 domain structure. *Nat. Struct. Biolog.* **7**: 403-407.
- Dauplais, M., Lecoq, A., Song, J., Cotton, J., Jamin, N., Gilquin, B., Vita, C., De Medeiros, C. L. C., Rowan, E. G., Harvey, A. L. and Ménez, A. 1997. On the convergent evolution of animal toxins. *J. Biol. Chem.* **272**: 4302-4309.
- Doyle, A. D., Cabral, J. M., Pfuetzner, R. A., Kuo, A., Gulbis, J. M., Cohen, S. L., Chait, B. T. and MacKinnon, R. 1998. The structure of the potassium channel: molecular basis of K<sup>+</sup> conduction and selectivity. *Science* **280**: 69-77.
- Goldin, A. L. 1992. Maintenance of *Xenopus laevis* and oocyte injection. *Methods Enzymol.* **207**: 266-279.
- Goldstein, S. A. N. and Miller, C. 1992. A point mutation in a *Shaker* K<sup>+</sup> channel changes its

- charybdotoxin binding site from low to high affinity. *Biophys. J.* **62**: 5-7.
- Goldstein, S. A. N. and Miller, C. 1993. Mechanism of charybdotoxin block of a voltage-gated K<sup>+</sup> channel. *Biophys. J.* **65**: 1613- 1619.
- Goldstein, S. A. N., Pheasant, D. J. and Miller, C. 1994. The charybdotoxin receptor of a *Shaker* K<sup>+</sup> channel-peptide and channel residues mediating molecular recognition. *Neuron* **12** (6): 1377-1388.
- Hamill, O. P., Marty, A., Neher, E., Sakmann, B. and Sigworth, F. J. 1981. Improved patch-clamp techniques for high-resolution current recording from cells and cell-free membrane patches. *Pflügers Arch.* **391**: 85-100.
- Harris, R. E., Larsson, H. P. and Isacoff, E. Y. 1998. A permeant ion binding site located between two gates of the *Shaker* K<sup>+</sup> channel. *Biophys. J.* **74**: 1808-1820.
- Heinemann, S. H. 1995. Guide to data acquisition and analysis. In: *Single-Channel Recording*. B. Sakmann and E. Neher. New York and London, Plenum Press. **Chapt. 3**: 53- 91.
- Hille, B. 1973. Potassium channels in myelinated nerve. Selective permeability to small cations. *J. Gen. Physiol.* **61**: 669-686.
- Hille, B. and Schwarz, W. 1978. Potassium channels as multi-ion single-file pores. *J. Gen. Physiol.* **72**: 409 - 442.
- Hille, B. 1992. Ionic channels of excitable membranes. Sunderland, Massachusetts: Sinauer Associates, Inc. Sec. Edition.
- Hille, B., Armstrong, C. M. and MacKinnon, R. 1999. Ion channels: from idea to reality. *Nature Med.* **5**: 1105-1109.
- Hodgkin, A. L. and Keynes, R. D. 1955. The potassium permeability of a giant nerve fibre. *J. Physiol., London* **128**: 61-88.
- Hoshi, T., Zagotta, W. and Aldrich, R. 1990. Biophysical and molecular mechanisms of *Shaker* potassium channel inactivation. *Science* **250**: 533-538.
- Hoshi, T., Zagotta, W. N. and Aldrich, R. W. 1991. Two types of inactivation in *Shaker* K<sup>+</sup> channels: effects of alterations in the carboxy-terminal region. *Neuron* **7**: 547- 556.
- Hoshi, T., Zagotta, W. N. and Aldrich, R. W. 1994. *Shaker* potassium channel gating I: transitions near the open state. *J. Gen. Physiol.* **103**: 249-278.
- Imredy, J. P. and MacKinnon, R. 2000. energetic and structural interactions between  $\delta$ -dendrotoxin and a voltage-gated potassium channel. *J. Mol. Biol.* **296**: 1283-1294.
- Isom, L. L., Jongh De, K. S., Patton, D. E., Reber, B. F. X., Offord, J., Charbonneau, H., Walsh, K., Goldin, A. L. and Catterall, W. A. 1992. Primary structure and functional expression of the  $\beta$ 1 subunit of the rat brain sodium channel. *Science* **256**: 839-842.
- Jacobsen, R. B., Koch, E. D., Lange-Malecki, B., Stocker, M., Verhey, J., Van Wagoner, R. M., Vyazovkina, A., Olivera, B. M. and Terlau, H. 2000. Single amino acid substitutions in  $\kappa$ -conotoxin PVIIA disrupt interaction with the *Shaker* K<sup>+</sup> channel. *J. Biol. Chem.* **275** (32): 24639-24644.
- Jiang, Y. and MacKinnon, R. 2000. The barium site in a potassium channel by X-ray crystallography. *J. Gen. Physiol.* **115**: 269-272.
- Korn, S. J. and Ikeda, S. R. 1995. Permeation selectivity by competition in a delayed rectifier potassium channel. *Science* **269**: 410-412.

- Kreusch, A., Pfaffinger, P. J., Stevens, C. F. and Choe, S. 1998. Crystal structure of the tetramerization domain of the *Shaker* potassium channel. *Nature* **392**: 945-948.
- López-Barneo, J., Hoshi, T., Heinemann, S. H. and Aldrich, R. W. 1993. Effects of external cations and mutations in the pore region on C-type inactivation of *Shaker* potassium channels. *Receptors and Channels* **1**: 61-71.
- MacKinnon, R. and Miller, C. 1988. Mechanism of charybdotoxin block of the high-conductance, Ca<sup>2+</sup>-activated K<sup>+</sup> channel. *J. Gen. Physiol.* **91**: 335-349.
- MacKinnon, R. and Miller, C. 1989. Mutant potassium channels with altered binding of charybdotoxin, a pore-blocking peptide inhibitor. *Science* **245**: 1382-1385.
- MacKinnon, R. 1991. Determination of the subunits stoichiometry of a voltage-activated potassium channel. *Nature* **350**: 232 - 235.
- Matteson, D. R. and Swenson, R. P. J. 1986. External monovalent cations that impede the closing of K<sup>+</sup> channels. *J. Gen. Physiol.* **87**: 795-816.
- McCleskey, E. W. and Almers, W. 1985. The Ca channel in skeletal muscle is a large pore. *Proc. Natl. Acad. Sci. USA* **82**: 7149-7153.
- Ménez, A. 1998. Functional architectures of animal toxins: a clue to drug design? *Toxicon* **36** (11): 1557-1572.
- Methfessel, C., Witzemann, V., Takahashi, T., Mishina, M., Numa, S. and Sakmann, B. 1986. Patch clamp measurements on *Xenopus laevis* oocytes: currents through endogenous channels and implanted acetylcholine receptor and sodium channels. *Pflügers Arch.* **407** (577): 577-588.
- Miller, C. 1995. The charybdotoxin family of K<sup>+</sup> channel-blocking peptides. *Neuron* **15**: 5-10.
- Morales, M. J., Castellino, R. C., Crews, A. L., Rasmusson, R. L. and Strauss, H. C. 1995. A novel  $\beta$ -subunit increases rate of inactivation of specific voltage-gated potassium channel  $\alpha$ -subunits. *J. Biol. Chem.* **270** (11): 6272-6277.
- Moran, O. 1996. Patch clamp technique. In: *Experimental Techniques in Bioelectrochemistry*. V. Brabec, D. Walz and G. Milazzo. Basel, Switzerland, Birkhauser Verlag.
- Neher, E., Sakmann, B. and Steinbach, J. H. 1978. The extracellular patch clamp: a method resolving current through individual open channels in biological membranes. *Pflügers Arch.* **375**: 219-228.
- Neher, E. 1995. Voltage offsets in patch clamp experiments. In: *Single-Channel Recording*. B. Sakmann and E. Neher. New York, Plenum Press: 147-153.
- Neyton, J. and Miller, C. 1988a. Discrete Ba<sup>2+</sup> block as a probe of ion occupancy and pore structure in the high-conductance Ca<sup>2+</sup>-activated K<sup>+</sup> channel. *J. Gen. Physiol.* **92**: 569-586.
- Neyton, J. and Miller, C. 1988b. Potassium blocks barium permeation through a calcium-activated potassium channel. *J. Gen. Physiol.* **92**: 549-567.
- Noda, M., Shimizu, S., Tanabe, T., Takai, T., Kayano, T., Ikeda, T., Takahashi, H., Nakayama, H., Kanaoka, Y., Minamino, N., Kangawa, K., Matsuo, H., Raftery, M. A., Hirose, T., Inayama, S., Hayashida, H., Miyata, T. and Numa, S. 1984. Primary structure of *electrophorus electricus* sodium channel deduced from cDNA sequence. *Nature* **312**: 121-127.
- Olivera, B. M. and Cruz, L. J. 2001. Conotoxins, in retrospect. *Toxicon* **39**: 7-14.
- Papazian, D. M., Timpe, L. C., Jan, Y. N. and Jan, L. Y. 1991. Alteration of voltage-

- dependence of *Shaker* potassium channel by mutations in the S4 sequence. *Nature* **349**: 305-310.
- Pardo, L. A., Heinemann, S., Terlau, H., Ludewig, U., Lorra, C., Pongs, O. and Stühmer, W. 1992. Extracellular K<sup>+</sup> specifically modulates a rat brain K<sup>+</sup> channel. *Proc. Natl. Acad. Sci. USA* **89**: 2466-2470.
- Park, C. and Miller, C. 1992. Interaction of charybdotoxin with permeant ions inside the pore of a K<sup>+</sup> channel. *Neuron* **9**: 307-313.
- Perozo, E., Cortes, D. M. and Cuello, L. G. 1999. Structural rearrangements underlying K<sup>+</sup>-channel activation gating. *Science* **285**: 73-78.
- Rettig, J., Heinemann, S. H., Wunder, F., Lorra, C., Parcej, D. N., Dolly, J. O. and Pongs, O. 1994. Inactivation properties of voltage-gated K<sup>+</sup> channels altered by presence of  $\beta$ -subunit. *Nature* **369**: 289-294.
- Robinson, R. A. and Stokes, R. H. 1965. Electrolyte solutions. London, Butterworth.
- Sakmann, B. and Neher, E. 1995. Single-Channel Recording. New York, Plenum Press.
- Sato, C., Ueno, Y., Asai, K., Takahashi, K., Sato, M., Engel, A. and Fujiyoshi, Y. 2001. The voltage-sensitive sodium channel is a bell-shaped molecule with several cavities. *Nature* **409**: 1047-1051.
- Savarin, P., Guenneugues, M., Gilquin, B., Lamthanh, H., Gasparini, S., Zinn-Justin, S. and Ménez, A. 1998. Three-dimensional structure of  $\kappa$ -conotoxin PVIIA, a novel potassium channel-blocking toxin from cone snails. *Biochemistry* **37**: 5407-5416.
- Scanlon, M. J., Naranjo, D., Thomas, L., Alewood, P. F., Lewis, R. J. and Craik, D. J. 1997. Solution structure and proposed binding mechanism of a novel potassium channel toxin  $\kappa$ -conotoxin PVIIA. *Structure* **5**: 1585-1597.
- Shon, K., Stocker, M., Terlau, H., Stühmer, W., Jacobsen, R., Walker, C., Grilley, M., Watkins, M., Hillyard, D. R., Gray, R. and Olivera, B. M. 1998.  $\kappa$ -conotoxin PVIIA is a peptide inhibiting the *Shaker* K<sup>+</sup> channel. *J. Biol. Chem.* **273**: 33-38.
- Skarzynsky, T. 1992. Crystal structure of  $\alpha$ -dendrotoxin from the green mamba venom and its comparison with the structure of bovine pancreatictrypsin inhibitor. *J. Mol. Biol.* **224**: 671-683.
- Sokolova, O., Kolmakova-Partensky, L. and Grigorieff, N. 2001. Three-dimensional structure of a voltage-gated potassium channel at 2.5 nm resolution. *Structure* **9**: 215-220.
- Spassova, M. and Lu, Z. 1999. Tuning the voltage dependence of tetraethylammonium block with permeant ions in an inward-rectifier K<sup>+</sup>-channel. *J.Gen. Physiol.* **114**: 415-426.
- Starkus, J. G., Kuschel, L., Rayner, M. D. and Heinemann, S. H. 1997. Ion conduction through C-type inactivated *Shaker* channels. *J.Gen. Physiol.* **110**: 539-550.
- Starkus, J. G., Heinemann, S. H. and Rayner, M. D. 2000. Voltage dependence of slow inactivation in *Shaker* potassium channels results from changes in relative K<sup>+</sup> and Na<sup>+</sup> permeabilities. *J.Gen. Physiol.* **115**: 107-122.
- Stühmer, W., Conti, F., Suzuki, H., Wang, X., Noda, M., Yahagi, N., Kubo, H. and Numa, S. 1989. Structural parts involved in activation and inactivation of the sodium channel. *Nature* **339**: 597-603.
- Stühmer, W., Terlau, H. and Heinemann, S. H. 1992. Two electrode and patch clamp recording from *Xenopus* oocytes. In: *Practical Electrophysiological Methods*. H.

- Kettenmann and R. Grantyn. New York, Wiley-Liss: 121-125.
- Stühmer, W. and Parekh, A. B. 1995. Electrophysiological recordings from *Xenopus* oocytes. In: *Single Channel Recording*. B. Sakmann and E. Neher. New York and London, Plenum Press. **Chap. 15**: 341-356.
- Swartz, K. J. and MacKinnon, R. 1997. Mapping the receptor site for Hanatoxin, a gating modifier of voltage-dependent K<sup>+</sup> channels. *Neuron* **18**: 675-682.
- Swenson, R. P. J. and Armstrong, C. M. 1981. K<sup>+</sup> channels close more slowly in the presence of external K<sup>+</sup> and Rb<sup>+</sup>. *Nature* **291**: 427-429.
- Taglietti, V. and Toselli, M. 1988. A study of stretch activated channels in the membrane of frog oocytes: interaction with Ca<sup>2+</sup> ions. *J. Physiol.* **407**: 311-328.
- Takahashi, T., Neher, E. and Sakmann, B. 1987. Rat brain serotonin receptor in *Xenopus* oocytes are coupled by intracellular calcium to endogenous channels. *Proc. Natl. Acad. Sci. USA* **84**: 5063-5067.
- Tempel, B., Papazian, D., Schwarz, T., Jan, Y. and Jan, L. 1987. Sequence of a probable potassium channel component encoded at *Shaker* locus of *Drosophila*. *Science* **237**: 770-775.
- Terlau, H., Heinemann, S. H., Stühmer, W., Pusch, M., Conti, F., Imoto, K. and Numa, S. 1991. Mapping the site of block by tetrodotoxin and saxitoxin of sodium channel II. *FEBS Letters* **293**: 93-96.
- Terlau, H., Shon, K., Grilley, M., Stocker, M., Stuehmer, W. and Olivera, B. M. 1996. Strategy for rapid immobilization of prey by a fish-hunting marine snail. *Nature* **381**: 148-151.
- Terlau, H. and Stühmer, W. 1998. Structure and function of voltage-gated ion channels. *Naturwissenschaften* **85**: 437-444.
- Terlau, H., Boccaccio, A., Olivera, B. M. and Conti, F. 1999. The block of *Shaker* K<sup>+</sup> channels by κ-conotoxin PVIIA is state dependent. *J.Gen.Physiol.* **114**:125-140
- Thompson, J. and Begenisish, T. 2000. Interaction between quaternary ammonium ions in the pore of potassium channels. *J. Gen. Physiol.* **115**: 769-782.
- Vergara, C., Alvarez, O. and Latorre, R. 1999. Localization of the K<sup>+</sup> lock-in and the Ba<sup>2+</sup> binding sites in a voltage-gated calcium-modulated channel. *J. Gen. Physiol.* **114**: 365-376.
- Woodhull, A. M. 1973. Ionic blockage of sodium channels in nerve. *J. Gen. Physiol.* **61**: 687-708.
- Yang, X. C. and Sachs, F. 1989. Block of stretch-activated ion channels in *Xenopus* oocytes by gadolinium and calcium ions. *Science* **243**: 1068-1071.
- Yang, X. C. and Sachs, F. 1990. Characterization of stretch-activated ion channels in *Xenopus* oocytes. *J. Physiol.* **431**: 103-122.
- Yellen, G. 1998. The moving parts of voltage-gated ion channels. *Q. Rev. Biophys.* **31** (3): 239-295.
- Zagotta, W., Hoshi, T. and Aldrich, R. 1990. Restoration and inactivation in mutants of *Shaker* potassium channels by a peptide derived from *ShB*. *Science* **250**: 568-571.

## Acknowledgements

I would like to acknowledge Prof. E. Sackmann, Prof. W. Stühmer, Dr. H. Terlau and Prof. F. Conti for their invaluable support, help, input and guidance throughout the course of my Ph.D.. In addition, I want to thank Mona Honemann, Sabine Schäpermeier and Wolfram Lessner for excellent technical assistance. Also, I'd like to thank Ute Rust for unconditional assistance with the management of never ending paperwork and, more important, for helping me in the understanding of the German-lifestyle. Thanks to the "artists" Lania Rubio and Oscar Moran for help with figures. Likewise, I would like to thank Ute Becherer and Rocio Finol for voluntarily assuming the hard task of correcting the manuscript.

I'd like to thank former and actual colleagues in the groups of *Molecular Biology and Neuronal Signaling* and *Molecular and Cellular Neuropharmacology* at the Max Planck Institute for Experimental Medicine, Göttingen, for their collaboration and solidarity. I would like to express my gratitude to the Institute of Cybernetics and Biophysics of the CNR in Genova for the kind hospitality; in particular Michael Pusch and Alessio Accardi for lending me the set-up.

I want to show my appreciation to my friends and colleague-friends that encouraged and helped me to overcome the difficult periods of the thesis sharing laughs and good humor.

Finally, I would like to express my sincere gratefulness to my friends Claudia and Thomas for invaluable moral and logistic support, to Paolo for his patience, understanding and for spending cold summers in Germany. Furthermore, thanks a lot to my "tomato-aunts" Carolina and Angioletta and, last but not least, to my parents.

Grazie

Anna

## Curriculum vitae et studiorum

- 15.11.1971** born in Genova, Italy
- 1977 - 1982** Ground school, Istituto Suore Benedettine, Genova, Italy
- 1982 - 1985** Middle school, A.G.Barrili, Genova, Italy
- 1985 - 1990** High school, Liceo Scientifico Istituto M.Champagnat, Genova, Italy
- 1990** “Diploma di Maturità Scientifica”, grade 60/60
- 1990 - 1996** Undergraduate studies in Physics at the Faculty of Mathematical, Physical and Natural Sciences, University of Genova, Italy
- 1995 - 1996** Pre-graduated student at the Institute of Cybernetics and Biophysics of the National Research Centre (CNR), supervised by Prof. Franco Conti, Genova, Italy
- Thesis: *Interaction of  $Ca^{2+}$  with  $Na^+$ -channel gating mechanism*
- 1996** Master degree in Physics at the Faculty of Mathematical, Physical and Natural Sciences, University of Genova, Italy, grade 110/110
- 1996 - 1998** Post-graduate fellow at the Institute of Cybernetics and Biophysics of the National Research Centre (CNR), by Prof. Franco Conti, Genova, Italy
- 1998 - 2001** Ph.D. Student at the Max-Planck-Institut for Experimental Medicine, department of Molecular Biology of Neuronal Signals by Prof. Dr. Walter Stühmer; supervised by PD. Dr. Heinz Terlau, Göttingen, Germany